AUTOPHAGY-TARGETING PEPTIDOMIMETICS AS POTENT ANTI-PROLIFERATIVE THERAPEUTIC CANDIDATES AGAINST OVARIAN CANCER

YU YINGTING

PhD

The Hong Kong Polytechnic University

2024

The Hong Kong Polytechnic University

Department of Applied Biology and Chemical Technology

Autophagy-targeting Peptidomimetics as Potent Anti-proliferative Therapeutic Candidates against Ovarian Cancer

Yu Yingting

A thesis submitted in partial fulfilment of the requirements

for the degree of Doctor of Philosophy

January 2024

CERTIFICATE OF ORIGINALITY

I hereby declare that this thesis is my own work and that, to the best of my knowledge and belief, it reproduces no material previously published or written, nor material that has been accepted for the award of any other degree or diploma, except where due acknowledgement has been made in the text.

Signature:

Name of student：YU Yingting

Abstract

Ovarian cancer, recognized as one of the most lethal gynecological malignancies, is characterized by an absence of early-stage biomarkers and efficacious therapeutic interventions, resulting in unfavorable prognoses. Predominantly, 90% of ovarian malignancies are of epithelial origin, with serous tumors accounting for 70%. These tumors are inherently heterogeneous, displaying a spectrum of clinicopathologic characteristics and behaviours attributable to their diverse tumor constituents. Consequently, the quest for potent therapeutics for ovarian cancer not only presents formidable challenges but also underscores the pressing need for expedited treatment solutions.

Autophagy, a highly conserved self-degradation process in eukaryotic cells, eliminates dysfunctional cellular components via lysosome-dependent pathways. Its potential role in modulating ovarian cancer cell responses to various treatments has garnered significant interest. Some studies suggest that ovarian cancers with increased autophagy flux exhibit less aggressive symptoms and greater chemotherapeutic responsiveness.

Beclin 1, a scaffold/adaptor protein, is a key regulator of autophagy, which responds to various autophagy stimuli and maintains the balance between pro-survival and pro-apoptotic processes. Our lab designed a serious of hydrocarbon stapled peptides that specifically bind to Beclin1, enhancing its interaction with UVRAG and promoting Vps34-dependent autophagy. Tat-SP4, one of the leading Beclin 1-targeting stapled peptides were further optimized by introducing

new staples and residue mutations, resulting in a new generation peptide with a stronger binding affinity to Beclin 1. The leading candidate of new generation peptide, SP9, demonstrated approximately 10-fold stronger binding affinity to Beclin 1 compared to Tat-SP4 and induced autophagy with comparable efficacy.

In this project, we demonstrate the anti-proliferative potency of SP9 against ovarian cancer cell lines and xenograft models, without significant toxicity. Mechanistic investigations reveal that SP9 triggers autotic cell death, along with calcium homeostasis disruption, elevated reactive oxygen species (ROS) level, mitochondria membrane potential depolarization, induction of mitochondrial permeability transition pore (mPTP) opening and defective OXPHOS activity. Autosis inhibitor digoxin can rescue SP9-induced cell death and mitigate calcium signal intervention, highlighting the crucial role of calcium in SP9-mediated cell death. Additionally, our cellular level findings suggest a synergistic effect between Beclin 1-targeting staple peptides and chemotherapy, offering reduced toxicity and enhanced anti-tumor efficacy.

In summary, our optimized designed Beclin-1 targeting stapled peptides have shown potent anti-proliferative efficacy in ovarian cancer model both *in vitro* and *in vivo*, indicating that our study provides a new strategy to target autophagy for ovarian cancer treatment. Autophagy-targeting peptidomimetics exhibit potential as robust anti-tumor therapeutic candidates for use in combination with existing therapies to enhance treatment outcomes for ovarian cancer.

Acknowledgements

I am grateful that finally reach this acknowledgement part. During my past four years PhD study, I received countless help and kindness. There are lots of people I want to appreciate and never appreciate enough.

First of all, I am very much obliged to my supervisor, Prof.Zhao Yan Xiang, for her guidance during my PhD study. Thanks for her professional guidance to my project, her patience and encouragement throughout my studies and being a great role model for us. I am always impressed by her outstanding academic competence, genuine passion to science and empathic capacity. Prof Zhao is an exceptional professor and possesses an impressive personal charisma, which inspire me a lot in both academic study and personal life. I am grateful for the opportunity to study in her group.

Next, I would like to express my sincere gratitude to all lab members. All of them are extremely pleasant and helpful person, very lucky to work with them. Especially thanks to Dr. Qiu Xianxiu and Dr.Li Na who lead me to our lab research in the beginning of my studies; thanks to Dr Zhang Xiaozhe, Dr. Chen Jingyi and Dr. Gao Shan who always ready to help and concern to me in both lab life and personal life; thanks for Dr Yang Xian, Miss Feng Yu and Miss Wang Lei who are so friendly and caring to me. They are wonderful people who make the world a better place and I feel so grateful to meet them.

Lastly, I would like to appreciate my dear parents, my family, my boyfriend and my best friends. Thanks for their support and unconditional love to me during this whole PhD study and my life.

Table of contents

List of figures and tables

Figure

Table

1.Introduction

1.1 Background of ovarian caner

Ovarian cancer is a late presentation malignancy with highest fatality rate of all gynecologic cancer. To women, the odds of diagnosis ovarian cancer is around 1 in 78 during her lifetime while the possibility die of ovarian cancer is about 1 in 108, the lethality-to-incidence ratio is over than 0.7 [1]. Ovarian cancer is often diagnosed at an advanced stage, which can contribute to higher mortality rates. In 2023, it is estimated 19,710 new cases and 13,270 deaths in US [2] . Ovarian cancer ranks sixth most prevalent caner and seventh deadliest cancer in female reproductive system based on the Hong Kong Cancer Registry (HKCaR) announcement [3]. According to population-based statistic study, the predicted tendency and incidence of ovarian cancer may continue rising in Hong Kong to 2030 [4]. It is acknowledged that ovarian cancer is a significant health concern globally.

The risk factor of ovarian cancer is various, some relatively explicit factors including aging, obesity, postponed pregnancy, hormone therapy and genetic history [5]. There are some factors with dubious impact on ovarian cancer, such as androgen and diets. Most of ovarian cancer develop after menopause and beyond 50% diagnosed patience are over 63 years or elder. Obesity is known as hazard element for different carcer type, women with BMI>30 might not only have higher incidence of ovarian cancer but also show negatively impact to long-term survival. Increasing morbidity is also found in women who postpone their

pregnancy later than 35 years old or never impregnant [6]. For the women after menopause, estrogens alone or with progesterone treatment might also raise the peril of developing ovarian cancer. Additionally, a family history of ovarian cancer, breast cancer and colorectal cancer is considered as ovarian cancer hazard, because these types of carcinomas caused by inherited mutation in specific gene (e.g., BRCA1/2 (BReast CAncer susceptibility gene) and MLH1, MSH2) which also leads to family cancer syndrome increasing the liability of ovarian cancer [7]. Understanding the change and pattern of these risk factors of ovarian cancer help the better prevention and prognosis in long term development.

1.1.1 Clinical and molecular classification of ovarian cancer

Ovaries are genital gland of female to generate ovum for reproduction, the ovum complete fertilized in uterus by travel through fallopian tubes, thus ovaries consist of three kinds of cell and each type of cell can develop into different forms of tumors. Nowadays, more and more evidence indicate ovarian cancer may commence in the cells located in the distal end of the fallopian tubes while it was earlier perceived to start only in ovaries. There are three main types of ovarian cancer which indicated by its origin: epithelial, sex-cord-stromal and germ cell (Figure 1.1). The epithelial tumors are start from the cell in the outer surface of ovary and it is the most common type in ovarian cancer when the latter two only constitute less than 5% of all ovarian cancer [8]. Stromal tumor origin from structural tissue cells that maintain the ovary structure and generate the female

hormones estrogen and progesterone, while germ cell tumor begins with the cell produced ovum.

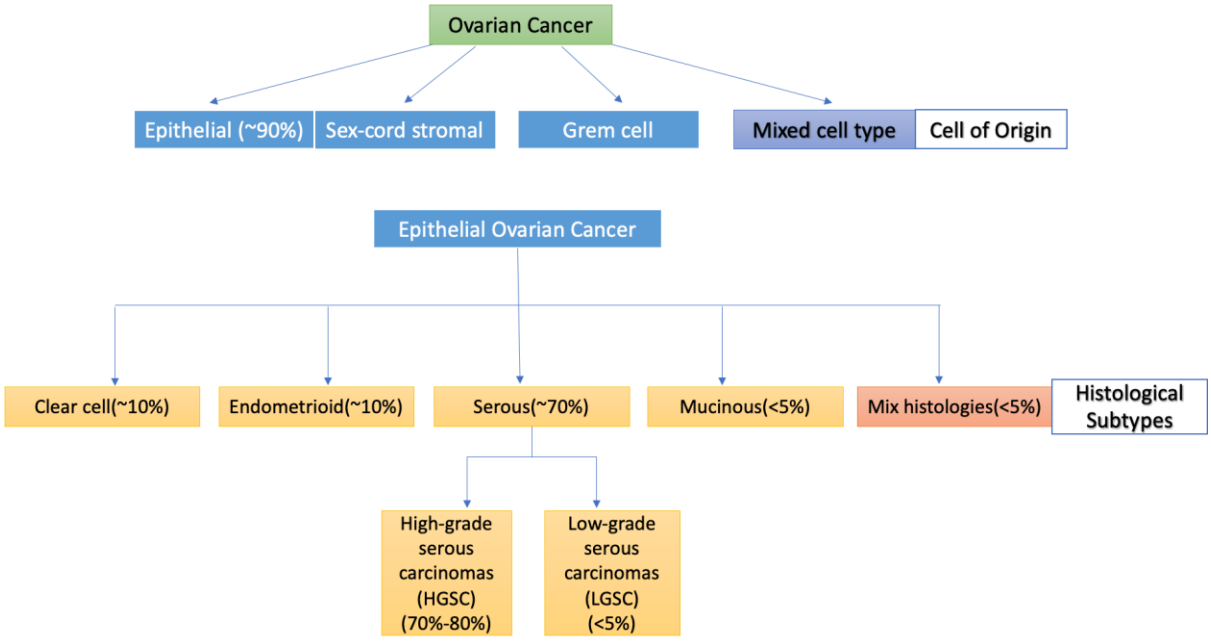

Figure 1. 1 General classification of ovarian cancer cells [9].

Our study is mainly focus on epithelial ovarian cancer which are characterized into four representative histological subtypes: serous, endometrioid, clear cell and mucinous. About 70% of epithelial ovarian cancer is defined as serous tumor which is considered as a heterogeneous disease showing assorted clinicopathologic features and behavior since it consisted of different kinds of tumors [10]. Based on morphologic and genetic studies, there are two categories of serous tumors: high-grade serous carcinomas (HGSC) or low-grade serious carcinomas (LGSC). HGSCs account for 70% to 80% of all subtypes of epithelial ovarian cancer, while LGSCs account for less than 5% [10].

Two classification systems are wildly adopted for the course of ovarian cancer, the FIGO (International Federation of Gynecology and Obstetrics) system and the AJCC (American Joint Committee on Cancer) TNM staging system are basically the same [11]. They both stage ovarian cancer with considering 3 factors: the expansion of the tumor, the spread to nearby lymph nodes(N) and how its metastasis(M) to distant location [12]. The number of T, N and M render the specific detail of tumor, higher number indicates the cancer is more advanced. Clinically ovarian cancer is classified as stages I to IV which refers to extend of cancer in the body (Figure 1.2). In stage I, disease is limited to ovaries only, yet it is defined as stage II when disease extending to the pelvis. Stage III and IV are considered as advanced stage which present regional or distant metastases [13]. The earlier detection of cancer, the higher chance a person has of surviving five years after treatment. For ovarian cancer, merely 16.3% are diagnosed at the early local stage and the 5-year relative survival for localized ovarian cancer reaches 92.6% [14]. The high mortality cause by late diagnosis with over 70% of ovarian cancer late present until they developed into advanced stage. 5-year relative survival of ovarian cancer drop to <30% with stage-related survival for stages III and IV [8].

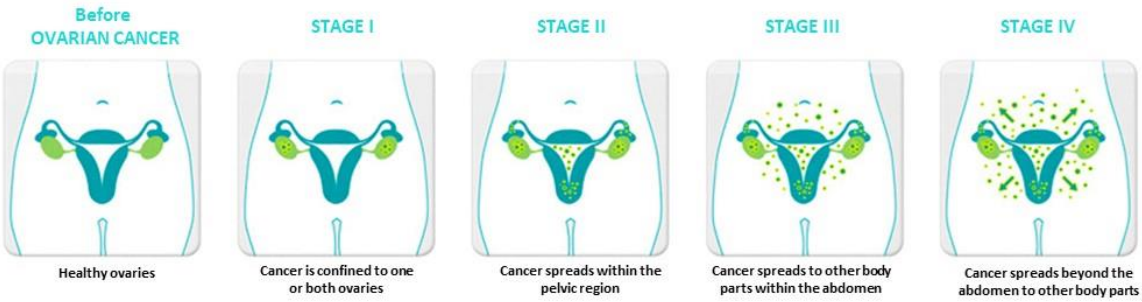

Figure 1. 2 Stage classification of ovarian cancer [15].

1.1.2 Current protocol for diagnosis and treatment of ovarian cancer

To early stage of ovarian cancer, the diagnostic ways including regular women's health pelvic exam and screening test: transvaginal ultrasound (TVUS) and the CA-125 blood test. Doctor can feel the ovaries and uterus for texture, shape, and size during pelvic exam yet most early stage of ovarian cancer shows no morphology symptom so that is difficult or improbable to feel [16]. Transvaginal ultrasound is a test that using sound waves to observe the uterus, fallopian tubes, and ovaries, which can assist to find if a mass in the ovary. Whereas it unable to access if the mass is benign or malignant. The CA-125 blood test is to measure the amount of protein CA-125 which often present high level in ovarian cancer patient in blood and showing decreased level after treatment take effect. However, there is higher chance that CA-125 protein level result from endometriosis and pelvic inflammatory disease instead of ovarian cancer, thus it is not a specific biomarker for ovarian cancer [17]. In general, early screening and detection of ovarian cancer is not effective for non-specific signs and symptoms and lack of a definitive screening tool. It is known that late presentation of ovarian cancer

results in high mortality, the onset of sign and symptom in ovarian cancer patient usually begins with tumor spread. The most prevalent symptom is listed as bloating, pelvic or abdominal pain and some urinary symptoms, these symptoms also caused by some benign diseases, but they incline to be more atypical and recurrent in advanced ovarian cancer case [18].

Currently, the combination of debulking surgery and adjuvant chemotherapy is still the mainstay treatment for ovarian cancer. Intraoperative imaging is required before surgery to assist tumor localization with using optical imaging agent named pafolacianine (Cytalux) [19]. Before surgery, the patient was injected with pafolacianine which is a fluorescent drug can bind to folate receptor -expressing cells (a specific protein found in ovarian cancer cells) few hours advance [20]. During surgery, near-infrared fluorescent light image system induces pafolacianine to give out light enable tumor to be removed [21]. Optimally debulked indicates no visible cancer or no larger than 1 cm diameter tumor after surgery, it is logically that better prognosis followed by optimally debulked than sub-optimally debulked which left larger tumor after surgery. In some instances, ovarian cancer debulking surgery impinge on other organs such as colony, small intestine, spleen, gallbladder, stomach, and bladder. Median progression-free survival for ovarian cancer is up to promising 18 months after debulking surgery [8].

To patient who is in advanced stage of ovarian cancer, surgical debulking is recommended to remove the tumors and followed by chemotherapy. It is

considered as systemic treatment, giving the chemo medication can reach almost every area in body thought blood stream. Chemotherapy is competent to eliminate the remanent cancer cell after surgery or those metastatic oncocytes, even shrivel the large size tumor into operable size before resection. There are varies methods of administration, it can be intravenous injection, intraperitoneal injection with catheter or oral administration. Combination treatment involved platinum compound and taxane are commonly adopted as first-line therapy in ovarian cancer, giving two drug combination shows stronger efficacy than one drug alone. The primary mechanism of platinum drugs is covalent binding to DNA, causing the cross-link of DNA strands and prohibition of DNA synthesis and replication, then further blocking cell cycle and DNA damage response [22]. Different from platinum compounds, taxane chemical carry out cytotoxicity by binding of tubulin to repressing microtubules' disassembly, leading to chromosome segregation and cell division irregular [23]. The typical course of combination treatment is 3 to 6 cycles depending on the stage and genre of the tumor, a cycle is standardized prescription of the drugs followed by a withdrawal period and the specific dosage is determined by progression of disease, regular chemo administration method is summarized in Table 1.1 [24].

Table1. 1 Regular administration of chemotherapy to ovarian cancer [25].

Medication	Route of administration	Stage treated	Duration
Paclitaxel and carboplatin	Intravenous	I	21 days
Paclitaxel and carboplatin	Intravenous	I	7 days
Docetaxel and carboplatin	Intravenous	I	21 days
Paclitaxel and cisplatin	Intravenous or intraperitoneal	II, III, IV	21 days
Paclitaxel and carboplatin	Intravenous or intraperitoneal	II, III, IV	21 days
Dose-dense paclitaxel and carboplatin	Intravenous	II, III, IV	21 days
Paclitaxel and carboplatin	Intravenous	II, III, IV	7 days
Docetaxel and carboplatin	Intravenous	II, III, IV	21 days
Carboplatin and liposomal doxorubicin	Intravenous	II, III, IV	28 days
Bevacizumab with paclitaxel and carboplatin	Intravenous	II, III, IV	21 days

Data from the National Comprehensive Cancer Network. Ovarian cancer: including fallopian tube cancer and primary peritoneal cancer.

As one of the most prevalently used chemo drug, cisplatin can effectively prohibit tumor growth by taking advantage of its multidirectional mechanism to anticancer action. Cisplatin is administrated by intravenous injection as a solution in saline. With the circulation of bloodstream, the cisplatin is easily attached with amino acids and proteins consisted in the blood, caused over 65-95% cisplatin inactivation [26]. The rested cisplatin with activity is imported into cells by the membrane transport proteins and by passive diffusion, followed one or two chloride ligands exchange for water to activate cisplatin. The hydrated and activated cisplatin exhibits a broad-spectrum cytotoxic effect, which functions by inducing intercellular oxidative stress and causing damage to DNA specifically in cancer cells. It has been discovered that genomic DNA is the primary target of

cisplatin [27]. Most of cases, cisplatin binds to two guanines, or two adenines situated on same strands, resulting in the formation of interstrand adducts, which leads to DNA impairment and then stimulates apoptosis pathways causing cell death [28]. Mitochondria DNA is another target to cisplatin, similar with genomic DNA, cisplatin also binds to mitochondrial DNA, resulting in the formation of interstrand adducts then the mtDNA becomes damaged. Impaired mitochondria DNA further change the permeability of the mitochondrial membranes and promote the apoptosis pathway by releasing cytochrome C and procaspase 9 from the organelle [29]. Additionally, cisplatin can effectively induce reactive oxygen species by facilitating the activation of nicotinamide adenine dinucleotide phosphate (NADPH) oxidase (NOX), which initiates the conversion of oxygen O_2into superoxide radicals (O_2•–) and subsequently, hydrogen peroxide (H_2O_2) [30]. Through the Fenton's reaction, H_2O_2 can be catalyzed by Fe^{2+}/Fe^{3+} to form highly reactive hydroxyl radicals (•OH), leading to oxidative damage in lipids, proteins, and DNA. Drug resistance and toxic side effect of cisplatin are serious handicaps of cisplatin administration, despite patients generally response well to chemotherapy in the beginning, recurrence rate is alarmingly high at more than 75% after 18 months [31], successive relapse associated with chemoresistance happens in advanced stage patients cause steep mortality. Most patients with cancer recurrent accept second-line chemo drug treatment until they show the worst prognosis with platinum-resistant disease. The cisplatin resistant can be divided into two kind bases on its origin: innate and acquired. The innated

resistance occur without any previous cisplatin exposure, while acquired resistant develop from drug exposure [32]. Though the exact mechanism of chemo resistant progress remains unclear, generally recognized that during repeated chemotherapy modality, chemoresistance develops gradually, cancer cell uptake less chemo drug and become resistant to current treatment regimen over time. In abdominal cavity, ovarian cancer grows and metastasizes then eventually develops into chemoresistance disease which forms a unique microenvironment with ascites, hypoxia and low glucose levels [33]. To adapt for survival, it has been shown that chemoresistance cancer cells are able to increase their effluence with alteration of key transporter and pumps and possess high detoxification activity against chemo drugs. The emergence of chemo resistance in ovarian cancer poses a substantial obstacle to achieving therapeutic success, the resistance of ovarian cancer cells to chemotherapy might involves a complex interplay of various mechanisms, including multidrug resistance (MDR), oxidative stress, DNA damage repair, cell metabolism, apoptotic pathways, immunity, and autophagy (Figure 1.3) [34].

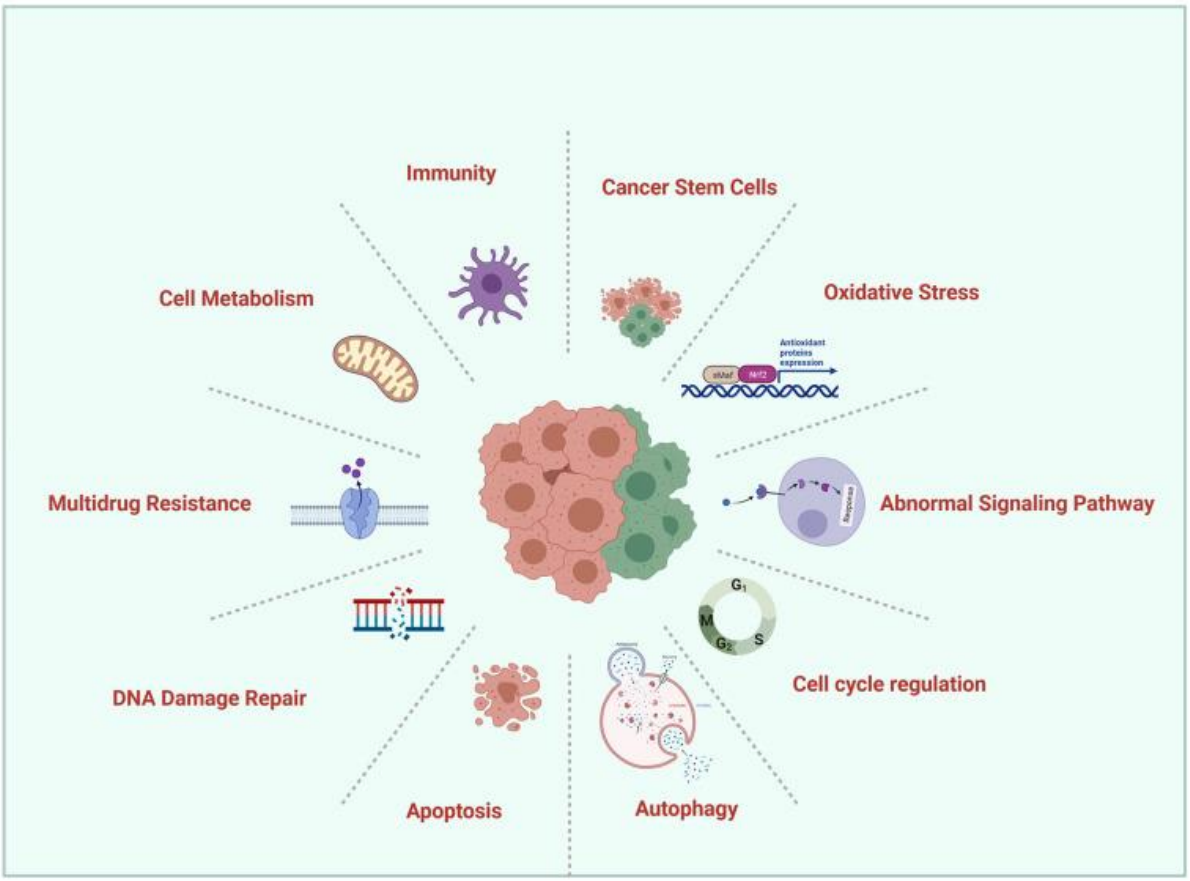

Figure 1. 3 Comprehensive illustration of the mechanisms underlying resistance to platinum-based chemotherapy in ovarian cancer [34].

1.1.3 Recently approved targeted therapeutics for ovarian cancer.

Other than traditional chemotherapy, there are some innovative targeted therapies showing promising curative effect in ovarian cancer with the pharmaceutical research development. The first targeted drug approved for ovarian cancer is anti-VEGF (vascular endothelial growth factor) monoclonal antibody, and Bevacizumab is the first available anti-VEGF antibody against VEGF to exert cytostatic anticancer effect [35]; Olaparib is the first clinically approved drugs for ovarian cancer treatment base on synthetic lethality rationale, targeting BRCA

gene mutation to improve therapeutic efficacy by prohibiting DNA repairing [36]; Immunotherapy is also the research hotspot since anticancer immune response can be promoted to against cancer cell with high specificity and few side effect [37].

The antiangiogenic compound curtails ovarian tumor growth by prohibiting angiogenesis since tumor require vessel generation for supplying oxygen and nutrition to facilitate cancer cell growth and metastasis. Vascular endothelial growth factor (VEGF) and its receptor (VEGF-R) are the most vital proangiogenic signal pathway to promotes blood vessel formation, it is highly activated in ovarian cancer cell and correlated with disease grade and metastasis tendency. Bevacizumab is the first FDA approved humanized monoclonal, which plays its curative effect by deterring VEGF binding to VEGF-R, further impairing existing vessel and hampering neovascularization [38]. Abundant clinical trials have proved that bevacizumab treatment can notably extend PFS of ovarian cancer patient in both monotherapy and combination therapy, whereas the enhancement of overall survival is not so evident [39]. Additionally, due to the limited response rate and bevacizumab resistance early arising, the efficacy of bevacizumab is compromised along with time.

The poly (ADP-ribose) polymerase inhibitors (PARPi) are capable to target polymerase then bring about synthetic lethality in BRCA mutation ovarian cancer cell. Synthetic lethality is characterized a type of genetic interaction leading cell death, it occurs when multiple genes got interrupted simultaneously.

BRCA1/BRCA2 gene is one of the most intensively studied gene in breast cancer genesis, it plays crucial role in DNA repair and transcriptional regulation that indispensable for chromosomal stability to prevent DNA lesion. BRCA gene take part in the DNA repair for double stranded damage by homologues recombination capability and PARP enzymes also involve with genomic stability by detecting and repairing single- and double-stranded DNA breaks [40]. Therefore, ovarian cancer patients with BRCA variation caused homologues recombination deficiency (HRD) lean more heavily on PARP mediated single-strand repair pathway, it also sensitizes the cell to platinum or other DNA damage agent [41]. PARPi takes advantage of HRD-positive status, exhibiting stronger cytostatic efficacy to develop into first-line maintenance therapy for ovarian cancer. Olaparib is the first PARPi drug introduced into clinical application of ovarian cancer in 2018, clinical trial data support that the Olaparib monotherapy can decrease 70% lethality compare with placebo treatment [40]. Furthermore, several studies proved that progression-free survival (PFS) for patients with BRCA mutation are notably extended by Olaparib maintenance treatment. However, the population-bases study revealed that only 5%-15% of BRCA1/2 variation presented in ovarian cancer which limit the medication use [42]. In 2022, the updated new overall survival data suggested PARP inhibitor administration is detrimental to patient's health, leading the revisions for FDA approved indications for PARP inhibitors in the management of epithelial ovarian cancer [20].

1.1.4 Novel combination therapies at different stages of clinical trials.

Immunotherapy for ovarian cancer shows tremendous potential for addressing this devastating disease and several clinical trials testing new treatments are currently underway. The ongoing trial of investigation including but not limited to immune checkpoint inhibition and tumor-directed immunotherapy of Wilms' Tumor 1 (WT1). One of the most famous immune checkpoints is programmed death receptor-1 (PD-1) and its ligand (PD-L1), which can distinguish pathogens from normal cell [43]. The presence of PD-L1 prevent self-cell from killing by T-lymphocyte (T-cell) immune response activity, giving the fact that cancer cell incline to upregulate PD-L1 to escape from auto immune response, immune checkpoint blockade target agent is competent to disrupt the immune checkpoint interaction between the tumor and T-cell, reviving cytotoxic T-cell response. Nivolumab is FDA approved anti PD-L1 agent for the recuring melanoma, non-small cell lung cancer, and renal cell carcinoma [44]. Additionally, Keytruda a drug developed by Merck used in cancer therapy. It is a monoclonal antibody, has already been approved by the FDA for the treatment of certain types of cancers including melanoma, non-small cell lung cancer, recurrent or metastatic head and neck cancer, classical Hodgkin lymphoma, and urothelial carcinoma. The drug is still under investigation for the treatment of ovarian cancer.

WT1 usually overexpress in epithelial ovarian cancer cell (WT1; 65% of patients) but barely express in non-cancerous tissue thereby it is the ideal target for tumor-directed immunotherapy [45]. WT1 peptide vaccine galinpepimut-S (GPS) is a

mixture of two native and two mutated analogue WT1 peptides, preliminary data suggested that acute myeloid leukemia patient with GPS monotherapy exhibiting satisfactory tolerance, high WT1-specific T-cell response efficiency and extended OS [46]. The ongoing clinical study investigate the safety and immunogenicity of WT1 peptide vaccine GPS with anti PD-1 nivolumab in WT-1 positive ovarian cancer individuals, phase I data suggested the combination treatment intensify the immune response and prolong PFS results [47]. Further clinical statistics is required to support immunotherapy operation in ovarian cancer. Though numbers of studies indicated the great potential of immunization therapy with encouraging therapeutic effect, the research remains in preliminary stage and no approved immunotherapies can be used in ovarian cancer clinical treatment so far. In the past few decades, researcher dedicated to improving the ovarian cancer treatment, whereas the survival rate remains discouraging. Statistic suggested that over 60%-80% of patient can attain fully remission after first-line treatment while 80% of them die from treatment resistant or cancer regression [48], indicating there is urgent unmet medical need to develop novel therapeutics that overcome chemoresistance in ovarian cancer.

1.1.5 The mechanisms and evaluation methodologies of synergistic interactions in oncological combination therapy

Combination therapy is often employed by combining chemo drugs with other medication or treatment modalities to reduce toxic effect and overcome the chemoresistance, achieving better therapeutic effect to cancer. For example, the

combination of cisplatin and gemcitabine is the clinical medication in the advanced bladder cancer and certain types of ovarian cancer [49, 50]. Gemcitabine is a nucleoside analog that can enhances the cytotoxic effects of cisplatin by inducing DNA damage and inhibiting DNA synthesis [51]. The combination treatment of cisplatin and Gemcitabine have been shown enhancing response rate and overall survival in patients with advanced ovarian cancer [49]. The exact mechanisms behind synergistic effects are manifold and can vary depending on the substances involved. There are a few general theories to surmise synergistic effects occur:

1. Complementary Pathways: Substances may work through different biochemical pathways to achieve a similar or related outcome. When combined, their actions may enhance each other, leading to a greater overall effect. This can occur, for example, when two substances target different steps within a biological process, resulting in improved efficiency. The combination of vemurafenib and cobimetinib allows for simultaneous inhibition of two different points in the same cancer cell growth signaling pathway [52].

2. Receptor Interactions: Substances may interact with the same or different receptors in the body. Combined treatment allows agents have additive or amplifying effects on receptor activity, causing enhanced response. e.g., breast cancer by simultaneously targeting different sites on the Epidermal Growth Factor Receptor (EGFR) receptor [53]. EGFR inhibitors, such as cetuximab or erlotinib, target the EGFR pathway, which is often overactive in certain types of

breast cancer. These inhibitors can potentiate the cytotoxic effects of cisplatin by inhibiting the EGFR signalling pathway, leading to increased cancer cell death [54].

3. Metabolic Interactions: Substances can undergo metabolic transformations within the body, leading to the formation of active metabolites or the alteration of metabolic pathways. When two substances influence the same or interconnected metabolic pathways, their combined effects can be synergistic. This can occur when one substance enhances the metabolism or bioavailability of another substance, resulting in a more robust effect. One example of a medication that demonstrates metabolic interactions applied in cancer treatment is the combination therapy of capecitabine (Xeloda) and oxaliplatin (Eloxatin) in the treatment of colorectal cancer [55]. Oxaliplatin can enhances the conversion of capecitabine to its active form, 5-FU, through its influence on the enzymes responsible for the metabolic process, achieving synergistic effective of anti-cancer activity [56].

4. Pharmacokinetic Interactions: Substances interact at the level of absorption, distribution, metabolism, or excretion within the body. These interactions can influence the bioavailability, half-life, or clearance of a substance, ultimately impacting its overall effect. When substances interact in a way that enhances these pharmacokinetic properties, it can lead to synergistic effects. One classic example of exerting synergistic effect by pharmacokinetic interactions in anti-cancer drugs is the combination of paclitaxel and ritonavir. Paclitaxel works by

inhibiting cell division and promoting cell death, yet paclitaxel can be metabolized by the liver enzyme CYP3A4, which lead to its rapid elimination from the body [57]. When paclitaxel is co-administered with ritonavir, the inhibition of CYP3A4 by ritonavir leads to a decrease in the metabolism of paclitaxel then further results in increased plasma concentrations and prolonged exposure of paclitaxel in the body. This combination therapy has been studied in clinical trials and has shown improved efficacy and tolerability compared to paclitaxel alone [58].

The mechanisms underlying synergistic effects is complex and context dependent. The specific interactions between substances are often studied on a case-by-case basis to comprehend the underlying mechanisms and potential benefits or risks. Evaluating the synergistic effect of combinations involves the use of mathematical models or indices. There are two primary ways to define drug independence, which refers to the way different drugs interact with each other when used together. (a) The first definition is based on the isobologram approach, also known as Loewe definition of additivity and implied combination index [59]. This model suggests that two drugs are independent if the effect of the combination is equal to the sum of the effects of each drug used separately. The second definition comes from the Bliss independence model, which is also referred to as the Webb fractional product method. According to this model, two drugs are deemed independent if the effect of their combination equals the product of the effects of each drug when used separately [60]. This suggests that

the combined effect is the expected outcome if each drug were acting on its own, without influencing the effect of the other.

The combination index is a quantitative indicator used to assess the degree of synergy, additivity, or antagonism in a combination of drugs or agents. It is based on the median-effect equation developed by Chou and Talalay. The CI is calculated using the formula [61]:

$$CI = (D)_1/(D_x)_1 + (D)_2/(D_x)_2 + (D)_1(D)_2/(D_x)_1(D_x)_2$$

Where $(D)_1$ and $(D)_2$ represent the doses of individual drugs required to achieve a specific effect, and $(D_x)_1$ and $(D_x)_2$ represent the doses of the individual drugs in combination needed to produce the same effect. The CI values indicate the nature of the combination effect: CI < 1: Synergism (greater effect than expected); CI = 1: Additivity (expected effect); CI > 1: Antagonism (less effect than expected), as shown in Table 1.2.

Table1. 2 Detail description of combination index [62].

Range of CI	Symbol	Description
<0.1	+++++	Very strong synergism
0.1–0.3	++++	Strong synergism
0.3–0.7	+++	Synergism
0.7–0.85	++	Moderate synergism
0.85–0.90	+	Slight synergism
0.90–1.10	±	Nearly additive
1.10–1.20	–	Slight antagonism
1.20–1.45	—	Moderate antagonism
1.45–3.3	—–	Antagonism
3.3–10	——	Strong antagonism
>10	———	Very strong antagonism

In addition to combination index value, Chou and Talalay developed the concept of dose-reduction index as an extension of their earlier work on CI analysis. The concept of the DRI was introduced as a quantitative measure to assess the degree of synergy between drugs in combination therapy, for address the limitation of CI, which only allow for the determination of whether the combination of two or more drugs produces synergistic, additive, or antagonistic effects, whereas it cannot directly provide information about the extent to which the individual drug doses can be reduced in combination therapy. The DRI quantifies the degree of synergy by calculating the ratio of the individual drug dose to the combination drug dose required to achieve the same level of effect [63]. Since its introduction, the DRI has been widely used in preclinical and clinical studies to assess the degree of synergy between drugs in combination therapy. It has helped researchers and clinicians in evaluating the effectiveness and cost-effectiveness of combination treatments, overcoming drug resistance, and guiding the design of optimal drug combinations.

The Loewe additivity model is also based on the principle of additivity, assuming that the combination effect is equal to the sum of the effects produced by each individual drug [64]. Loewe synergy scores can be obtained from the SynergyFinder tool which is a web-application that enables researchers to pre-process, analyse and visualise pairwise drug combinations in an interactive manner [65]. Drug interactions are classified as likely synergistic (score >10), antagonistic (score <-10), or additive (score -10 to +10). Apart from the Loewe

model, other frequently used reference models such as the Highest Single Agent (HSA), Bliss, and Zero Interaction Potency [66] models are also utilized in the SynergyFinder tool. These models measure the level of synergy in different ways. The HSA model quantifies synergy as the amount exceeding the response of the most effective single drug [67]. The Bliss model calculates synergy as the multiplicative effect of individual drugs, assuming they act independently [68]. Lastly, the ZIP model measures synergy based on the expected response as if the individual drugs did not influence each other's potency [69]. Loewe additivity model and the Bliss independence model are two commonly used models in the anticancer drug study field. In summary, the choice of model for a synergy study depends on several factors, including the nature of the drugs being studied, the desired outcome, and the specific context of the study.

1.2 Autophagy and its role in ovarian cancer

1.2.1 The role of Beclin 1 in autophagy and carcinoma.

Autophagy known as self-eating process, is evolutionarily high conserved mechanism in all eukaryotic cells for eliminating dysfunctional cellular contents through lysosome-dependent pathways [70]. There are four defined forms of autophagy: macroautophagy, microautophagy, chaperone-mediated autophagy, and crinophagy. Macroautophagy is the most wildly studied autophagy form and considered as predominant pathway, herein referred to as autophagy. The autophagy activity involves with the sequestration of damaged cytoplasmic component with double membranes vesicle autophagosome, then transported to

fuse with lysosome/vacuole forming autolysosome, eventually the content of autolysosome got breakdown and recycled [71]. The cytosolic double-membrane vesicles enveloped with cargo is the most representative features of autophagy, hence the formation of the double-membrane bound phagophore and autophagosome is wildly considered as golden standard for certifying autophagy activity. There are selective and nonselective autophagy with different type of sequesters cytosolic components. Nonselective autophagy occurs for the turnover of bulk cytoplasm under starvation conditions or stress induction, whereas selective autophagy specifically targets impaired or redundant organelles, including mitochondria and peroxisomes, as well as invasive microbes. Selective autophagy receptors, such as p62/SQSTM1, recognize specific cargo proteins or organelles and target them for degradation by binding to both the cargo and LC3 on the autophagosome membrane.

Autophagy activity is initiated by the formation of a phagophore, a cup-shaped membrane structure that emerges from the endoplasmic reticulum or other membrane sources. This initiation is regulated by the ULK1 (uncoordinated-51 like kinase-1) complex, which is activated in response to nutrient deprivation or other stress signals [72]. Next stage is the vesicle nucleation process, the phagophore expands and engulfs a portion of the cytoplasm, forming a double-membrane autophagosome. This course is intermediated by the class III phosphatidylinositol 3-kinase (PI3K) complex, which generates phosphatidylinositol 3-phosphate (PI3P) on the phagophore membrane, serving

as a docking site for effector to mediate phagophore elongation. After specific cargo proteins or organelles are targeted and fully sequestered by the mature autophagosome, it further fuses with a lysosome, forming an autolysosome. The autolysosome formation is mediated by the interaction of the autophagosome membrane protein, soluble N-ethylmaleimide-sensitive factor attachment protein receptor (SNARE), and lysosomal membrane proteins. The lysosomal hydrolases then degrade the cargo, generating breakdown products, such as amino acids, fatty acids, and sugars, are released from the autolysosome and recycled for cellular metabolism and biosynthesis. Overall, the major process of autophagy can be concluded as the induction of autophagy, vesicle elongation, autophagosome formation by docking and fusion, vesicle breakdown and degradation (Figure 1.4).

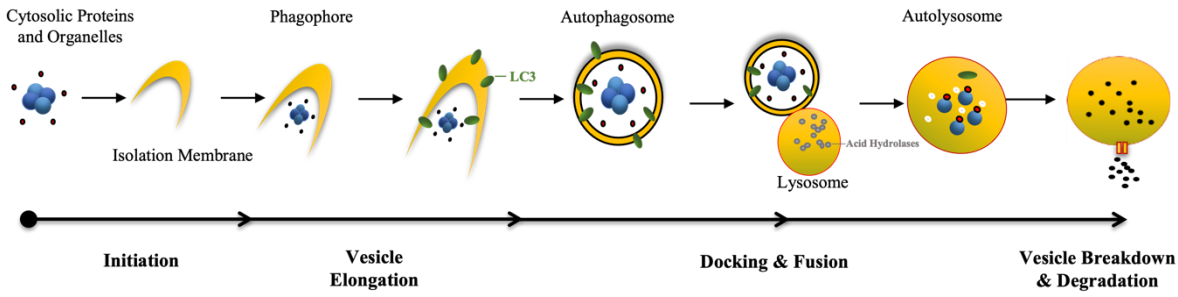

Figure 1. 4 The autophagy process includes four phases: initiation, vesicle elongation and autophagosome formation, autolysosome formation and the degradation.

Beclin 1 (Bcl-2-interacting coiled-coil protein 1) is a 450-amino-acid, 60-kDa coiled-coil protein that is encoded by the BECN1 gene in humans [84]. Beclin 1 is scaffold/adaptor protein known as the positive regulator of autophagy, it is a

core element of class III phosphatidylinositol 3-kinase (PI3KC3) complex which constituting Beclin 1, VPS34, VPS15, and ATG14 proteins [85]. The stimulation of PI3K complex enable initialize the autophagy pathway through Beclin 1 functioning as allosteric protein to attune the lipid kinase activity of PI3K-III catalytic unit VPS34 for producing Phosphatidylinositol (3)P (PI(3)P), as the generation of PI(3)P is required for the autophagy induction and autophagosome nucleation [86]. Beclin 1 is considered as major regulator of autophagy, playing essential role in autophagosome formation, phosphorylation, and ubiquitination of Beclin 1 response to difference autophagy stimulation and sustaining the balance between pro-survival and pro-apoptotic, given the Beclin 1 also interacting with B-cell lymphoma 2 (BCL-2) family protein, the famous anti-apoptotic mediators and proto-oncogene, though BH3 domain to regulate autophagy-related apoptotic cell death behavior [86].

Autophagy plays a crucial role in maintaining nutrient and energy homeostasis by eradicating defective cytosolic component and the reuse of degradation product for energy production and biosynthesis. It serves as a quality control mechanism by selectively degrading damaged organelles, misfolded proteins, and protein aggregates. This process helps to prevent the accumulation of toxic cellular waste and maintains the integrity and functionality of cellular components. Through autophagy pathway, reused cellular components, such as amino acids, fatty acids, and sugars, which can be used as energy sources during nutrient deprivation or other stress conditions. Autophagy is activated in response

to various stress signals, including nutrient deprivation, oxidative stress, and pathogen invasion. By removing damaged components and providing essential nutrients, autophagy helps cells to survive and recover from stress-induced damage. Meanwhile, autophagy involves with immune response by eliminating intracellular pathogens, such as bacteria and viruses, through a process known as xenophagy. Additionally, autophagy coordinates the production and secretion of immune mediators, contributing to the modulation of immune responses. Autophagy is essential for cellular and organismal health, the regulation of autophagy engages in diverse physiological activities, varying from intracellular homeostatic, cell differentiation and development, cell death to stress adaptation, immune function, and aging [73]. Defective autophagy flux is observed in various pathophysiological process including neurodegenerative diseases, metabolic disease, and cancer, highlighting the critical role of autophagy in maintaining overall organismal health [74].

Despite the dual role of autophagy in tumorigenesis, many studies acknowledge that Beclin 1 act as tumor suppressor in various cancer type. Mice with BECN1 gene knockout can be survival but exhibit higher malignancy ratio than wild-type animals [87]. The human BECN1 gene is situated on chromosome 17q21, and monoallelic deletions within this genomic region have been identified in up to 75% of ovarian cancers. [88]. The loss of one allele of the Beclin 1 gene is associated with diminished Beclin 1 protein levels, thereby disrupting the normal autophagy process in ovarian cancer cells. Furthermore, the incidence of somatic mutations

in the Beclin 1 gene in ovarian cancer is notably low[75]. The infrequent occurrence of somatic mutations in Beclin 1 suggests that alternative mechanisms, such as epigenetic regulation or post-translational modifications, may exert a more significant influence on Beclin 1 function in ovarian cancer. In addition, study demonstrated that Beclin 1 could be stimulated to ubiquitination and degradation through interplaying with an E3 ubiquitin ligase CUL3 (cullin3), then further discourage autophagy activity and promote tumor growth in breast and ovarian cancer [89]. Furthermore, with analyzing the tumor tissue from ovarian cancer patient receiving chemotherapy, Toshiko's team discovered the clinicopathological significance of some pivotal autophagy-related molecular: BECN1, LC3, and HMGB-1, revealing the connection of these protein expression with progression-free survival and overall survival, they demonstrated that the evaluation of BECN-1 can be a potential biomarker for anticipating the unfavorable response to platinum-based chemotherapy in ovarian cancer [90]. Collectively, the autophagy-related function of BECN-1 is of importance to carcinogenesis.

1.2.2 Autophagy in ovarian cancer therapy

The involvement of autophagy in carcinoma pathogenesis has been wildly explored. An array of study indicates the binary role of autophagy in cancer by restraining benign tumor growth but aggravating advanced malignant cancer [76]. In the early stage of tumorigenesis, autophagy acts as a tumor suppressor mechanism as evidenced by constrain of inflammation and intracellular reactive

oxygen species (ROS) levels, thereby supporting genomic stability and integrity. Elevated autophagy can effectively prevent cell from toxin accumulation and oncogenic protein aggregation such as p62 protein [77], for autophagy contributing to cellular protein and organelle quality control. P62, also known as sequestosome1, is a protein encoded by the SQSTM1 gene and functions as an autophagy adaptor. It consists of multiple domains, including a ZZ-type zinc finger domain, ubiquitin-associated domain [78], and LC3-interacting region [49]. Research has demonstrated that the overexpression of p62 or its abnormal aggregation is associated with the development of cancer [79]. P62 acts as a selective autophagy substrate and receptor, engaging with autophagy processes. It interacts with LC3 (Microtubule-associated protein 1A/1B-light chain 3) through its LIR domain to enhance autophagosome formation [80].

On the contrary, some studies consider that autophagy restriction could be potent therapeutic approach in advanced cancer since autophagy can benefit tumor cell survival and metastasis by improving stress tolerance and sustaining cellular metabolism in the later stages of cancer development [81]. Autophagy may act as a tumor promoter, in part via enhancing the property of cancer cells to cope with metabolic stress conditions like nutrient deprivation and hypoxia. Although the modulated system of autophagy in carcinoma can be divergent in different context, the importance of autophagy regulation in tumorigenesis is undisputable. Autophagy in ovarian cancer therapy has gained significant attention due to its potential role in modulating the response of ovarian cancer cells to various

treatment modalities. Research has shown that autophagy plays a dual role in ovarian cancer therapy, the potential of autophagy inhibitors or activators as adjuvant therapies in ovarian cancer treatment has been investigated, aiming to enhance the efficacy of existing therapeutic approaches. On one hand, autophagy can confer resistance to chemotherapy and promote tumor cell survival by facilitating the adaptation of cancer cells to stress conditions induced by chemotherapeutic agents. Cloroquine (CQ) belongs to lysosomotropism agents, which can restrain autophagy by repressing lysosomal acidification further leading the failure of autophagosome degradation, it has been extensive studied in anti-cancer treatment [66]. Combination CQ with chemo drug enable to sensitize various cancer cells, study found the pretreatment of CQ can remarkedly boost the anticancer effects by reversing the drug sequestration of lysosomes in ovarian cancer cells[82] [83].

On the other hand, some studies found that ovarian cancer with increased autophagy flux presenting less aggressive symptom and more responsive to chemo drug [84, 85], therefore autophagy can also be targeted as a therapeutic strategy to induce cell death in ovarian cancer cells, particularly in combination with other treatment regimens. It is proved that loss of Beclin 1 expression cause reduced autophagy activity and increased tumorigenesis result [86]. Furthermore, the researchers demonstrated that Beclin 1 expression levels were associated with clinical outcomes in ovarian cancer patients, with higher Beclin 1 expression correlating with improved response to chemotherapy and overall survival [87].

This finding suggests that targeting Beclin 1-mediated autophagy could be a potential therapeutic strategy in ovarian cancer treatment. These researches highlight the diverse approaches and findings in the study of autophagy in ovarian cancer therapy, demonstrating the potential for targeting autophagy as a therapeutic strategy to overcome treatment resistance and improve patient outcomes.

1.3 Beclin 1-targeting stapled peptides developed by our lab

1.3.1 Structure-based rational design of Beclin 1-targeting stapled peptides

Beclin 1 is the first characterized mammalian autophagy protein containing three different domains (as shown in Figure 1.5) [88]: Bcl-2-homology-3 (BH3), coiled coil (CCD) and evolutionarily conserved (ECD) (from N- to C-terminal) (1) BH3 domain is a well-characterized BCL-2 homology-3 (BH3) domain required for interactions with BCL-2 proteins, located in extended N-terminal region (residues 105–130) that is innately disordered and contains multiple phosphorylation sites [89, 90]; (2) a coiled-coil (CC) domain (residues 141–171) that enable to interacts with the CC domains of UVRAG or ATG14 [91]; and (3) ECD domain also known as the β-α autophagy-specific domain (residues 265–450) for the high degree of overlap between these regions, which engages with membranes. The mammalian class III PI3K is widely acknowledged for its critical function in membrane-mediated transport processes including autophagy and endosomal trafficking, and it is also known as Beclin 1–Vps34 complex [92]. Atg14L or

UVRAG are two mutually exclusive binding partners to Beclin 1 coil-coil domain by allosteric interaction with its metastable homodimeric state, composing functionally distinct Atg14L/UVRAG- containing Beclin 1–Vps34 subcomplexes. It is known that Atg14L is liable for guided complex I to ER sites then encourage autophagosome biogenesis [93]. As for the UVRAG-containing form which is termed “complex II” (PI3KC3-C2), mainly corelated with late-stage autophagosome maturation and degradative endolysosomal trafficking activities. The Beclin 1–Atg14L/UVRAG interaction relies critically on their coiled-coil domains and the N-terminal region among Beclin 1 coiled-coil domain is the most important region for binding to Atg14L and UVRAG [94], as shown in Figure 1.5 [95].

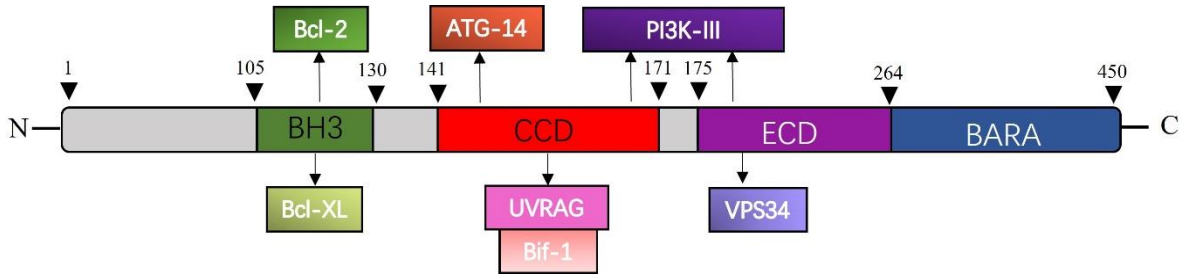

Figure 1. 5 The structure of Beclin 1 consists of three domains: the Bcl-2 homology 3 (BH3) domain, the central coiled-coil domain (CCD) and PI3-III, and the evolutionarily conserved domain (ECD), also term as the β-α repeated autophagic-specific domain (BARA) [95] .

Our previous study has shown that UVRAG can not only show stronger bind affinity with Beclin 1 than Atg14L in vitro but also enable to outcompetes Atg14L in recruiting endogenous Beclin 1 to the UVRAG-containing complex when

overexpressed in vivo [96]. We proved that the potency of the Beclin 1–UVRAG coiled-coil interaction is critical for UVRAG to outcompete Atg14L in recruiting endogenous Beclin 1 by the in vitro and in vivo competitive-binding results. It is reveal that Leu-to-Glu mutations in the UVRAG coiled-coil domain that weaken the potent Beclin 1–UVRAG interaction render UVRAG less or non-competitively against Atg14L. We were motivated to design small-molecule compounds that could target the Beclin 1 coiled-coil domain and enhance the Beclin 1–UVRAG interaction in vivo. To enhance the Beclin 1–UVRAG interaction in vivo, we deducted that a practical approach would be to reduce Beclin 1 self-association so that more endogenous Beclin 1 could be recruited by Atg14L or UVRAG to form Atg14/UVRAG-containing Beclin 1–Vps34 complexes. Guided by this design principle, an 11-residue segment corresponding to residues 191–205 within the Beclin 1 coiled-coil domain were adopted as the template for our designed compounds (Figure 1.6 A). This template is predicted to associate with the C-terminal end of the Beclin 1 coiled-coil domain, i.e., residues 231–245 according to our Beclin 1 coiled-coil homodimer structure, so that it could disrupt Beclin 1 self-association but not expected to compete with UVRAG for Beclin 1 interaction. Given it made up part of the Beclin 1 homodimer interface yet did not overlap with the binding site for UVRAG.

For the short length of 11 residues may not favour such secondary structure due to thermodynamics, a hydrocarbon staple of 11-carbon length was introduced in silico to connect residues 197 and 204 via (i, i + 7) linkage that spanned two

helical turns. Then we have computationally generated a small library of stapled peptides with sequence permutation (Figure 1.6 C). The structural model of the SP1-Beclin 1 interaction was created by aligning SP1 with the Beclin 1 coiled-coil homodimer structure (Figure 1.6 B). To enhance the binding affinity of SP1, computational optimization was performed, resulting in a collection of stapled peptides (SP2-SP12). During this optimization, certain residues considered to be essential for target-site binding were left unaltered, while computational mutations were introduced to other amino acid residues. After conducting computational screening, in vitro binding studies, and analysing in vivo imaging data, a few promising peptides were identified. To understand the binding modes of these stapled peptides with the Beclin 1 molecule, molecular dynamics (MD) simulations were performed. Additionally, the binding energies of these peptides were calculated using the force field-based molecular mechanics generalized born surface area (MM-GB/SA) method. It is proved that certain sequence changes, such as replacing Gln194 with Ser and Val205 with Ala in SP4, SP9, and SP12, promoted binding energy to enhance notably.

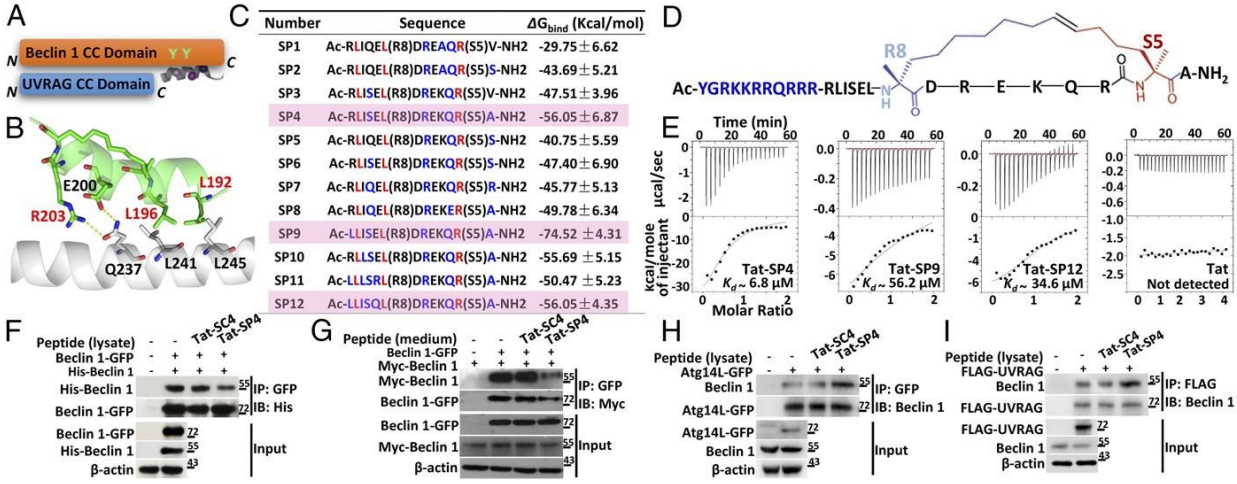

Figure 1. 6 Rationally designed stapled peptides were developed to target the Beclin 1 coiled-coil domain and facilitate Beclin 1–UVRAG interaction [97]. A. The design principle of Beclin 1-specific α-helical stapled peptides is illustrated, with the peptide depicted as a short ribbon binding to the C-terminal half of the Beclin 1 coiled-coil domain, and hydrocarbon staples represented as spheres stabilizing the α-helical structure. B. A model of the designed stapled peptide SP1 binding to the C-terminal region of the Beclin 1 coiled-coil domain is shown, with dashed lines indicating hydrogen bonds. Residues are numbered according to the Beclin 1 sequence. C. A list of computationally designed stapled peptides is provided, with modified residues colored blue, and residues colored red or black remaining unchanged. R8 and S5 represent two residues chemically modified to form the hydrocarbon linkage. Three highlighted candidates, SP4, SP9, and SP12, exhibit significantly improved theoretical interaction energy compared with SP1. D. The sequence and chemical structure of Tat-SP4 are presented, with the Tat signal peptide (colored in blue) added to facilitate cell penetration. E. An ITC profile is shown to measure the interaction between Beclin 1 and designed peptides. F. Tat-SP4 reduces Beclin 1 self-association in vivo. GFP- and His-tagged Beclin 1 were cotransfected into HEK293T cells, and their self-association was probed by co-IP. Tat-SC4 and Tat-SP4 were added to the cell lysate at a 20-μM concentration before the immunoprecipitation procedure. Tat-SC4 is a control peptide with a scrambled Tat-SP4 sequence and without the hydrocarbon staple. G. A repeat of the co-IP experiment in F but with Tat-SC4 and Tat-SP4 added to the cell culture medium at 20 μM 6 h post-transfection. H and I. Tat-SP4 promotes the Beclin 1–Atg14L/UVRAG interaction in vivo. GFP-Atg14L (H) and FLAG-UVRAG (I) were transfected into HEK293T cells, and their interaction with endogenous Beclin 1 was probed by co-IP. Tat-SC4 and Tat-SP4 were added to the cell lysate at a 20 μM concentration before the immunoprecipitation procedure.

To increase solubility and improve cell penetration, the YGRKKRRQRRR sequence known as Tat was added at the N terminus to synthesize Tat-SP4, Tat-SP9, and Tat-SP12 (Figure 1.6 D). Tat, which stands for "Trans-Activator of Transcription," is a regulatory protein produced by the tat gene in HIV-1, boosting the efficiency of viral transcription [98]. Commercial used peptide TAT-Beclin 1 can enhance autophagy activity by binding to the autophagy suppressor GAPR-1/GLIPR2 [99]. The TAT (47-57) sequence belongs to a group of cell-penetrating cationic peptides called CCP, which are capable of attaching genes, proteins, or nanoparticles to assist in transporting these substances across the cell membrane [100]. The ITC profile proved that adding TAT to the stapled peptides does not disturber the interaction with Beclin 1, for Tat peptide show no binding affinity to Beclin 1(Figure 1.6 E). And the co-IP experiments further verified that these designed peptides could disrupt Beclin 1 self-association and promote the Beclin 1–Atg14L/UVRAG interaction in vivo as expected (Figure 1.6 F-I). Additionally, with using the lead peptide Tat-SP4, our designed Beclin 1-specific stapled peptide was characterized to positively involved with autophagy flux by western blots of LC3 and p62 [97].

1.3.2 Optimization of Beclin 1-targeting stapled peptides with higher binding affinity

In the following work, our lab realized the optimization of designed peptides Tat-SP4 by introducing new staples and residue mutations, resulting in a new generation peptide with a stronger binding affinity to Beclin 1 [101]. In our

previous study, we chose a 11-residue segment (residues 191-205) from the Beclin 1 coiled-coil domain as the template peptide sequence for designing the stapled peptides. We referred to this segment as Native-P1 based on our previous structural studies, which showed that this segment contributed to the Beclin 1 homodimer interface but did not overlap with the UVRAG binding site. We presumed that the Native-P1 peptide would adopt an α-helical structure when binding to the Beclin 1 coiled-coil domain (Figure 1.7 A). To enhance the stability of the peptide structure, we utilized a hydrocarbon staple to connect two residues on the Native-P1 sequence, which were originally separated by six residues. This allowed the staple to traverse two complete turns of the helix. We explored six potential scaffolds for incorporating this hydrocarbon staple (Figure 1.7 B), ensuring that the four critical binding residues (L192, L196, V199, and R203) remained undisturbed. Additionally, we made a chemical modification to the hydrocarbon staple by replacing the α-methyl group found in the unnatural amino acids of our previous study with α-hydrogen (Figure 1.7 C). This alteration increased the conformational flexibility and minimized potential steric clashes when installing the hydrocarbon staple at various positions along the peptide sequence (i7-01s to i7-06s, as shown in Figure 1.7 B). Thought molecular dynamics (MD) simulations, we observed that the helical structures of all six stapled peptides remained intact, particularly within the L192 to R203 residue range. Although 100 ns MD simulations for each peptide were not of sufficient duration to achieve complete conformational convergence, the calculated binding

energies indicated that i7-01s, i7-02s, i7-04s, and i7-06s exhibited a tendency to establish more stable interactions with the Beclin 1 coiled-coil domain.

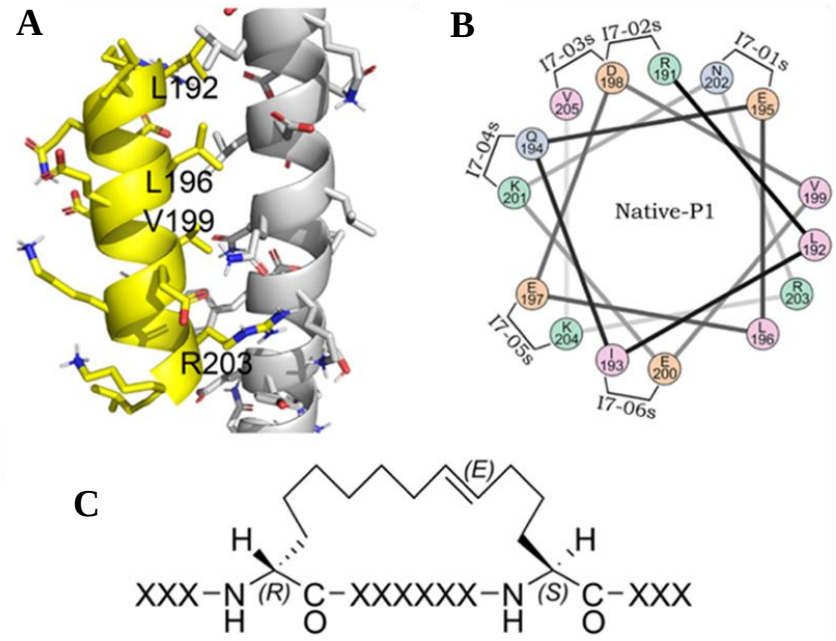

Figure 1. 7 Illustration of how the hydrocarbon staple was installed on the peptide sequence [101]. A. Molecular model of the Native-P1 peptide (in yellow) in the complex with the Beclin 1 coiled-coil domain (in gray, from PDB entry 3Q8T). Here, Native-P1 is assumed to be in a helical structure for binding. This complex model was used as the template for deriving the initial model of all designed stapled peptides described in this study. B. Staple position scanning in peptide design. The hydrocarbon staple was added at six positions on the Native-P1 sequence. C. Chemical structure of the hydrocarbon staple. Two amino acids containing olefin side chains were separated by six residues on the peptide sequence. The two side chains were connected by a Ruthenium-catalyzed ring-closing metathesis reaction, resulting in the 11-carbon long linker shown in this figure.

Out of the i7-01s, i7-02s, i7-04s, and i7-06s, these four scaffolds, we selected the i7-01s scaffold for further examination due to the presence of mutations E195 and N202 on the Native-P1 sequence, precisely located near the hydrophobic region

on the surface of the coiled-coil domain (Figure 1.8). This mutation is expected to minimize the unfavourable hydrophobic-hydrophilic mismatch between the peptide and the coiled-coil domain. Moreover, our predicted model reveals that the hydrocarbon staple in i7-01s effectively stacks onto the surface of the coiled-coil domain, potentially augmenting the binding of this stapled peptide. Subsequently, we performed systematic single-point mutations on the Native-P1 sequence base on i7-01s scaffold. The calculated binding energies for all these mutated peptides indicated that mutations at Q194, E197, D198, E200, K201, K204, and K205 were more likely to enhance the binding affinity.

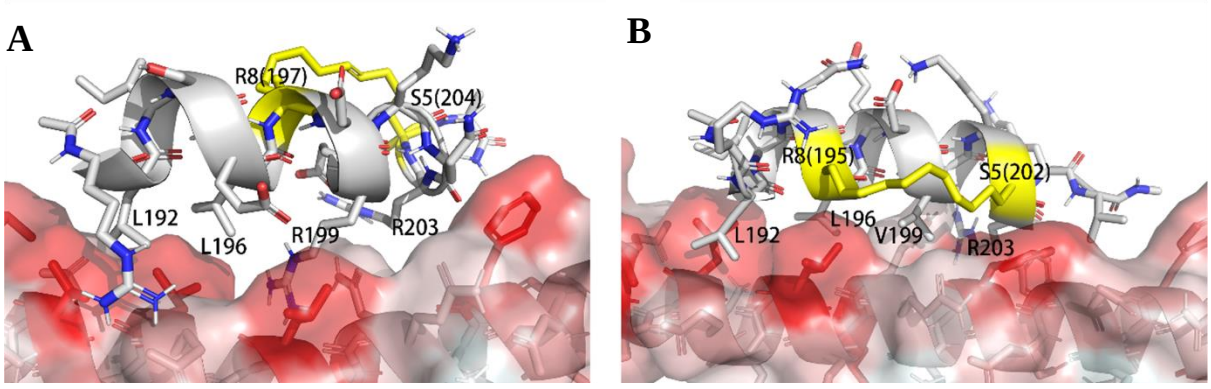

Figure 1. 8 Anticipated binding modes to the Beclin 1 coiled-coil domain of A. the stapled peptide SP4 from our prior study and B. the newly formulated I7-01s scaffold [101]. The hydrocarbon staple is depicted in yellow. The molecular surface of the Beclin 1 coiled-coil domain is color-coded based on the hydrophobicity scale, with darker red indicating greater hydrophobicity.

To further enhance the binding affinity, we strategically combined particularly favourable single-point mutants into novel multiple-point mutant designs through

manual selection. A total of 75 designed peptides were synthesized and their binding energies are detected by MD. Remarkably, the average binding energy of most of these peptides (72 out of 75) was more desirable compared to that of the Native-P1 peptide, utilizing the same i7-01s scaffold, this outcome aligns with our molecular design expectations. After considering multiple factors including predicted binding mode, binding affinity, and physicochemical properties such as total charge, 17 stapled peptides were carefully selected from all the designs for chemical synthesis (Table 1.3). To determine their binding affinity with the Beclin 1 coiled-coil domain, an Isothermal Titration Calorimetry assay was performed on these 17 peptides (Table 1.3, Figure 1.9). In comparison to SP4, the best-affinity stapled peptide obtained in our previous study (Kd = 3.2 μM), 12 of the newly synthesized peptides demonstrated similar or stronger binding to Beclin 1. Notably, two peptides (i7-01s-20 and i7-01s-31) exhibited binding affinities approximately 10-fold and 30-fold stronger than Tat-SP4, respectively. This highlights the significant improvement achieved through our design and synthesis efforts. In summary, our findings reported that positioning the hydrocarbon staple closer to the Beclin 1 coiled-coil surface significantly enhanced the interaction between Beclin 1 and the peptide.

Table 1. 3 Sequence and binding affinity of newly designed stapled peptides with the i7-01s scaffold [101].

ID	SEQUENCE *	K_d (μM) #
Native-P1	RLIQELEDVEKNRKV	
Tat-SP4	Ac-[Tat]-RLISEL(R8)DREKQR(S5)A-NH_2	3.21 ± 0.49
i7-01s-02	Ac-[Tat]-RLIQ(R8)REDREK(S5)RAV-NH_2	0.86 ± 0.16
i7-01s-10	Ac-[Tat]-RLIQ(R8)REDREK(S5)RAR-NH_2	2.03 ± 0.56
i7-01s-12	Ac-[Tat]-RLIS(R8)REDREK(S5)RAE-NH_2	2.84 ± 0.48
i7-01s-20	Ac-[Tat]-RVIQ(R8)LVIIEK(S5)RDV-NH_2	**0.10 ±0.05**
i7-01s-30	Ac-[Tat]-RLLQ(R8)LKTVLK(S5)RSV-NH_2	No binding
i7-01s-31	Ac-[Tat]-VLFN(R8)LVDVIK(S5)RKV-NH_2	**0.33 ± 0.28**
i7-01s-34	Ac-[Tat]-RFIQ(R8)LEVVIK(S5)RSV-NH_2	No binding
i7-01s-36	Ac-[Tat]-RLIQ(R8)REDVEK(S5)RKR-NH_2	No binding
i7-01s-37	Ac-[Tat]-RLIQ(R8)KEDVEK(S5)RKR-NH_2	2.41 ± 0.35
i7-01s-45	Ac-[Tat]-RLKQ(R8)LEDVEK(S5)RKR-NH_2	1.41 ± 0.32
i7-01s-46	Ac-[Tat]-RLIQ(R8)KIDVEK(S5)RKR-NH_2	0.71 ± 0.23
i7-01s-54	Ac-[Tat]-ALIQ(R8)QEDVEK(S5)RKR-NH_2	311 ± 54.62
i7-01s-57	Ac-[Tat]-RRIQ(R8)MEDVLK(S5)RKR-NH_2	2.20 ± 0.36
i7-01s-58	Ac-[Tat]-RLIE(R8)REIVEK(S5)RKR-NH_2	0.61 ± 0.17
i7-01s-64	Ac-[Tat]-RLII(R8)QEDVEK(S5)RKR-NH_2	356 ± 78.53
i7-01s-70	Ac-[Tat]-RLIQ(R8)KGDVEL(S5)RKR-NH_2	2.14 ± 0.47
i7-01s-75	Ac-[Tat]-RLIY(R8)MEDVEK(S5)RKR-NH_2	1.29 ± 0.40

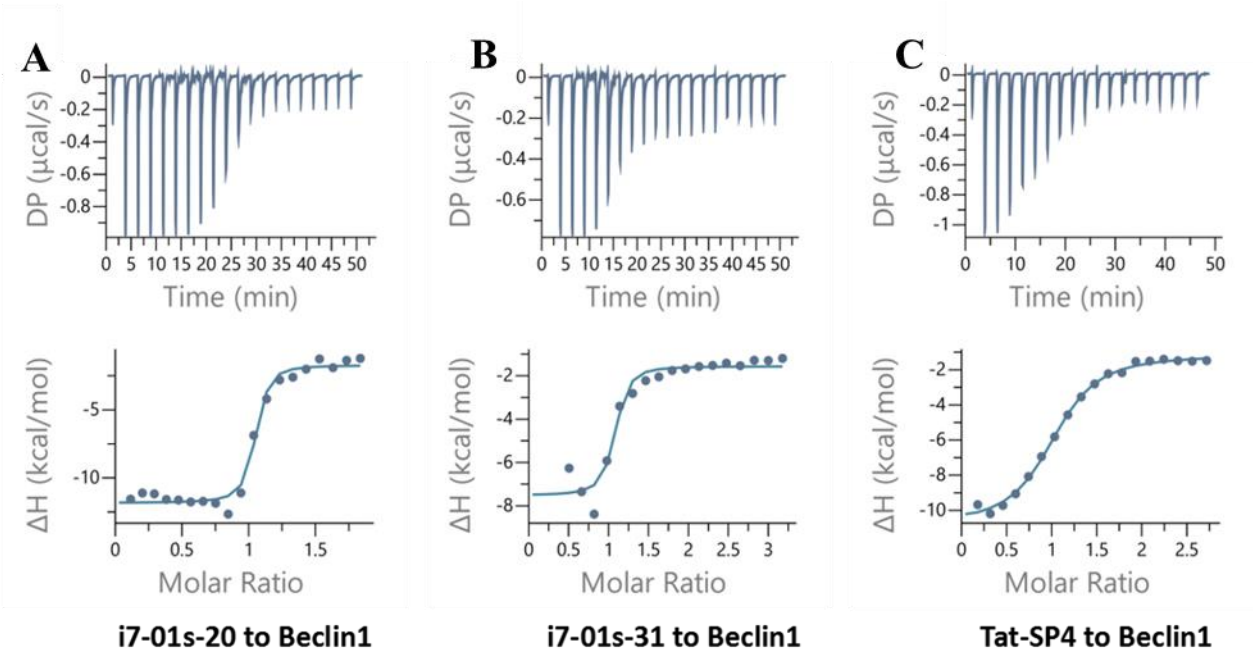

Figure 1. 9 Stapled peptides with the i7-01s scaffold demonstrated increased binding affinity to Beclin 1 coiled-coil domain [101]. Representative ITC profiles for I7-01s-20 (A) and I7-01s-31 (B) showed notably enhanced binding affinity to Beclin 1 as compared to tat-SP4 (C).

The influence of these two peptides on cellular autophagic activity was assessed through the detection of LC3 and p62 protein levels, which serve as molecular markers of autophagy. Our results indicate that the administration of i7-01s-31 at 10 and 20 μM for 3 hours resulted in a discernible albeit modest elevation in LC3-II levels in HEK293T cells (Figure 1.10 A, B). This increase became more pronounced in the presence of CQ (Figure 1.10 A, C). The protein level of p62 did not exhibit any noticeable change following peptide treatments, either in the presence or absence of CQ (Figure 1.10 A, D, E). Considering that p62 may exhibit lower sensitivity compared to LC3-II in terms of autophagic flux, it is plausible that the minor alteration in p62 levels may not be reliably detectable via western blot analysis. The observed pattern of changes in LC3-II and p62 levels is akin to the findings reported for Tat-SP4 in our previous study [91]. Therefore, the newly developed peptides i7-01s-20 and i7-01s-31, despite demonstrating approximately 10-30 folds stronger binding affinity to Beclin 1 compared to Tat-SP4, induce autophagy with comparable efficacy. The findings confirmed that the optimized Beclin 1-targeting stapled peptides effectively stimulate autophagy. Within these candidates, i7-01s-31 is adopted and term as SP9 in this project for further study.

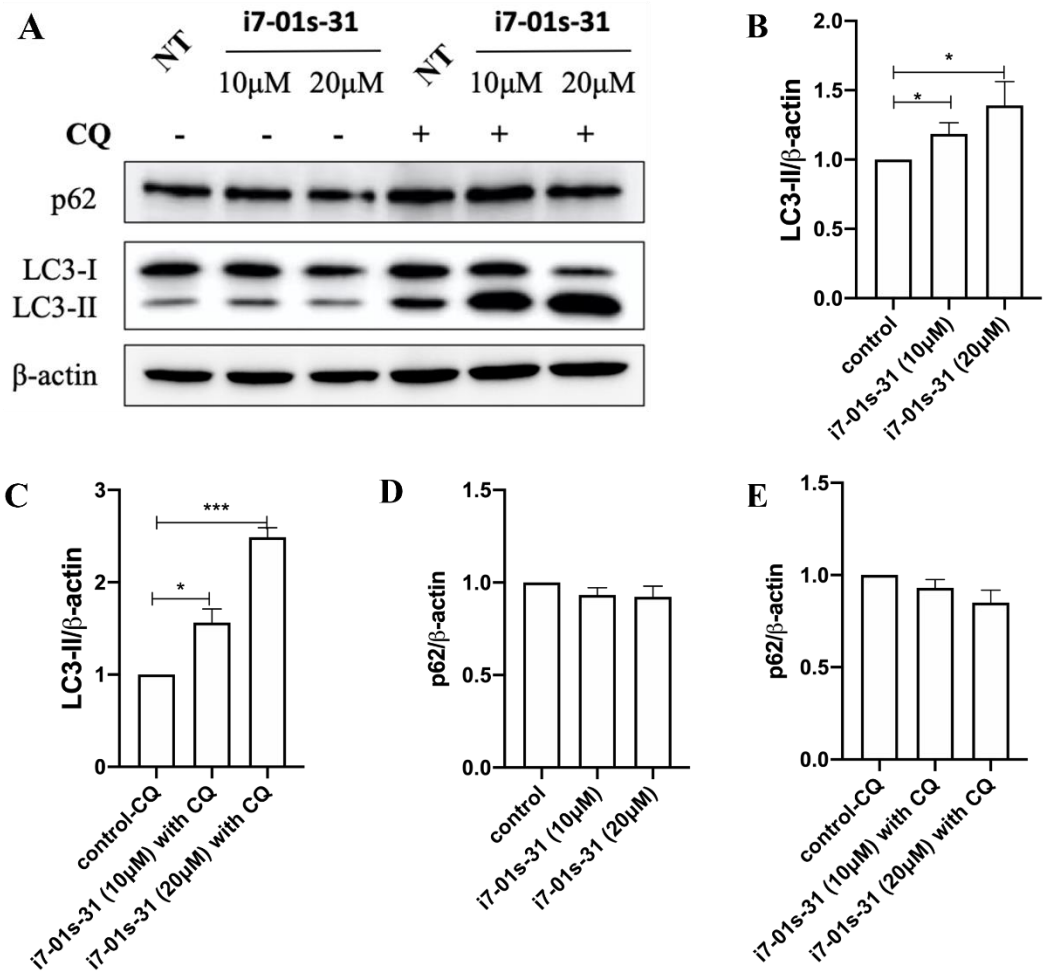

Figure 1. 10 Peptides derived from the i7-01s scaffold demonstrate efficacy as autophagy inducers [101]. A. Western blot analysis was conducted to evaluate p62 levels and LC3 lipidation profiles in HEK293T cells following treatment with 10 and 20 μM of i7-01s-31 for 3 hours, with or without CQ. B & C. Quantitative assessment of LC3 lipidation profiles derived from the western blot data. D & E. Quantitative analysis of p62 levels from the western blot data. LC3-II or p62 levels were normalized to the β-actin level. The data are presented as mean ± SEM (n = 3).

1.4 The implication of mitochondria function and calcium signal pathways in ovarian cancer

1.4.1 Mitochondria dysfunction in ovarian cancer cells

In both healthy and cancerous cell, mitochondrion is one of the most crucial organelles with unique double-membrane bound structure, which function in the primary purpose of acting as powerhouse to generate energy currency adenosine triphosphate (ATP) by oxidative phosphorylation (OXPHOS) [102]. Beyond energy generation, mitochondria are also involved with different cellular activities, including intracellular calcium regulation, heat production, the manufacturing and scavenging of reactive oxygen species and the intervention between cell growth and death [103]. Impaired mitochondria function could contribute to various human disease and pathology, such as metabolic diseases, aging and neurodegenerative disorders [104]. Additionally, mitochondria play critical role in carcinoma cell metabolism by providing energy in the form of ATP to meet the demand of dramatically tumor cell proliferation [105].

OXPHOS also called electron transport-linked phosphorylation or terminal oxidation, is a metabolic pathway that cells attain energy and comprise by the electron transport chain and chemiosmosis. ETC is a collection of the multi-subunit enzymes (complexes I to IV) bounded to inner mitochondria membrane [106], allowed electrons derived from citric acid cycle of NADH and $FADH_2$ to pass through in a series of redox reactions combine with O_2 and release energy

(Figure 1.11) [107, 108]. Both electron transport chain and the ATP synthase are embedded in the inner membrane, the energy released from oxidation/reduction reactions form a proton gradient facilitate transferring energy from the electron transport chain to the ATP synthase by movements of protons across this membrane, this process is named chemiosmosis [109]. Electrons from NADH enter ETC in Complex I (NADH-coenzyme Q oxidoreductase) which is a giant enzyme containing 40 polypeptides chains, while electron from $FADH_2$ transferred by Complex II (Succinate-Q oxidoreductase), the second entry point of ETC [108]. Both complex I and complex II deliver their electrons to a small and movable electron carrier called ubiquinone, which is reduced to form QH_2 and travels through the membrane, carrying the electrons to complex III (Q-cytochrome c oxidoreductase) [110]. As electrons move through complex III, more H^+ ions are pumped across the membrane, and the electrons are further delivered to another mobile carrier called cytochrome C (cyt C) which brings the electrons to complex IV, a final batch of H^+ ions are pumped across the membrane [108]. Complex IV passes the electrons to O_2, which splits into two oxygen atoms and accepts protons from the matrix to synthesis water. Four electrons are required to reduce each molecule of O_2, and two water molecules are formed in the process. ATP synthase is a membrane-spanning protein and only channel for H^+ ions in the IMM to catalyse an extra phosphate to ADP, capturing energy from the proton gradient as ATP [111]. In 1920s, Otto Warburg first introduced the connection between mitochondria metabolic and carcinogenesis, his study

postulated that tumor cell is inclined to consume glucose by glycolysis pathway for ATP generation even with sufficient oxygen, leading the redundant of lactate and contributing to the impairment of OXPHOS [112]. However subsequent studied provides several evidence showing advanced stage tumors strongly depend on OXPHOS for energy supplied beside glycolysis pathway, this paradoxical perspective attribute to complex signalling cascade process of mitochondria metabolic regulation, which is modulated by numbers of factor [113, 114]. Besides energy production function, OXPHOS support diverse biogenesis activities to maintain cellular homeostasis.

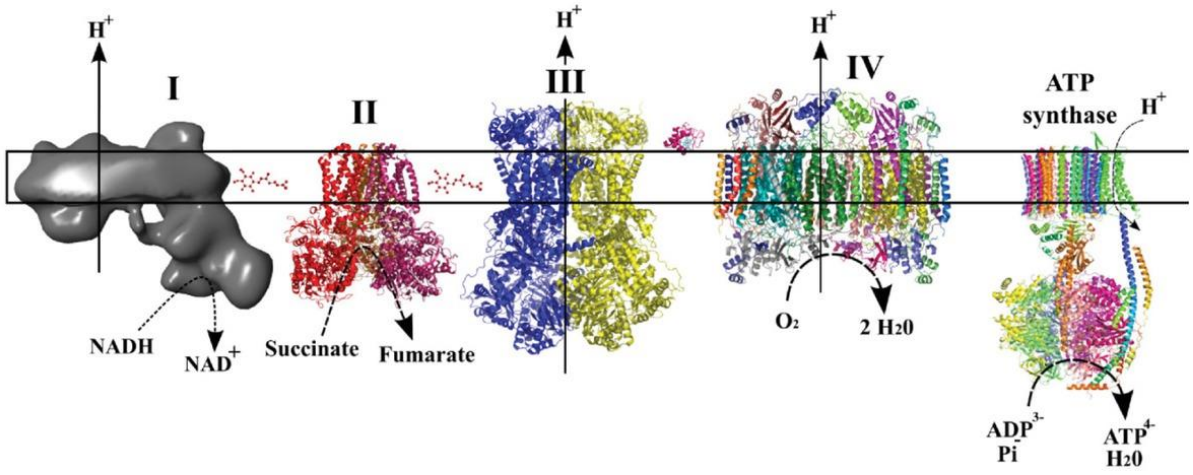

Figure 1. 11 Electron Transport Chain and ATP synthase [107, 108].

The pathophysiological alterations of mitochondria in cancer progression have been extensively studied, oxidative stress is among the number. Mitochondria is the primary source of ROS, which comprise at least one oxygen atom and one or more unpaired electrons, including oxygen free radicals, e.g. superoxide anion radical, hydroxyl radical, hydroperoxyl radical, singlet oxygen, as well as free

nitrogen radicals [115]. ROS accumulation leading oxidative stress, which is considered as hallmark of mitochondria dysfunction. It is observed that mitochondria could produce abundant of ROS which tend to invoke DNA impairment further leading genetic liability and oncogenicity, whereas some evidence suggest the deregulation of antioxidant activity could induce cancer cell death [116, 117]. Thioredoxin can be reduced by nicotinamide adenine dinucleotide phosphate (NADPH) to motivate the electron for redox system coordination, signal conversion and DNA synthesis [118], yet auranofin which is the inhibitor of thioredoxin, presenting cytotoxicity effect to cancer cell. Its conducive therapeutic effect with increasing ROS level in carcinoma is further confirmed by the prevention effect of ROS scavenger N-acetylcysteine (NAC) supplement, this agrees with the perspective that many anti-cancers drug including chemo drug, raising intracellular level of ROS to induce cancer cell death [119].

The double-membrane bound structure of mitochondria consist by an outer mitochondria membrane, intermembrane space and an inner mitochondria membrane [106], each membrane has different functions [120] (Figure 1. 12）.

Outer mitochondria membrane (OMM) permits small molecules from cytosol to freely traverse, and the pore-forming membrane protein known as porin composed channel for protein across[121]. By contrast, the IMM shows more restricted permeability to ions and small molecules than the OMM for only be permeable to oxygen, carbon dioxide and water [121]. IMM is considered as an

electrical insulator and chemical barrier, embedded with sophisticated ion transporters and antiport systems for corresponding protein transportation and anions exchange, such as Voltage Dependent Anion Channel (VDAC), Na^+/Ca^{2+} (NCLX) and H^+/Ca^{2+} (mHCX) exchangers [122]. The ETC proton pumps complex I, III and IV located in IMM, bring about redox transformations associated with the activity of the citric acid cycle, establishing the mitochondrial membrane potential ($\Delta\Psi m$) which is determined as the capacity of mitochondria to sustain an electrochemical gradient required for ATP synthesis [123]. Mitochondrial membrane potential is a general indicator of mitochondrial function, it not only reflects the process of electron transport and OXPHOS, but also tightly related to ROS production, cell migration and cell life-death transition [78]. Mitochondrial membrane potential in many cancer cells is detected with higher level than non-cancerous cell types and even correlated to malignancy level such as invasive properties and metastases features, providing a unique metabolic marker for accessing metabolic states of cancer cell [124]. The potentiometric fluorescent dye tetramethylrhodamine methyl ester (TMRM) and JC-1 assay kit with cationic carbocyanine dye are commonly used for the measurement of the mitochondrial membrane potential [125]. A growing number of research present that many agents with beneficial therapeutic effect to cancer cell could depolarize the mitochondrial membrane potential [106].

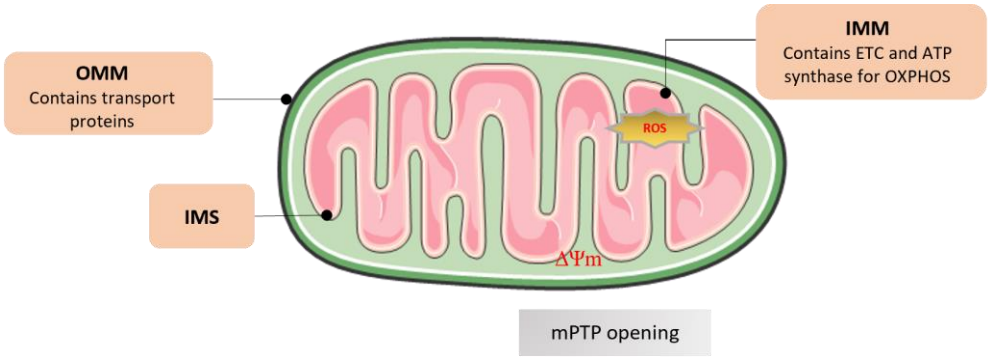

Figure 1. 12 Membrane structure of mitochondria

The mitochondrial permeability transition pore (mPTP) is a large conductance channel located in IMM to mediate the rapid exchange of small molecules across the membrane and it regard as essential role in mitochondrial function and cellular signalling [126]. The idea of mPTP is first raised in 1979 by Haworth and Hunter, who discovered the surge of IMM permeability after the addition of calcium to bovine myocardial mitochondria and this phenomenon is reversible by calcium chelator [127]. Subsequent researcher proved there are diverse endogenous modulators activator of mPTP such as Mg^{2+}, NADH, H^{+}, and ROS, and it is proved that the opening of mPTP disrupt the mitochondrial membrane potential [128]. Thus, the opening regulation of the mitochondrial permeability transition pore (mPTP) is considered as mitochondrial response to calcium overloading and other cellular stresses such as oxidative. Furthermore, mPTP has been iterative involved with mitochondrial dysfunction as non-selective channel, the delayed mPTP opening could induce mitochondrial depolarization, OXPHOS uncoupling, and leading apoptotic and necrotic cell death through ATP shrinkage.

Many pharmacological modulators of the PTP have been applied to disease affected by mPTP channel induced-mitochondria dysfunction. For example, Cyclosporin A (CsA) is effective therapeutic drug for ischemia-reperfusion injury by prohibiting mPTP opening [129]. The activator of mPTP shows therapeutic effect to cancer cell which are insensitive to cellular signal by promoting mPTP opening to induce cell death [130]. The intersection between mitochondrial metabolism and carcinogenesis has been extensively studied by numerous researchers. It is widely recognized that targeting mitochondrial metabolism holds promise in the discovery of new approaches for cancer treatment.

1.4.2 Calcium dysregulation in carcinogenesis and chemoresistant

Calcium ion is a vital secondary massager that engages in a range of cellular processes from muscle contraction, exocytosis, gene transcription to cell proliferation, differentiation, and apoptosis [131, 132]. There are varies components made up the Ca^{2+} signalling toolkit, located in ER (endoplasmic reticulum) which is the major Ca^{2+} store in the cell [133]. ER Ca^{2+} concentration can reach 1mM, while the cytosolic Ca^{2+} concentration ($[Ca^{2+}]cyt$) at rest is about 100nM, which is various from the cell type [134]. ER also exert a buffering function to maintain $[Ca^{2+}]cyt$ by taking up reductant Ca^{2+} or releasing Ca^{2+} through inositol 1,4,5-trisphosphate receptors (IP3Rs) and ryanodine receptors (RyRs) [135]. The interplay between Ca^{2+} stores and cytosolic Ca^{2+} pool determine the Ca^{2+}-dependent function. Upon physiological stimulation, Ca^{2+} released from ER influence the plasma membrane Ca^{2+} flow, continued high

[Ca^{2+}]cyt then further upregulate the Ca^{2+}-dependent effector proteins such as kinases, ion channel and phosphatases [136, 137]. In the course of time, Ca^{2+} is pumped back to the ER and [Ca^{2+}]cyt returns to resting level, assisted by the coordination of protein and channel.

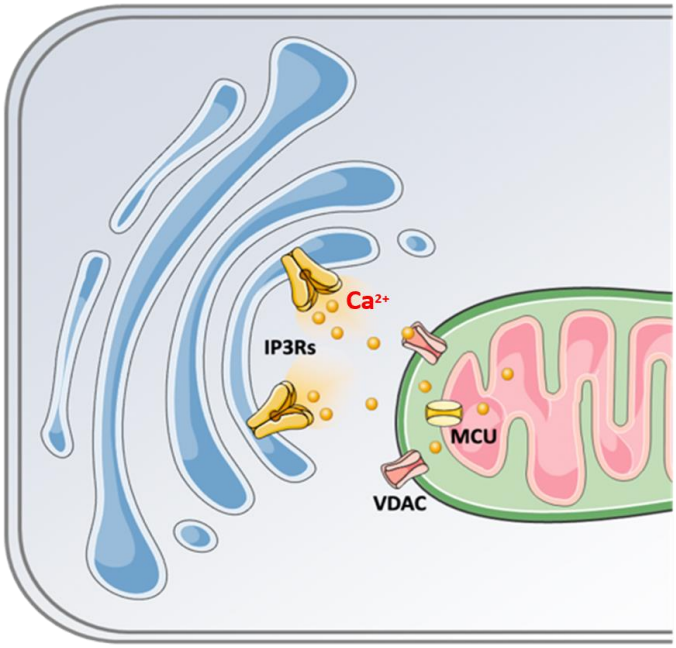

Figure 1. 13 The cartoon represents the Ca^{2+} interplay between ER-mitochondria interface to sustain Ca^{2+} transfer mediated by Ca^{2+}-dependent effector proteins (IP3Rs, VDAC and MCU), yellow dots represent the Ca^{2+} irons.

Beyond the close contacts between ER and plasma membrane, mitochondria are also involved with the modulation of Ca^{2+} homeostatic by its Ca^{2+} uptake ability (Figure 1.13). In the early 60's, mitochondria became the first discovered organelle that approve of Ca^{2+} influx [138]. Both ER Ca^{2+} release and Ca^{2+} absorption from the plasma membrane could increase [Ca^{2+}]cyt to encourage mitochondrial Ca^{2+} uptake. Chemiosmotic theory reveals that the electrochemical gradient generated by the respiratory chain across the IMM offer thermodynamic

basis of mitochondrial Ca^{2+} uptake. The transport of Ca^{2+} ions across the inner and outer mitochondrial membranes of mitochondria refer to several proteins. These proteins include the voltage-dependent anion channel 1 (VDAC1) located in the OMM, and the Na+-dependent mitochondrial Ca^{2+} efflux transporter (NCLX) and the mitochondrial Ca^{2+} uniporter (MCU), both present in the IMM [139]. Over the years, additional regulatory components of the mitochondrial calcium uniporter complex have been discovered, highlighting the intricate regulation and fine-tuning of mitochondrial calcium uptake.

Calcium signal have profound impact to physiological activity of organelles, which participate the regulation of cell cycle via intracellular Ca^{2+} channels, promoting cell transition from the G1/S phase to mitosis [140]. Accordingly, the shortage of Ca^{2+} flow can arrest cell cycle at the G0/G1 and S phases. A growing body of evidence suggest that dysregulation of Ca^{2+} signalling contribute to diverse pathological changes [141, 142]. Upregulation of calcium channels is a significant alteration in cancer cells, leading to mitochondrial calcium overload, which further activates several processes related to cancer progression, including cell cycle progression, apoptosis, proliferation, and metastasis [143]. In particularly, ovarian cancer development has been proposed to be tightly corelated with the disequilibrium of membrane-based and organelle-based Ca^{2+} signalling [144]. Studies have shown that hypoxia regulates the intensity of Ca^{2+} signalling in cancer cells by influencing IP3Rs [145]. In addition, previous research by Lencesova's group revealed that hydrogen sulfide induces ER stress

and apoptosis in hypoxic conditions, indicating a close association between IP3Rs and apoptosis in ovarian cancer cells [146]. It has been found that the mitochondrial calcium uptake 1 (MICU1/CBARA1) protein facilitates the uptake of mitochondrial Ca^{2+} and drives aerobic glycolysis in ovarian cancer [147]. MICU1 has been observed to be overexpressed in various ovarian cancer cell lines, such as CP20 and OV90, and this overexpression is correlated with reduced overall survival [147].

Chemoresistance is one of the adverse impact caused by defective calcium signalling in cancer cells, it has been observed that higher mitochondrial calcium levels contribute to chemoresistance by promoting multiple adaptive mechanisms [148]. Increased calcium levels within mitochondria can enhance mitochondrial bioenergetics and support the production of ATP, which is essential for cell survival and resistance to chemotherapy-induced cell death [149]. Abnormally high level of mitochondrial ATP production sustains cell viability by supporting various anti-apoptotic pathways and promoting DNA repair mechanisms, rendering cancer cells more resistant to chemotherapy agents [150]. Elevated mitochondrial calcium signalling can lead to alterations in the mitochondrial permeability transition pore (mPTP), a channel responsible for regulating mitochondrial membrane permeability. Dysregulated mPTP opening can result in the release of pro-apoptotic factors, such as cytochrome c, triggering apoptosis [151]. However, it is proved that increased mitochondrial calcium levels in cancer cells can prevent mPTP opening, inhibiting apoptosis and conferring resistance

to chemotherapy-induced cell death [130]. Mitochondrial calcium overload can trigger the production of reactive oxygen species within the mitochondria. While ROS are essential signalling molecules at low levels, excessive ROS generation can cause oxidative stress and damage DNA, proteins, and lipids [152]. This oxidative stress-induced damage can activate survival signals and promote chemoresistance [153]. Additionally, altered mitochondrial calcium signalling can modulate signalling pathways involved in cancer cell growth, such as the PI3K-AKT and MAPK pathways [154]. Dysregulated calcium flux can activate these pathways, leading to increased cell survival, growth, and resistance to chemotherapy drugs [155]. In summary, the dysregulation of calcium signalling in cancer cells plays a vital role in chemoresistance through diverse mechanisms. Increased mitochondrial calcium levels promote enhanced ATP production, apoptosis inhibition, ROS production, and activated signalling pathways that support cancer cell survival and resistance to chemotherapy.

2.Objective

Objective 1: Assessing the anti-proliferative efficacy of Beclin 1-targeting stapled peptides in vitro using a panel of ovarian cancer cell lines.

As one of the most fatal gynecologic cancer, ovarian cancer lack of specific biomarker for screening in early stage and short of effective medication for radical cure while current treatments share the poor prognosis. Therefore, powerful remedy for ovarian cancer is impending. As our previous study has proved the leading candidate of our new generation of design peptides, SP9, shows stronger binding affinity to the tumor suppressor Beclin 1 than its prototype SP4 after optimization. Furthermore, the designing rationale is delineated, and the potency of inhibiting tumor cell growth is also primary verified in breast cancer cell. In this study, our focus is centered on examining the effect of SP9 in ovarian cancer and investigating its underlying mechanism.

To access the anti-tumor ability of SP9 in ovarian cancer, we plan to determine the IC50 value of SP9 with using four different ovarian cancer cell lines: SK-OV3, OVCAR3, HEY-T30 and CAOV3 by standard Trypan Blue assay. The IC50 value of the chemotherapy drug cisplatin and paclitaxel will also be assessed as a reference, considering these medications are frequently used treatment for ovarian cancer. 5 days proliferation assay also will be conducted to observe SP9 blocking effect in cell growth over an extended period. A distinct cell viability assay, the CellTiter-Glo® Luminescent cell viability assay, is also applied to confirm the efficacy of SP9.

Objective 2: Mechanistic study to delineate the cell death process triggered by Beclin 1-targeting stapled peptides in ovarian cancer cells.

After affirming SP9-induced cell death effect, we will try to reveal the cell death mechanism caused by SP9. There are many classic or novel cell death pathways worth investigating, such as apoptosis, necroptosis, ferroptosis, pyrotosis or autosis. We propose to adopt corresponding inhibitor to check if they can prohibit the SP9 induced cell death effect by cell viability rescue assay. Additionally, some specific biomarker protein like cleaved Poly (ADP-ribose) polymerase (PARP) and cleaved caspase3 for apoptosis activation and N-terminal fragments of gasdermin E protein for pyrotosis pathway will be detected by western blot technique.

Objective 3: Investigating the impact of Beclin 1-targeting stapled peptides on mitochondria bioenergetics and calcium signalling in ovarian cancer cells

Mitochondrion is an essential membrane-bound organelle for its powerhouse function generating energy currency adenosine triphosphate (ATP) in cell. In cancer cell, mitochondria are abnormally activated to supply energy assisting tumor cell over proliferation, thus mitochondria are wildly recognized as critical target for cancer therapy. Reasonably, we wonder if SP9 take effect by compromising mitochondria function in ovarian cancer cells.

To evaluate the influence of SP9 over mitochondria metabolism, we plan to estimate mitochondria membrane potential ($\Delta\varphi$) level and reactive oxygen species [30] level by flow cytometry with fluorescent dye tetramethylrhodamine

methyl ester (TMRM) and cell permeable CellROX™ Green reagent respectively. Furthermore, we propose to appraise oxidative phosphorylation (OXPHOS) activity by measuring the oxygen consumption rate (OCR) and mitochondrial permeability transition pore (MPTP) opening with using MitoProbe™ Transition Pore Assay Kit.

Ca^{2+} is the crucial secondary messengers, which can stimulus cell reaction by maintaining cytoplasmic Ca^{2+} concentration low at rest and raising Ca^{2+} respond to excitement, it is accountable for extensive physiology activities. The mitochondria-associated membranes indicate the contact site between mitochondria and endoplasmic reticulum (ER), which is described as hotspot for calcium iron communication and being responsible for Ca^{2+} regulation. Accordingly, we suspect SP9 may perturb the calcium signal pathway and it can be involved with its cell growth repression effect in ovarian cancer cell.

In this objective, extra calcium and its selective cell-permeant chelator BAPTA-AM will be added for evaluate the role of calcium in SP9 induced cell death event. To further observing calcium signal dynamic, OVCAR3 will be employed to genetical encoded with three plasmids mito-GCaMP5G, cyto-RCaMP1h and G-CEPIA1er, which are Ca^{2+} sensor of mitochondria, cytosol and endoplasmic reticulum (ER) respectively. Signal data will be obtained by CCD camera and quantitatively analysed by Cell R imaging software.

Objective 4: Validating the anti-tumor activity of Beclin 1-targeting stapled peptides in vivo using xenograft models for ovarian cancer

Once we have outlined the molecular process of cell death caused by the Beclin 1-targeting stapled peptide in vitro, the next step is to assess the effectiveness of SP9 in inhibiting ovarian cancer growth in animal model. We plan to construct a xenograft ovarian cancer model in nude mice with a human ovarian cancer cell line which is susceptible to SP9. The growth rate and the final weight of the tumors will be measured to evaluate the tumors prohibition effectiveness of our optimized stapled peptide. Additionally, histopathological analyses will be conducted to examine any differences in autophagy markers and the morphology of the tumors.

Objective 5: Exploring the synergistic impact of the Beclin 1-targeting stapled peptide in combination with the chemotherapeutic agent cisplatin on the inhibition of ovarian cancer proliferation.

Combination therapy involves with two or more agents or different means of treatment joint together, which is a fundamental strategy for cancer treatment. This treatment modality might exhibit synergistic effect to improve treatment efficacy, prevent drug resistance and lower toxicity. Synergist effect refers to nonlinear cumulative effects resulting by two or more substances interact together and produce stronger healthy effect than the sum of individual drug. Thus, we wonder if SP9 can exert synergistic effect by combining with classic chemo drug cisplatin.

In vitro, colony formation assay will be performed to visualize cell growth ability after combination treatment. Combination index shall be calculated via Calcusyn

Software using Chou-Talalay method to quantitate the combination effect of cisplatin and SP9. For in vivo assay, we plan to use OVCAR3 xenograft animal tumor model to evaluate the combination effect of cisplatin and SP9 by observing tumor growth.

3.Methodology and materials

3.1 Synthesis of Beclin 1-targeting stapled peptides

All peptide samples were acquired commercially from GL Biochem (Shanghai) Ltd. Generally, the peptides were synthesized by automated solid-phase peptide synthesis, incorporating olefin-containing amino acids at the designated positions. Then, the hydrocarbon staple was formed on olefin-containing amino acids by ring-closing metathesis reaction using the Grubbs catalyst. Details regarding synthesis process is similar with our previous study.

3.2 Cell lines and cell culture

The HEY-T30, OVCAR-3, CAOV-3 and HEK293 were obtained from ATCC (American Type Culture Collection). SK-OV3 were kindly provided by Prof. Larry Chow's lab at Hong Kong polytechnic university. Cells cultured in four kinds of medium: RPMI1640 with 10%(v/v) FBS(Gibco), 1%(v/v) penicillin/streptomycin (Gibco) and 30nM Paclitaxel for HEY-T30; RPMI1640 with 10%(v/v) FBS(Gibco), 1%(v/v) penicillin/streptomycin (Gibco) for SK-OV3; RPMI1640 with 20%(v/v) FBS(Gibco), 1%(v/v) penicillin/streptomycin (Gibco) and 0.01 mg/ml bovine insulin for OVCAR-3, DMEM(Gibco) supplemented with 10% (v/v) fetal bovine serum (FBS)(Gibco) and 1% (v/v) penicillin/streptomycin (Gibco) for CAOV-3 and HEK293. Cell lines regularly tested and verified to be mycoplasma negative by DAPI staining before and

during experiments. Cells were grown in a humidified incubator with 5% CO_2 at 37°C. Cell with low passage carefully maintained in lab liquid nitrogen.

3.3 Cell viability assay and proliferation assay

To assess peptide-triggered cell death effect, cell viability was examined by measuring IC50 (half-maximal inhibitory concentration) with standard Trypan Blue cell counting method. Trypan Blue exclusion is a common method to detect the number of live cells from dead cells in cells suspension. The principle is that only live cells with intact cell membranes can exclude trypan blue dye and live cells will have a clear cytoplasm whereas dead cells will have a blue cytoplasm thus only live cell can be observed under microscope. Ovarian cancer cells were seeded into 96-wells plates based on optimal cell growth rates determined for each cell line with 80-90% final confluency and incubated overnight before adding peptides. Cells were treated with gradual concentrations of peptides. After 24 hours incubation, the cells were digested by 100μL trypsin per well and counting by the Z1 Particle Counter (Beckman Coulter).

For the proliferation assay, cells were seeded into 24-well plates and the initial cell number was determined by optimal cell growth rates for each cell line. Cells were incubated overnight before adding peptides or chemo drugs. Cell growth will be monitored daily. Cells were trypsinized and counted using the Z1 Particle Counter (Beckman Coulter) 24 hours after plating of cells, daily for 5 days.

3-(4,5-dimethylthiazol-2-yl)-2,5-diphenyltetrazolium bromide MTT (CAS No.:298-93-1, Sigma) staining assay was conducted to access the cancer cells viability after chemo-drug cisplatin and paclitaxel treatment. Seeding cells in 96-wells plate, after 48 hours incubation with cisplatin or paclitaxel, removing medium then 5mg/mL MTT solution was added. With 4 hours incubation, MTT solution was removed then wash the well by PBS twice gently. 100μl of DMSO per wells was added to dissolve the formazan dye which indicate the cell viability. Absorbance value of formazan dye was measured by Bio-Rad Microplate Reader (Model 680, Bio-Rad Laboratories, Hercules, CA, USA) at the wavelength of 570nm.

CellTiter-Glo luminescent cell viability assay is homogeneous method to access the cell viability by quantitation of the ATP present. Following the instruction of CellTiter-Glo Luminescent Cell Viability Assay kit (Promega), cells were seed in opaque-walled multiwells plate with indicated confluence, cell culture and peptide treatment is the same procedure as previous descripted in cell viability assay, single reagent (CellTiter-Glo Reagent) were added into culture medium directly with equal to the volume of cell culture medium present in each well. Then mix contents for 2 minutes and allow the plate to incubate at room temperature for 10 minutes to stabilize luminescent signal before reading luminescence.

3.4 Western blot assay

Indicated cells were seeding in 6-wells plate with 70% confluence and treat with peptides or other chemical compound for positive control after overnight cell adherence. After indicated incubation period, we collect the medium and wash the well with PBS twice (washed PBS is also collected with medium), then centrifuge to collect the floating cell. Subsequently lysis all cells with lysis buffer which containing 2% SDS, 25% glycerol and 5% β-Me and freshly supplied with 1% protease inhibitor cocktail (Bimake, B14001) before using, then cells are scraped with cell scraper followed the cell lysate is transferred to 1.5mL Eppendorf tubes to boil at 100°C for 10 minutes with dry bath to obtain lysate protein sample.

Before loading to SDS-gel, we mixed the lysate protein sample with 5× SDS sample buffer and boiled at 100°C for 5 minutes. After SDS-gel running with indicated voltage and time, next transferred the gel to 0.45μm PVDF membrane (Bio-Rad) with Mini-Trans-Blot Electrophoretic Transfer Cell (Bio-Rad). After that, 5% skim milk in TBST buffer (137mM NaCl, 20mM Tris, 0.1% Tween 20) were using to block non-specific binding on the membrane in PVDF membrane. The blocked membrane was incubated in specific primary antibody at 4°C overnight. In the end, washing the membrane with TBST buffer 3 times every 10 minutes, the membrane next incubated with homologous HRP-conjugated secondary antibody at 1:2000 diluted with 5% skim milk in TBST buffer for 1hour then repeating the washing procedure. At last, signal detection with

Western HRP Substrate (Millipore) and by ChemiDoc Imaging Systems (Bio-Rad).

The primary antibodies in this study included: anti-cleaved PARP 1:2000 (Cell Signaling Technology), anti-Caspase3 1:1000 (Cell Signaling Technology), anti-cleaved Caspase3 1:1000 (Cell Signaling Technology), anti-β-actin 1:2000 (Cell Signaling Technology), Recombinant Anti-DFNA5/GSDME antibody N-terminal 1:1000 (abcam).

3.5 **Apoptosis detection by Annexin V/PI staining**

The FITC Annexin V/Dead Cell Apoptosis Kit with FITC annexin V and PI for flow cytometry is a rapid and convenient assay for apoptosis detection. The kit contains recombinant annexin V conjugated to fluorescein (FITC annexin V), as well as red fluorescent propidium iodide nucleic acid binding dye. Annexin V is the Ca^{2+} dependent phospholipid-binding protein that has a high affinity for phosphatidylserine [156]. In normal live cells, PS is located on the cytoplasmic surface of cell membrane while they translocate to outer leaflet of the plasma membrane in apoptosis cell. Thus, PS exposing to the outer environment which allow Annexin V labelled with a FITC fluorescein to bind then identify as apoptotic cells. PI is impermeant to live cells and apoptotic cells, but stains dead cells with red fluorescence, binding tightly to the nucleic acids in the cell. Cells are seeding in 6-wells plate, after treatment, we collected cells and stained with following every step with protocol of FITC Annexin V/Dead Cell Apoptosis Kit.

Lastly, cells were harvested for flow cytometry analysis using the Accuri C6 Flow Cytometer (BD Biosciences). According to manufacturer's introduction, cellular population of live cells are incapable to be stained by neither dye located in the lower left quadrant, the early staged apoptotic cell showed green fluorescence on the lower right quadrant only with Annexin V positive; Necrosis cell population can be stained by both Annexin V and PI shown on the upper right quadrant.

3.6 Determination of mitochondria membrane potential (Δψ)

We measure the mitochondrial membrane potential (ψm) with tetramethylrhodamine methyl ester (TMRM) (ThermoFisher), a cell-permeant, cationic, red fluorescent dye, following the protocol in this kit. Cells are cultured in 6-well plates and incubated overnight. To measure specifically the mitochondrial membrane potential (ψm) we quantified the fluorescence intensity before and after applying 100μM CCCP, a mitochondrial electron chain uncoupler as a positive control, and peptides as experiment groups. Cells were pretreated by peptides for 1hours. Then using 100μM TMRM stained cells for 30 mins. Finally, cells were harvested and analyzed with the Accuri C6 Flow Cytometer (BD Biosciences), TMRM can be captured by the 532nm laser and PE equivalent bandpass filter should be used to detect TMRM.

3.7 Measurement of cellar Reactive oxygen species level

To detect the ROS level change after peptide treatment in cells, we empoly CellROX™ Green Flow Cytometry Assay Kit (Thermo Fisher, catalog number: C10492), which enable the flow cytometric detection of reactive oxygen species in live cells. According to the manufacturer's instructions, the CellROX™ Green reagent is capable of binding DNA to exhibit a strong fluorogenic signal that has absorption/emission maxima of 508/525 nm, but it is originally non-fluorescent in reduced state.

Cells were collected and resuspend in complete growth medium with ~5×10^5 cells/mL cell concentration, then cells sample were treated with or without peptides for 1 hour and followed by 30 mins 500nM CellROX™ Green staining. Tert-butyl hydroperoxide (tBHP), an exogenous inducer for ROS was used for positive control in this assay. Lastly, cell samples were analyzed by Accuri C6 Flow Cytometer (BD Biosciences).

3.8 Detection of mitochondrial permeability transition pore (MPTP)

The MitoProbe™ Transition Pore Assay Kit (Thermo Fisher, MP34153 and MP 35103) was applied to determine whether peptides can trigger mitochondrial permeability transition pore opening in ovarian cancer cell. Calcien AM is a non-fluorescent and colorless acetoxymethyl esterase substate, which can passively diffuse into the cells without selectivity in cytosol and mitochondria. When

calcien AM dye entre the cell it cleaves into calcein and acetoxymethyl esters by intracellular esterases, then the fluorescent dye calcein released to be detected. Calcien dye can be chelated with cobalt iron leading the cytosolic calcein fluorescent quenching, as the cobalt cannot enter mitochondria for the closed MPTP. Therefore, after staining of Calcien AM and cobalt iron treatment, only fluorescent in mitochondria is reserved, outside the mitochondria got quenched after adding $CoCl_2$. The Ca^{2+} ionophore ionomycin was used for positive control to trigger MPTP in this assay for Ca^{2+} is the crucial regulator of MPTP opening. Based on this rationale, the change of fluorescent intensity can be the indicator of MPTP activation.

For flow cytometer assay, cells were seeding in 6 wells plate firstly, treated with peptide or ionomycin 1 hour then collected for staining Calcien AM and $CoCl_2$ followed by kit instruction. Cell samples were analyzed by Accuri C6 Flow Cytometer (BD Biosciences). For confocal image assay, cells were seed in confocal dish and incubated overnight for adherence. Then treated cells with 1μM calcein AM, 1mM CoCl2, 1μM Hoechst in 1 mL No FBS culture medium, incubating for 15 minutes at 37℃, protected from light. After twice wash by no FBS culture medium, cells were observed Leica invert confocal microscope (TCS-SP8-MP system).

3.9 Oxygen consumption rate (OCR) analysis

The activity of oxidative phosphorylation (OXPHOS) was analysed by measuring the oxygen consumption rate (OCR) of ovarian cancer cell upon treatment by

peptides. OCR is a parameter for the mitochondrial OXPHOS process. OCR was measured using a Seahorse Bioscience Extracellular Flux analyzer (XF24). Cells were plated in 24-well plates at a seeding density of 50,000 cells per well in 250 μl of cell culture medium before overnight incubation. The next day, medium was changed to mitochondrial assay buffer supplement with 180 mg/ml glucose and 100μM L-Glutamine at pH 7.4. Cells were washed twice in mitochondrial assay buffer and added 500 μl the same buffer. After 1 hour of incubation at 37°C without CO_2, cells were tested by XF Analyzer.

Following the OCR measurements, the first injection contained corresponding concentration of peptides or vehicle, the second injection is 1μM oligomycin, followed by 1 μM FCCP, and 0.5 μM rotenone and antimycin A, and those chemicals are injected into wells at the indicated time points. Oligomycin inhibits ATP synthase and reduces OCR, FCCP uncouples oxygen consumption from ATP production and raises OCR to a maximal value, and antimycin A and rotenone target the electron transport chain and reduce OCR to a minimal value. This is also named mitochondria stress test protocol that provides information on basal respiration, ATP-linked respiration, proton leak, and maximal respiration capacity. At the end of this experiment, using cell numbers in each well normalized the different groups. Measurement data were showed by Wave software.

3.10 Calcium signal detection

To detect calcium signal response to peptide treatment in ovarian cancer cell, we first genetically encode OVCAR3 cells with three plasmids cyto-RCaMP1h, mito-GCaMP5G and G-CEPIA1er, which are Ca^{2+} sensor of cytosol, mitochondria and endoplasmic reticulum (ER) respectively. Cells were seed in 24-wells plate 3×10^4 per well, able to reach around 60% cell density after overnight adherence, then lipofectamine 3000 (ThermoFisher, L3000075) were used for transiently transfection procedure. 1 ug/well plasmid was used, and the subsequent steps were instructed by manufacture's protocol.

After 48 hours incubation, transfected efficacy can be observed by fluorescence microscope. Culture medium was replaced by HBSS buffer with or without Ca^{2+} before calcium signal is detected. Cell plate were put on the stage of Olympus inverted epifluorescence microscope to be observed. Images were collected by a CCD camera and analysed by Cell R imaging software.

3.11 Colony formation assay

Colony formation assay is in vitro cell survival assay based on the competence of single cells to grow into colonies. 500 cells/well OVCAR3 or 800 cells/well SK-OV3 were seeding in 6-well plates for overnight adherence, indicated concentration of peptides or chemo drug or combination were added into plates and cultured for 6 days or 7 days depend on cell proliferation speed. Then we removed culture medium and washed cells by PBS twice and added 500 μl 4%PFA to fix colony at room temperature for 15 mins. 0.5% crystal violet were

used for colony staining at room temperature for 30 mins and washed by PBS twice again. The image of plates was scanned and captured by ChemiDoc Imaging Systems (Bio-Rad).

3.12 Drug combination analysis

To investigate the combination effect of peptides and cisplatin in ovarian cancer cell, the combination effect of peptides and cisplatin was determined by CalcuSyn software using Chou-Talalay method. Cells were seeded at 96-well plate at based on optimal cell growth rates determined for each cell line with 80-90% final confluency and incubated overnight, indicated peptide or cisplatin or combination (we applied constant ration in this study) were added. After 24 hours incubation, the cell viability was counting by trypan blue method. The data was analysed by CalcuSyn software to calculate combination index value. CI<1 indicates synergist effect.

3.13 Xenograft animal experiment

Xenograft animal experiment were performed following by the guidelines of the Centralised Animal Facilities of the Hong Kong Polytechnic University. 4-6 weeks old female BALB/c nude mice were purchased from the Centralised Animal Facilities of the Hong Kong Polytechnic University. For each animal, 5 $\times 10^5$ OVCAR3 cells were harvested in PBS then mixed with Matrigel (Corning,

356237) in volume ration= 1:1, the total volume of cell suspension is 100 μl, which is subcutaneously injected into the female nude mice to grow xenograft tumor. When tumor size grows to ~100mm^3, start to treat with peptides or cisplatin or combination by intraperitoneal injection. Then tumor volume 1/2 (length × width^2) and animal body weight were recorded every 2 days. Experiment was terminated when tumor size over 1500 mm^3.

3.14 Statistic analysis

All comparison analysis in this study presented as mean ± SDM, accomplished by GraphPad Prism 8.0 elsewise additional suggested. Each assay independently repeated at least three times to obtain replicates for statistical analysis. $P<0.05$ is acknowledged as statistically significant difference.

4.Result

4.1 Beclin 1-targeting stapled peptides can repress cell growth in ovarian cancer whereas it shows less toxicity in non-cancer cell

4.1.1 Beclin 1-targeting stapled peptides demonstrates anti-proliferate efficacy in ovarian cancer cells.

The sensitivity to SP9 of ovarian cancer cell lines was accessed by 24 hours IC50 determination first. This value was determined by measuring cell viability using the standard Trypan Blue exclusion assay. Results show the estimated IC value of SP9 is 4.12μM, 5.45μM 4.93μM and 6.08μM in SK-OV3, OVCAR3, HEY-T30 and CAOV3 these four cell lines respectively (Figure 4.1 A-D). The non-cancer cell line HEK293 (Human embryonic kidney 293) cell was adopted to value the toxicity of SP9, the IC50 value is up to 27.90μM (Figure 4.1 E). The SP9 IC50 value in different cell lines measured by Trypan Blue exclusion method is summary in histogram plot (Figure 4.1 F), indicating relatively low cytotoxicity of SP9 in non-cancer cells compare with ovarian cancer cells. There are various cell viability assays are designed to measure different aspects of cell viability base on different principles and mechanisms of action. Given each assay has its own advantages and limitations, we adopt another distinct cell viability assay, the CellTiter-Glo® Luminescent cell viability assay, to measure the IC50 value of SP9. The result is obtained as 5.78μM and 4.83μM in OVCAR3 and SK-OV3 cells, respectively (Figure 4.1 G and H). These IC50 value are very similar with

the value obtained by the standard Trypan Blue exclusion assay (Figure 4.1 A and B), which further confirm the cytotoxicity effect of SP9 in ovarian cancer cells.

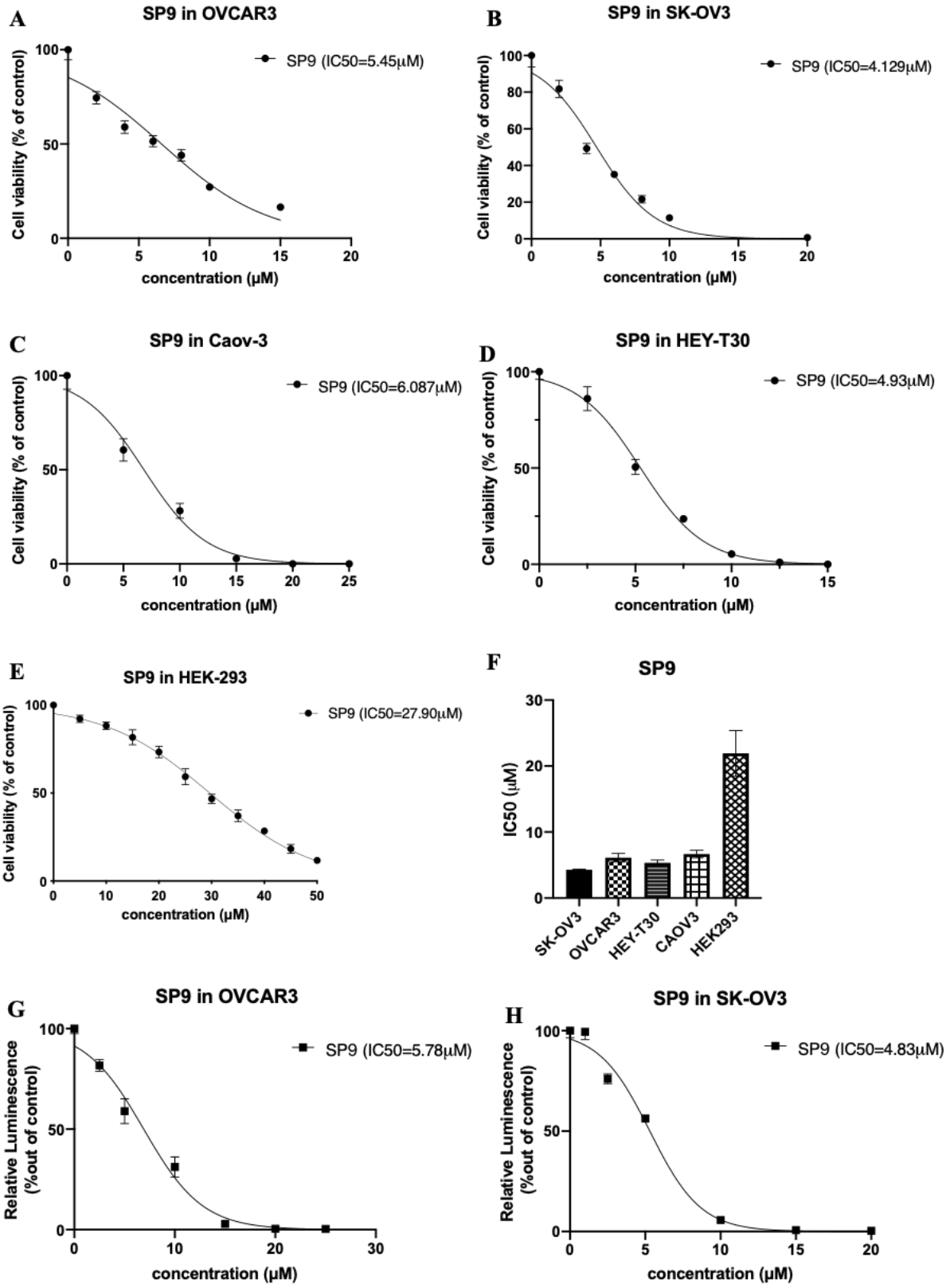
A
SP9 in OVCAR3
SP9 (IC50=5.45μM)
Cell viability (% of control)
concentration (μM)
B
SP9 in SK-OV3
SP9 (IC50=4.129μM)
Cell viability (% of control)
concentration (μM)
C
SP9 in Caov-3
SP9 (IC50=6.087μM)
Cell viability (% of control)
concentration (μM)
D
SP9 in HEY-T30
SP9 (IC50=4.93μM)
Cell viability (% of control)
concentration (μM)
E
SP9 in HEK-293
SP9 (IC50=27.90μM)
Cell viability (% of control)
concentration (μM)
F
SP9
IC50 (μM)
SK-OV3
OVCAR3
HEY-T30
CAOV3
HEK293
G
SP9 in OVCAR3
SP9 (IC50=5.78μM)
Relative Luminescence (%out of control)
concentration (μM)
H
SP9 in SK-OV3
SP9 (IC50=4.83μM)
Relative Luminescence (%out of control)
concentration (μM)

Figure 4. 1 Assessment of IC50 in Ovarian cancer cell lines and non-cancerous cell line with the treatment of SP9 after 24 hours. A. Cell viability of OVCAR3 after treatment with different concentrations of SP9. The predicted IC50 value is 5.45 μM. B. Cell viability of SK-OV3 after treatment with different concentrations of SP9. The predicted IC50 value was 4.129 μM. C. Cell viability of Caov-3 after treatment with different concentrations of SP9. The predicted IC50 value was 6.087μM. D. Cell viability of HEY-T30 after treatment with different concentrations of SP9. The predicted IC50 value was 4.93 μM. E. Cell viability of HEK-293 after treatment with different concentrations of SP9. The estimated IC50 value was 27.90 μM. F. The summary histogram of SP9 IC50 value in five different cell lines. Data were mean ±SEM of three replicates. G. and H. Cell Titer Glo Luminescent cell viability curve for SP9 cytotoxicity effect in OVCAR3 and SK-OV3 cells. Data were mean ±SEM of three replicates.

4.1.2 Beclin 1-targeting stapled peptides exhibits enhanced anticancer potency with reduced toxicity compared to chemotherapeutic drugs.

Cisplatin and paclitaxel are the first line chemotherapy for ovarian cancer, to compare the potency between chemo drug and SP9, the 48 hours IC50 value of cisplatin and paclitaxel in four ovarian cancer cell lines were measured by MTT method in accordance with references. The result showed IC50 value of cisplatin is 35.23μM, 13.82μM 1.54μM and 9.59μM, IC50 value of paclitaxel is 22.89μM, 12.04μM 5.98μM and 9.45μM in SK-OV3, OVCAR3, HEY-T30 and CAOV3 respectively. It has been reported that SK-OV3 cells are resistant to tumor necrosis factor and to several cytotoxic drugs including diphtheria toxin, cisplatin, and Adriamycin, OVCAR3 also present resistance to clinically relevant concentrations of Adriamycin. According to our IC50 data, SK-OV3 and OVCAR3 two cell lines did exhibit less susceptibilities than other non-resistant ovarian cancer cell lines (Figure 4.2 B & D), which is consistent with previous statement. In contrast, ovarian cancer cells showed highly sensitive to SP9 in assigned ovarian cancer cell lines regardless of chemo-resistance (Figure 4.1 F). However, in HEK293 cells cisplatin and paclitaxel displayed strong cytotoxicity with low IC50 value, 1.26μM and 0.03μM, respectively (Figure 4.2 E) while SP9 show less lethal effect with relatively high IC50 value (Figure 4.1 E&F), suggesting SP9 might provide a therapeutic window between efficacy and toxicity for ovarian cancer treatment.

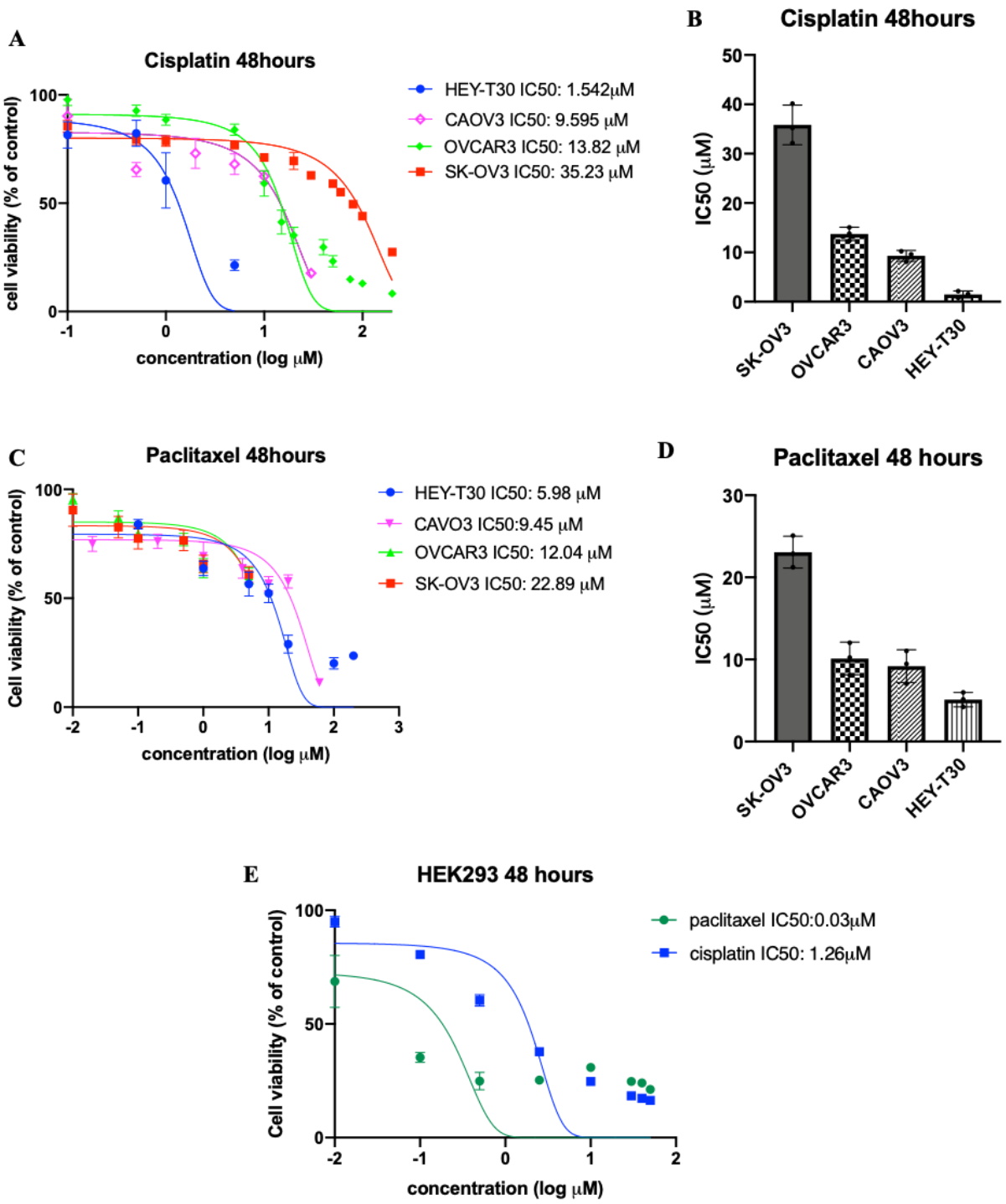
A
Cisplatin 48hours
cell viability (% of control)
concentration (log μM)
HEY-T30 IC50: 1.542μM
CAOV3 IC50: 9.595 μM
OVCAR3 IC50: 13.82 μM
SK-OV3 IC50: 35.23 μM
B
Cisplatin 48hours
IC50 (μM)
SK-OV3
OVCAR3
CAOV3
HEY-T30
C
Paclitaxel 48hours
Cell viability (% of control)
concentration (log μM)
HEY-T30 IC50: 5.98 μM
CAVO3 IC50:9.45 μM
OVCAR3 IC50: 12.04 μM
SK-OV3 IC50: 22.89 μM
D
Paclitaxel 48 hours
IC50 (μM)
SK-OV3
OVCAR3
CAOV3
HEY-T30
E
HEK293 48 hours
Cell viability (% of control)
concentration (log μM)
paclitaxel IC50:0.03μM
cisplatin IC50: 1.26μM

Figure 4. 2 Assessment of IC50 in Ovarian cancer cell lines and non-cancerous cell line with the treatment of chemo drugs after 48hours. A. Cell viability of four ovarian cancer cell lines HEY-T30, CAOV3, OVCAR3 and SK-OV3 after treatment with different concentrations of cisplatin, the predicted IC50 value is 1.542μM, 9.595μM, 13.82μM and 35.23μM respectively. B. The summary histogram of cisplatin IC50 value in four ovarian cancer cell lines. C. Cell viability of four ovarian cancer cell lines HEY-T30, CAOV3, OVCAR3 and SK-OV3 after treatment with different concentrations of paclitaxel, the predicted IC50 value is 5.98μM, 9.45μM, 12.04μM and 22.89μM respectively. D. The summary histogram of paclitaxel IC50 value in four ovarian cancer cell lines. E. Cell viability of non-cancerous cell line HEK-293 after treatment with different concentrations of paclitaxel and cisplatin, the predicted IC50 value is 0.03μM and 1.26μM respectively. Data were mean ±SEM of three replicates.

Given the chemo drug takes longer time to come into effect than SP9, the 5 days proliferation assay was performed to assess the efficacy of chemo drug and SP9 in terms of blocking cell growth over an extended period. Similar with IC50 experiments, we used trypan blue assay to monitor cell proliferation. OVCAR3 and SK-OV3 were treated with the same dosage of SP9 or chemo drug at Day 0 and the number of cells was recorded from Day 1 to Day 5 to draw a 5-day cell proliferation curve. The 5-day cell growth results showed that SP9 can significantly inhibit the proliferation of ovarian cancer cells within 1 day, though survival cells resumed proliferation from the second day on, the growth rate is distinctly slowdown. From overall cell survival rate, SP9 still present evident inhibitory action on cell growth compare with the control group over 5 days in both ovarian cancer cell lines OVCAR3 and SK-OV3 (Figure 4.3 A and B, red curves). In contrast, the same dosage of cisplatin showed no prominent cytotoxicity in day1 but start to take effect of cell growth inhibition from Day2 (Figure 4.3 A and B, blue curves). For paclitaxel, similar trend with cisplatin is observed in SK-OV3 cell lines (Figure 4.3 B. green curve), yet 8μM paclitaxel showed strong inhibitory cell proliferation efficacy and started from day1 in OVCAR3 cell line. It displayed the similar potency with SP9 in day 1 but the cytotoxicity is growing along with times (Figure 4.3 A. green curve). Taken together, our data certified the cytostatic efficacy of SP9 in ovarian cancer cell growth.

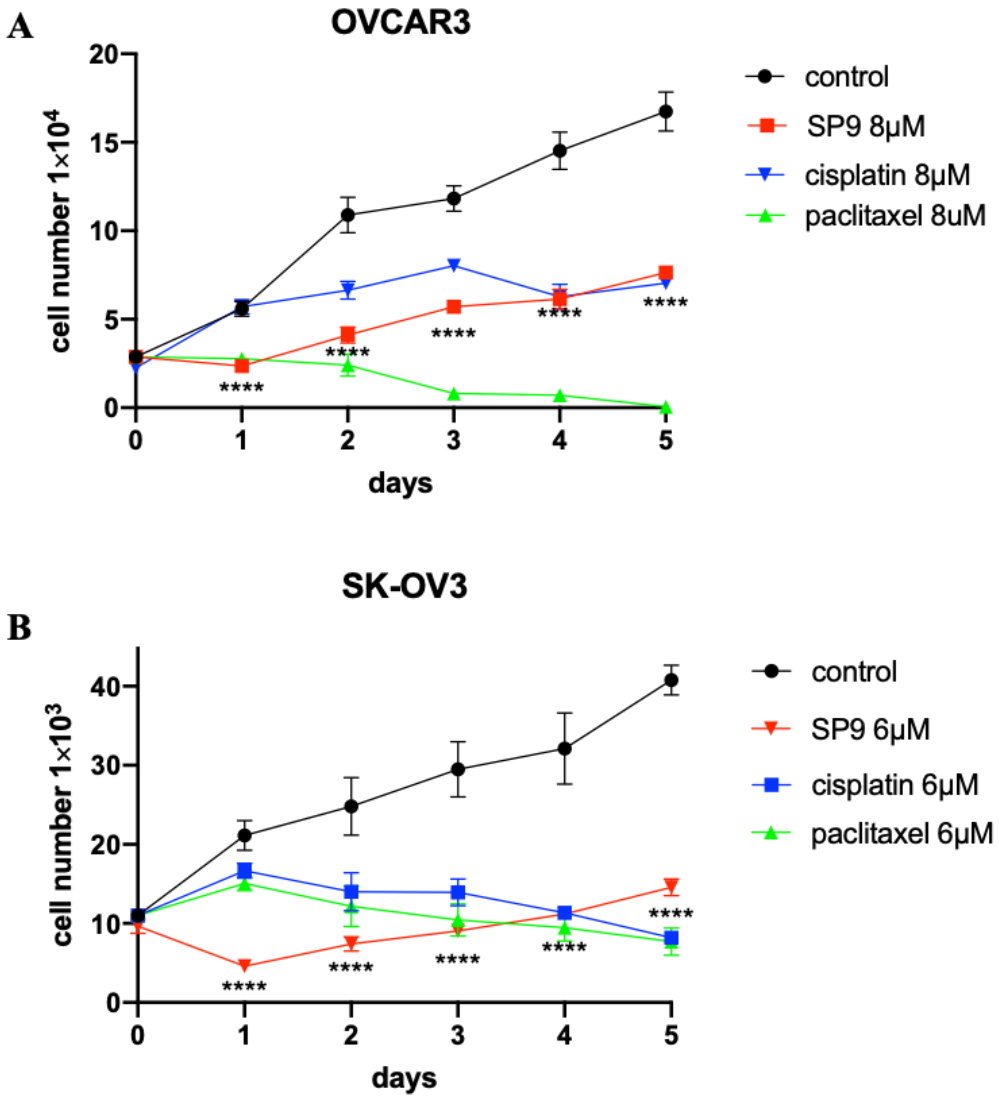

Figure 4. 3 Long-term anti-proliferation efficacy of SP9 and chemo drugs in ovarian cancer cell lines. A. Cell viability results of OVCAR3 after treatment with 8μM SP9 or chemo drugs for five days, the number of viable cells was counted every 24 hours. B. Cell viability results of SK-OV3 after treatment with 6μM SP9 or chemo drugs for five days, the number of viable cells was counted every 24 hours. Data represent mean ± SEM of three replicates. **** $P<0.0001$; two-way ANOVA.

In general, we determined the IC50 value using the Trypan Blue exclusion assay and the CellTiter-Glo luminescent cell viability assay across a range of ovarian cancer cell lines. The results obtained were consistent and confirmed the cytostatic effectiveness of SP9 in inhibiting the growth of ovarian cancer cells (Figure 4.1). Considering the chemotherapy remains the primary treatment for ovarian cancer, we try to compare the anti-proliferation efficacy and toxicity between chemotherapeutic reagent (cisplatin and paclitaxel) and SP9. We assessed the IC50 values over a short-term period (Figure 4.2) and evaluated the impact on cell growth inhibition over an extended period with 5 days proliferation assay (Figure 4.3). Our findings demonstrated that SP9 exhibits significant anti-proliferative effects on ovarian cancer cells, while displaying lower cytotoxicity towards non-cancerous cells in comparison to conventional chemotherapeutic agents. These results suggested that SP9 may offer a therapeutic advantage by providing a favorable balance between efficacy and toxicity for the treatment of ovarian cancer.

4.2 Mechanistic Study of cell death induced by Beclin 1-Targeting stapled peptides.

4.2.1 The induction of cell death by Beclin 1-targeting stapled peptides is not dependent on the apoptosis pathway

To understand which type of cell death pathway SP9 triggered in ovarian cancer cells, we first investigate if SP9 induce apoptotic cell death by adopt classical apoptosis inhibitor, given most clinical used anti-cancer drug trigger cell death by apoptotic pathway. Apoptosis is a common form of programmed cell death, and it is regulated by caspases which is a unique family of cysteine proteases. Z-VAD-FMK is a well-known pan caspase inhibitor which can bind to the catalytic site of caspase proteases to restrain the apoptosis signalling pathway. Doxorubicin is a commonly used anti-cancer chemotherapy which can induce apoptosis cell death via caspase pathway activation, as the first-line chemotherapy for ovarian cancer, cisplatin and paclitaxel also trigger caspase cascade to induce apoptosis, so they will be adopted as positive control in this study.

The result of cell viability assay presented noticeable rescue effect to doxorubicin treated group with 50μM Z-VAD-FMK supplement in ovarian cancer cell lines (Figure 4.4 A, rescue cell survival from around 36% to 56%, 30% to 50% in OVCAR3 and SK-OV3, respectively), verifying Z-VAD-FMK can suppress caspase signal and apoptosis activation, leading less cell death. Whereas our results showed that there is no significant difference to cell survival percentage of peptide treated group with or without Z-VAD-FMK in ovarian cancer cell lines (Figure 4.4 A, the cell survival rate remains around 50% after peptide treatment with or without Z-VAD-FMK exposure), signifying that peptide induce cell death

independent to apoptosis pathway since caspase inhibitor fail to recuse peptide caused cell death.

Next, Annexin V/PI double staining assay is exploited for apoptosis detection by flow cytometer. According to manufacturer's introduction, the early staged apoptotic cell showed Annexin V positive but PI negative, the percentage of apoptotic cells are shown in the lower right quadrant; dead cell presents both Annexin V and PI positive, the percentage of necrotic cell death positive is shown in the upper right quadrant. The different populations could be easily separated by flow cytometry. In this assay, 25μM cisplatin is administered to OVCAR3 cells as positive control to induce apoptotic cell death, around 60% apoptotic cell death event shown in lower right quadrant (Figure 4.4 B upper plot). As shown in our data, there are over 20% of OVCAR3 cells underwent non-apoptotic cell death with 7.5μM SP9 treatment, while 7.4% showed apoptosis cell death event. When cells were treated with 15μM SP9, over 30% of OVCAR3 cells underwent non-apoptotic cell death but only 6.4% apoptosis cell death event happened, indicating SP9 induce non-apoptotic cell fatality by dosage dependent, higher dosage of peptide result in more cell dead events, but the percentage of apoptotic cell show indistinctive change compare with dead cell ratio. Similar results are observed in other ovarian cancer cell lines SK-OV3 and HEY-T30 (Figure 4.4 B middle and bottom plot), suggesting SP9 might exert cell death effect independent on apoptotic pathways in ovarian cancer cells.

We further detect the caspase cleavage activity by western blot technology to confirm our previous suspect. Caspase3 is a decisive executor of apoptosis for responding to proteolytic cleavage of various key proteins including nuclear enzyme poly (ADP-ribose) polymerase (PARP). Our results showed that there is no cleavage caspase3 and cleavage PARP signal are observed with peptide treatment while the positive control group with chemo drug presented detectable cleavage caspase3 and cleavage PARP signal even with dosage dependent (Figure 4.4 C). The results are all similar in other ovarian cancer cell lines SK-OV3 and HET-T30, so we concluded that SP9 induced non-apoptotic cell death in ovarian cancer cell lines.

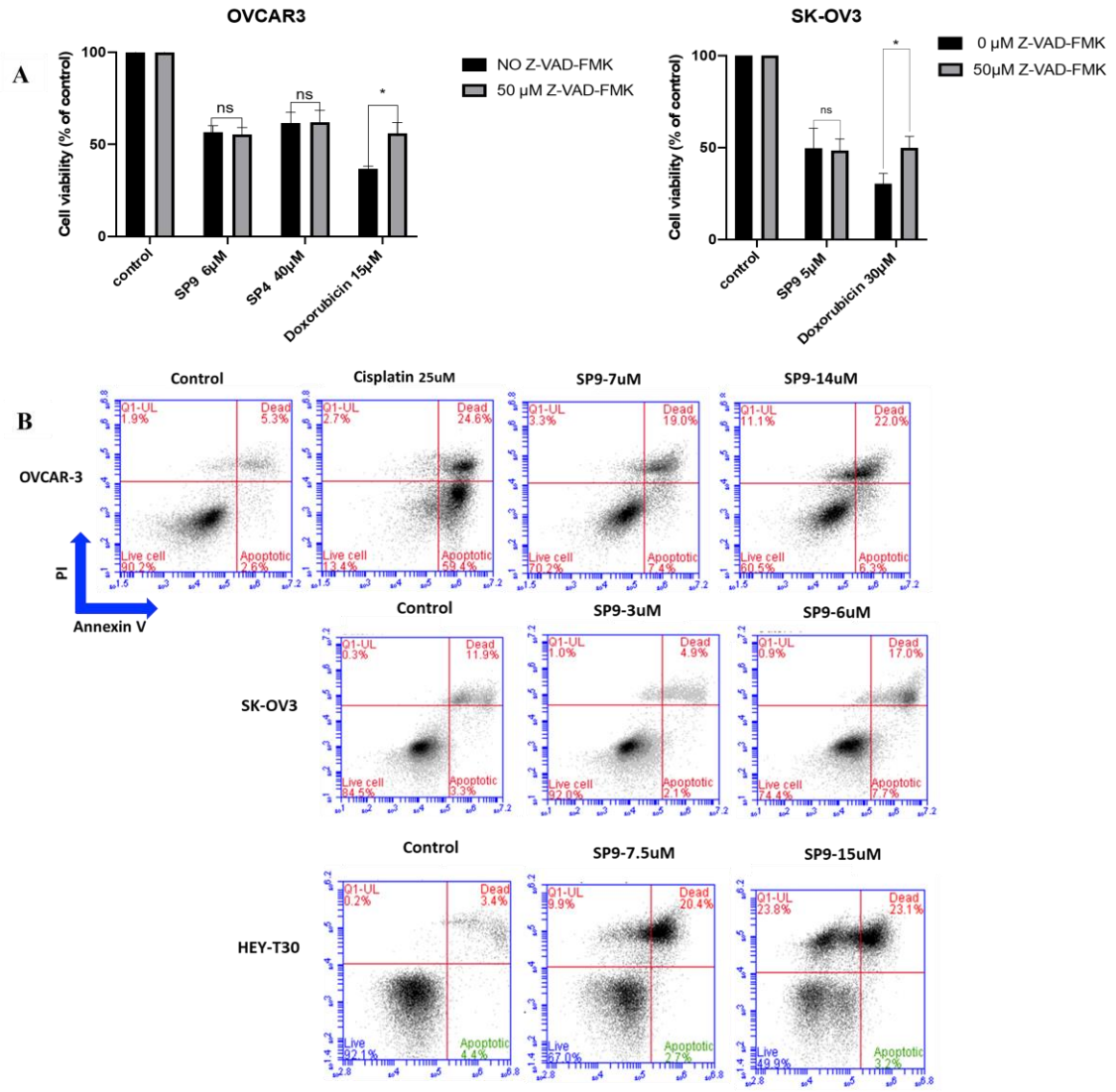
A
OVCAR3
Cell viability (% of control)
100
50
0
ns
ns
*
control
SP9 6μM
SP4 40μM
Doxorubicin 15μM
NO Z-VAD-FMK
50 μM Z-VAD-FMK
SK-OV3
Cell viability (% of control)
100
50
0
ns
*
control
SP9 5μM
Doxorubicin 30μM
0 μM Z-VAD-FMK
50μM Z-VAD-FMK
B
Control
Cisplatin 25uM
SP9-7uM
SP9-14uM
OVCAR-3
Q1-UL 1.9%
Dead 5.3%
Live cell 90.2%
Apoptotic 2.6%
Q1-UL 2.7%
Dead 24.6%
Live cell 13.4%
Apoptotic 59.4%
Q1-UL 3.3%
Dead 19.0%
Live cell 70.2%
Apoptotic 7.4%
Q1-UL 11.1%
Dead 22.0%
Live cell 60.5%
Apoptotic 6.3%
PI
Annexin V
Control
SP9-3uM
SP9-6uM
SK-OV3
Q1-UL 0.3%
Dead 11.9%
Live cell 84.5%
Apoptotic 3.3%
Q1-UL 1.0%
Dead 4.9%
Live cell 92.0%
Apoptotic 2.1%
Q1-UL 0.9%
Dead 17.0%
Live cell 74.4%
Apoptotic 7.7%
Control
SP9-7.5uM
SP9-15uM
HEY-T30
Q1-UL 0.2%
Dead 3.4%
Live 92.1%
Apoptotic 4.4%
Q1-UL 9.9%
Dead 20.4%
Live 67.0%
Apoptotic 2.7%
Q1-UL 23.8%
Dead 23.1%
Live 49.9%
Apoptotic 3.2%
C
NT
SP9 4 μM
SP4 20 μM
Cis 10 μM
Doxorubicin 1.5 μM 1.0μM
Cleaved PARP
89 kDa
Caspase 3
35 kDa
Cleaved-Caspase 3
17 kDa
β-actin
43 kDa
SK-OV3
NT
SP9 4 μM
SP4 20 μM
Cis 10 μM 5 μM 2.5μM
Cleaved PARP
Caspase 3
Cleaved-Caspase 3
β-actin
HEY-T30
NT
SP9 4 μM
Taxel 0.5 μM 1.0μM
Dox 0.5 μM 1.0μM
89 kDa
35 kDa
17 kDa
43 kDa

Figure 4. 4 SP9 induced non-apoptotic cell death in ovarian cancer cell lines. A. Survival of OVCAR3 and SK-OV3 after treatment with indicated concentration of peptide and 15μM doxorubicin with or without addition of apoptosis inhibitor 50μM Z-VAD-FMK. Data represents mean ± SEM. B. Flow cytometry plot for OVCAR3, SK-OV3 and HEY-T30 cells with Annexin V and PI dual staining after one hour treatment of indicated concentration of SP9 and 25 C. Representative western blot result of OVCAR3, SK-OV3 and HEY-T30 cells treated with different concentrations of SP9, and chemo drug indicated incubation time. The cell lysate was detected by cleaved Caspase-3 antibody, cleaved-PARP and β-actin (loading control). Data represent mean ± SEM of three replicates. ns, not significant; *P <0.5; t-test.

4.2.2 The cytostatic effect of Beclin 1-targeting stapled peptides cannot be rescue by the inhibitor of necrosis, ferroptosis and pyrotosis.

Necrosis phenotypes exhibit in different manner of cell death, including ferroptosis, necroptosis and pyrotosis. Thus, we next apply the typical ferroptosis inhibitor Ferrostatin and necroptosis inhibitor Necrostain-1 to conduct the cell viability assay to study if peptide take effect by ferroptosis or necroptosis manner. Ferrostatin is a selective inhibitor of Erastin induced ferroptosis, so Erastin is used as positive control to exhibit the Ferrostatin protective effect against ferroptosis cell death in this assay. Our result showed that in OVCAR3 cell line, 60μM erastin and 7.5μM SP9 lead cell demise in a similar level (approximately 50%) but ferrostatin supplement only can protect Earstin treated group noticeably from ferroptosis cell death while the cell viability rate of peptide treated group showed no difference with or without ferrostatin addition (Figure 4.5 A), implying ferrostatin has no protected effect to peptide treated group for the cytotoxicity of peptide is irrelevant with ferroptosis pathway.

Necroptosis is identified regulated form of cell death with necrotic features. RIP1 (receptor interacting protein 1) kinase are critical signalling molecular to mediate necroptosis pathway and Necrostain-1 is known as RIP1-targeted inhibitor of necroptosis. Our data showed the Necrostain-1 did not affect the cell survival percentage of peptide treated group (Figure 4.5 B), indicating peptide-triggered cell death effect is independent on necroptosis pathway. Pyroptosis is a mode of

programmed necrosis which defined as a form of cell lysis involved with inflammation. It is known as Gasdermin-mediated cell death, and studies proved that GSDME cleavage into N-GSDME followed by chemotherapy-induced pyroptosis cell death. Our western blot data revealed that N-GSDME is unable to be detected with peptide treatment while the cisplatin treatment caused GSDME cleavage into N-GSDME by dosage dependent is observed (Figure 4.5 C). This result suggested the cytostatic effect of peptide might not involve with pyroptosis pathway.

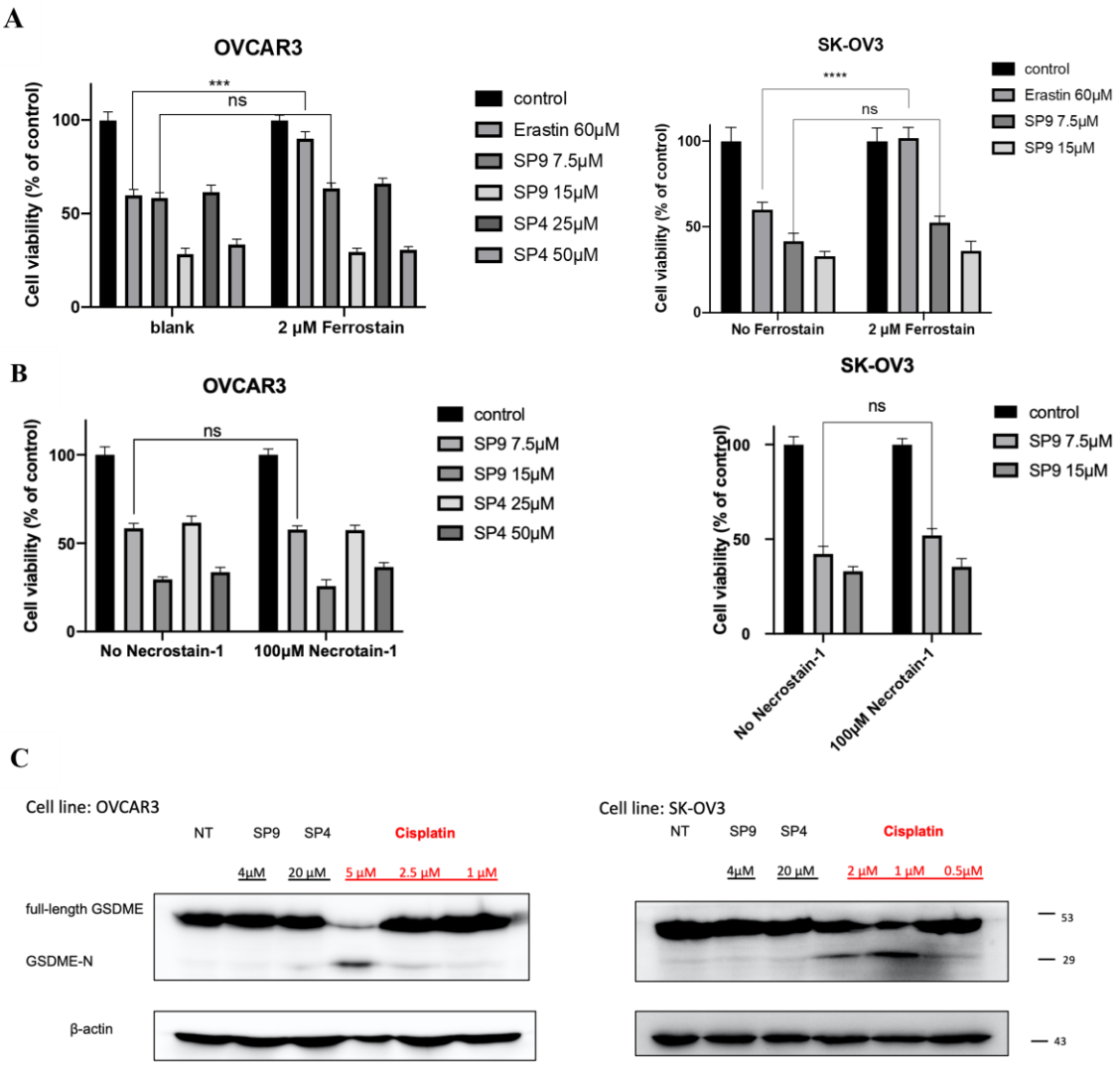

Figure 4. 5 SP9 induced cell death without involvement of ferroptosis, necroptosis and pyrotosis. A. Survival of OVCAR3 and SK-OV3 cells treated by indicated concentrations of peptide and 60μM Erastin (positive control), a ferroptosis activator, with or without the addition of 2μM Ferrostain, a ferroptosis inhibitor. B. Survival of OVCAR3 and SK-OV3 cells treated by indicated concentrations of peptide with or without addition of 100μM Necrostain-1, an inhibitor of necroptosis. C. Representative western blot result of OVCAR3 and SK-OV3 cells treated with indicated concentrations of SP9 24hours and chemo drug 48hours. The cell lysate was detected by GSDME antibody and β-actin (loading control). ns, not significant; ***P <0.001; **** P<0.0001; t-test.

4.2.3 Beclin 1-targeting stapled peptides induced cell death is dependent on autosis.

We further explore if the cytotoxicity of peptide caused by autosis, which is defined as autophagy gene dependent and non-apoptotic cell death manner [39]. Digoxin is one of cardiac glycosides verified protective effect against autosis, hence we applied digoxin as autosis inhibitor to perform cell viability assay of peptide to investigate if peptide induce cell death by autosis manner. Our result demonstrated that 7.5μM digoxin supplement enable to noticeably enhance cell viability of peptide treatment even in different dosage (Figure 4.6), suggesting SP9 might takes cytostatic effect by autosis which can be inhibited by digoxin.

Taken together, to elucidate the mechanism underlying SP9-induced cell death, we examined various programmed cell death pathways by utilizing specific inhibitors. Our findings revealed that SP9-induced cell death is not primarily associated with apoptosis, necroptosis, ferroptosis, or pyroptosis (Figure 4.4 & 4.5). However, the use of an autosis inhibitor significantly rescued majority of SP9-induced cell death in both ovarian cancer cell lines (Figure 4.6 A), suggesting that SP9 may predominantly rely on the autosis pathway. Furthermore, a classic autophagy inhibitor 3-Methyladenine (3-MA) were adopted to confirm if the cytostatic effect caused by SP9 is involved with autophagy pathway. Our result demonstrated that 3-MA can notably increase the cell viability presenting by high luminescence (Figure 4.6 B), which suggested SP9-induced cell death is rely on autophagy pathway.

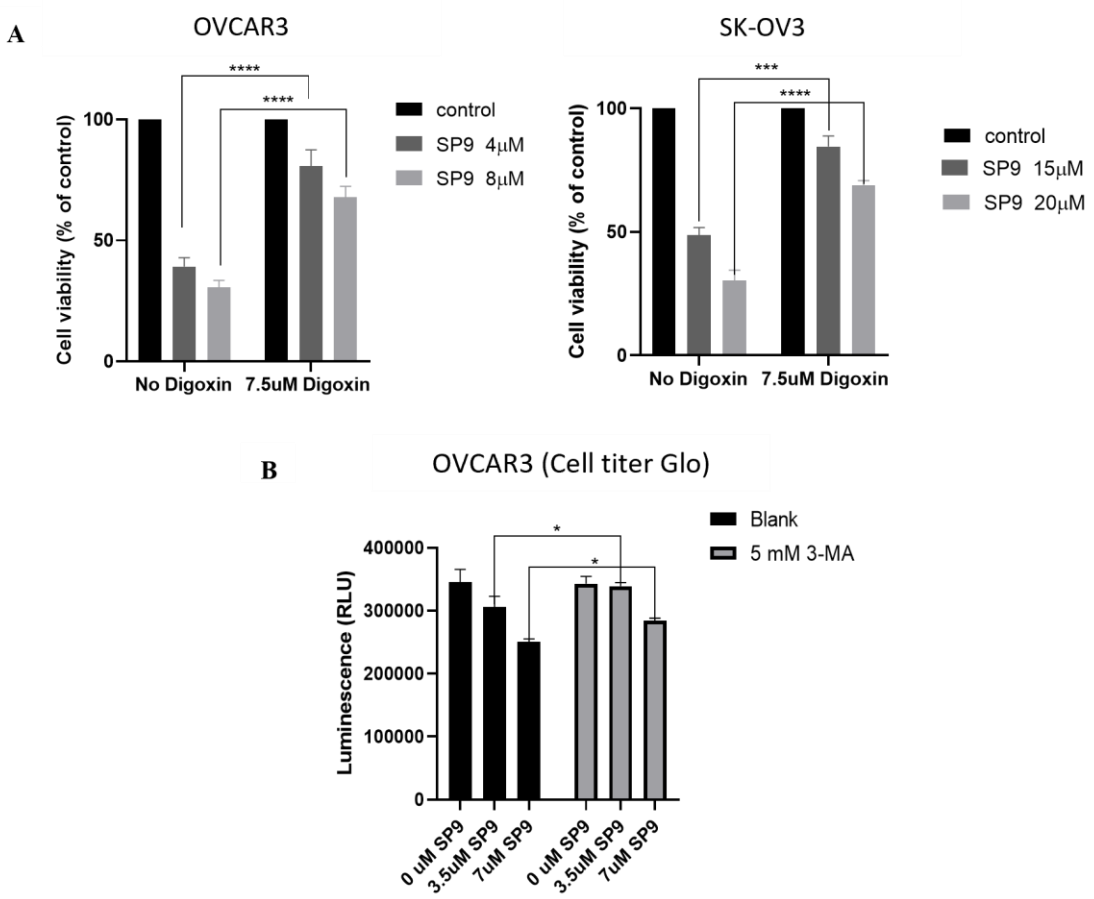

Figure 4. 6 SP9 induced cell death could be rescued by autosis inhibitor. A. Measurement of the viable cell number of OVCAR3 and SK-OV3 cells after treatment with indicated concentration of SP9 for 4 hours in the presence or absence of 7.5 μM digoxin. B. Cell Titer Glo Luminescent cell viability curve for SP9 cytotoxicity effect in OVCAR3 with or without 5mM 3-MA exposure. Results shown represent mean ± SEM (n=3). **P* <0.5, ****P* <0.001; **** P<0.0001; t-test.

4.3 The impact of Beclin 1-targeting stapled peptides on mitochondria function in ovarian cancer cells.

4.3.1 Beclin 1-targeting stapled peptides elevates intracellular reactive oxygen species level.

Mitochondria is the major cell organelle to generate ROS, mitochondria ROS is produced through the process of electron transport chain and oxidative phosphorylation (OXPHOS) during aerobic respiration, the imperative role of ROS in tumorigenesis have been extensively studied. Thus, we evaluate the ROS level in ovarian cancer cell to assess the influences of peptide to mitochondria function. CellROX™ Green reagent was used to quantify the intracellular ROS level and CellROX fluorescence measured by BD Accuri C6 flow cytometer. 500μM TBHP is added in OVCAR3 cells as positive control group, which can induce ROS production to enhance fluorescent intensity, represented by right shift from control group (Figure 4.7 left plot). Our data showed stronger MPfluorescence determination with higher concentration of peptide treatment in both cell lines (Figure 4.7), indicating our peptide can increase intracellular ROS level and the induction potency of peptide present dosage dependent.

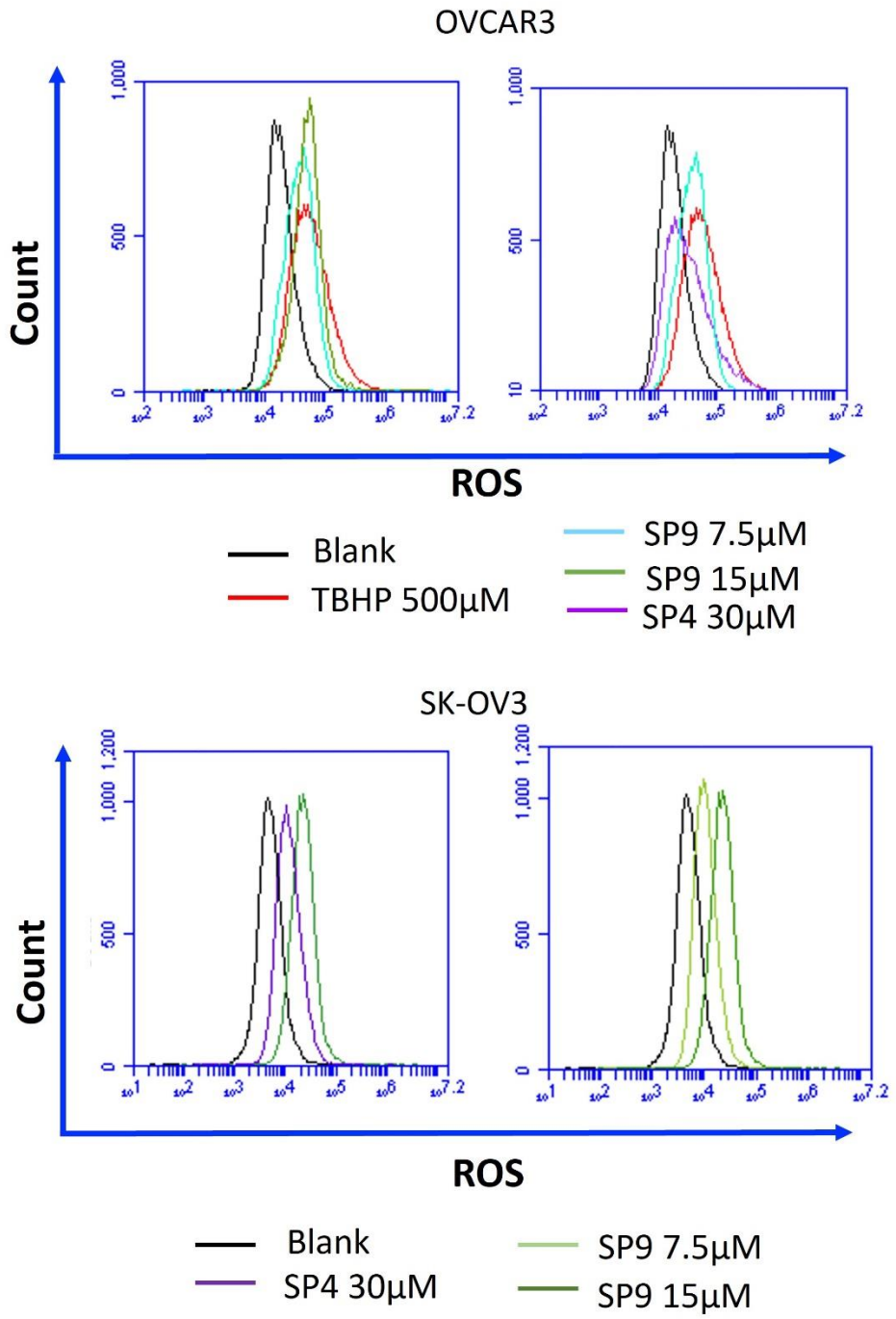

Figure 4. 7 SP9 induced intracellular ROS generation by dosage dependent in ovarian cancer cell lines. The representative flow cytometry plot of OVCAR3 and SK-OV3 treated with indicated concentration of peptide (SP9: 7.5, 15µM, SP4: 30µM) and 500µM TBHP (an ROS inducer, positive control) for one hour.

4.3.2 Beclin 1-targeting stapled peptides dissipates the mitochondria membrane potential by TMRM detection.

Mitochondria membrane potential (ΔΨm) play essential role in homeostasis, maintaining cellular physiological activity including cell death. Since mitochondria membrane potential is generated by proton pumps and identified as the capacity of mitochondria to sustain electrochemical gradient for producing ATP, reflecting the mitochondria function in varied aspect. Thus, we detected the mitochondria membrane potential by a fluorescent dye tetramethylrhodamine methyl ester (TMRM), measuring by BD Accuri C6 flow cytometer. Our data displayed that compare with the control group (shown as red curves in Figure 4.8,), the fluorescent intensity is reduced with peptide treatment, shown the corresponding fluorescent signal curve left shift and closer to the blank group (shown as black curves in Figure 4.8) with higher dosage in both OVCAR3 and SK-OV3 cells. CCCP was used as a positive compound to induce mitochondria membrane potential depolarization, TMRM fluorescence intensity decreased as expected (shown as green curve in Figure 4.8 right plot). This result suggested peptide can induce the loss of mitochondria membrane potential by dosage dependent in ovarian cancer cells.

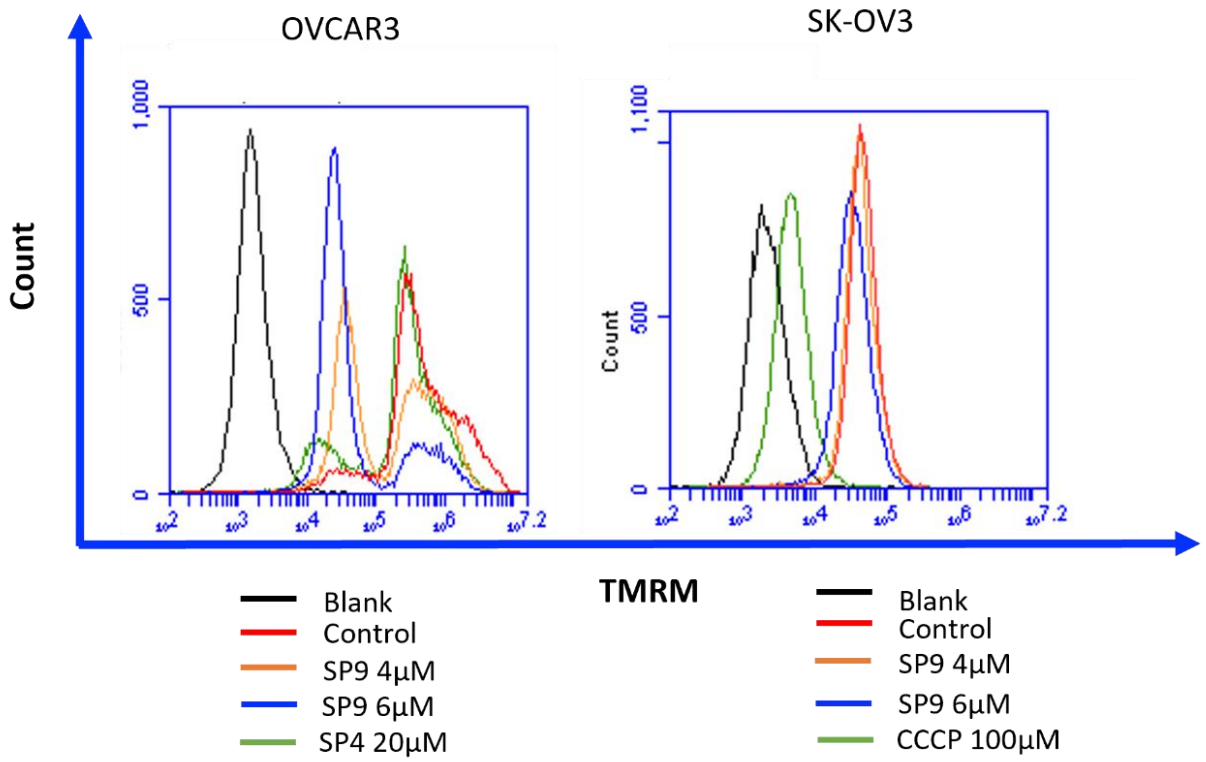

Figure 4. 8 SP9 dissipate mitochondrial membrane potential (Δψm) in ovarian cancer cell lines. The representative flow cytometry plot of OVACR3 and SK-OV3 treated with peptide (SP9 4μM and 6μM; SP4 20μM) for one hour. Blank group indicated cells without any staining; control group indicated cell without any treatment.

4.3.3 Beclin 1-targeting stapled peptides-mediated induction of Mitochondrial permeability transition pore (MPTP) opening

Mitochondrial permeability transition pore (MPTP) is a transmembrane protein which is calcium-dependent and ion non-selective channel, locating in the inner mitochondrial membrane with distinct functions. MPTP usually closed in normal condition, besides calcium, various oxidant byproduct could induce opening of MPTP including ROS. MPTP opening acts as a vital element in pathology pathway to cell fatality, it is observed that tumor cell can be resistant to cell death by desensitizing MPTP to calcium of ROS induction. With by BD Accuri C6 flow cytometer technology, we apply MitoProbe^{TM} Transition Pore Assay Kit to measure MPTP opening level to evaluate if peptide treatment can induce MPTP opening in ovarian cancer cells. Calcein AM is a non-fluorescent substrate for esterases, which, upon entering cells, is cleaved by these enzymes to release the fluorescent compound calcein so fluorescent can distribute throughout the entire cell with strong fluorescent intensity (shown as red curve in Figure 4.9). The calcein quencher, $CoCl_2$, can pass through the plasma membrane but is halted by the mitochondrial membrane. As a result, under normal conditions, the addition of $CoCl_2$ quenches the fluorescence of calcein in the cytosol, while the fluorescence of calcein in the mitochondria is preserved (shown as blue curve in Figure 4.9).

In this assay, ovarian cancer cells were pretreated with indicated concentrations of SP9 for an hour, then were stained with Calcein AM followed by calcein

quencher $CoCl_2$. Therefore, the diminish of fluorescence indicate the opening of MPTP. We adopt ionomycin, a calcium ionophore, served as a positive control in this assay, we attested that ionomycin is capable of triggering MPTP opening, presenting by decreasing Calcein AM fluorescence signal (Figure 4.9.B left). Our data showed that in OVCAR3 cells, 2μM SP9 can decrease the Calcein AM fluorescence signal (Figure 4.9 A. left plot), and the lower intensity of fluorescence presented by shifting to left with peptide concentration increased (Figure 4.9 A. middle plot), similar result is also observed in another ovarian cancer cell line SK-OV3 (Figure 4.9 B), suggesting the capability of peptide induced MPTP opening by dosage dependent.

To further visualize the SP9-induced MPTP opening, the confocal image study was conducted. Following by the standard protocol provided by the manufacturer, cells were stained with calcein AM and $CoCl_2$ for evaluated MPTP opening level, and Hoechst was added to label nuclear DNA of cells. Our result showed the calcein AM fluorescence signal diminished after 2μM SP9 added to medium (Figure 4.9 C), confirmed that peptide can reduce MPTP opening.

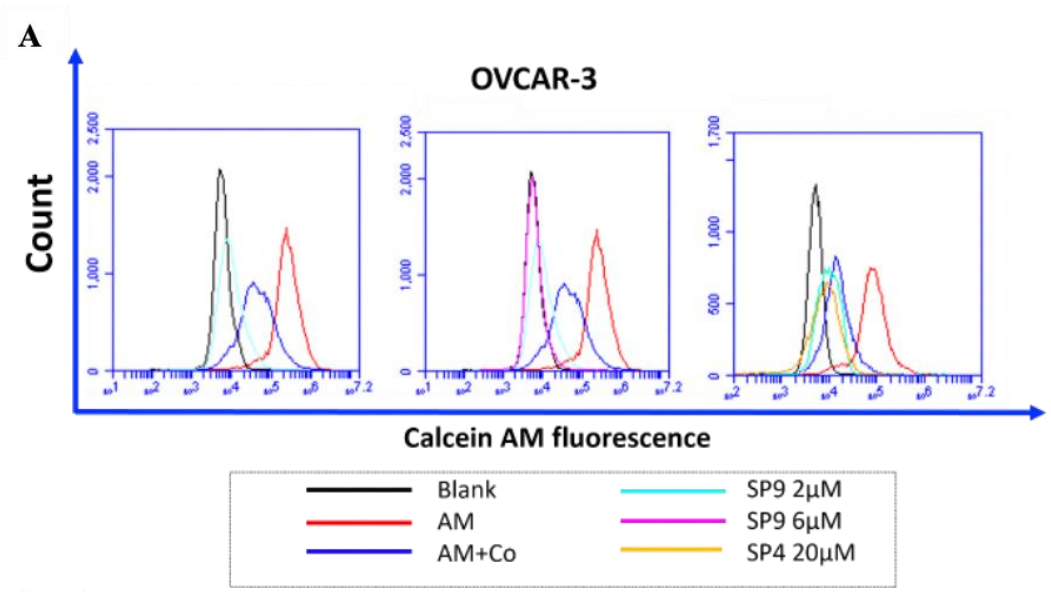
A
OVCAR-3
Count
Calcein AM fluorescence
Blank
AM
AM+Co
SP9 2μM
SP9 6μM
SP4 20μM

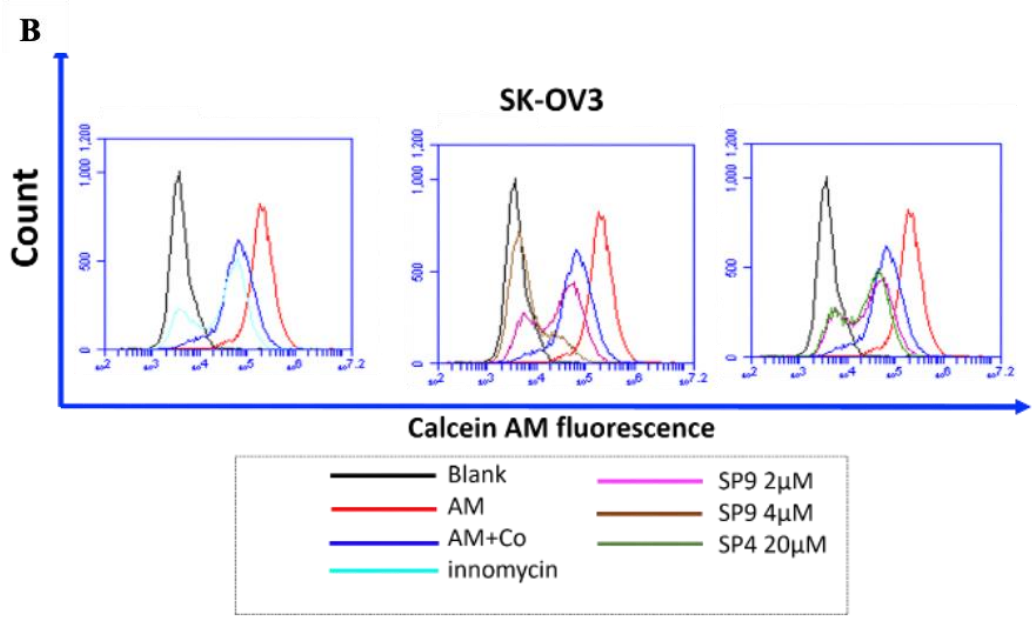
B
SK-OV3
Count
Calcein AM fluorescence
Blank
AM
AM+Co
innomycin
SP9 2μM
SP9 4μM
SP4 20μM

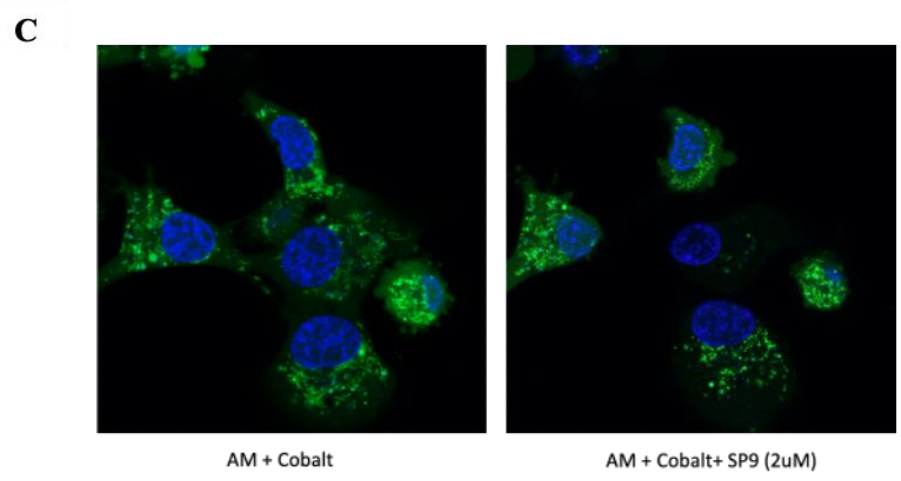
C
AM + Cobalt
AM + Cobalt+ SP9 (2uM)

Figure 4. 9 SP9 induce the opening of MPTP in ovarian cancer cell lines. A. The representative flow cytometry plot of OVACR3 treated with MPTP staining and indicated concentration of peptide for one hour. B. The representative flow cytometry plot of SK-OV3 treated with MPTP staining and indicated concentration of peptide or ionomycin for one hour. Blank group indicated control group cells without any staining; AM indicated control group cells only stained with calcein AM; AM+Co indicated control group cells stained with calcein AM followed by calcein quencher $CoCl_2$; ionomycin treated group is positive control for MPTP opening; all treated group stained with calcein AM and $CoCl_2$. C. The representative confocal image of OVACR3 stained with 1μM calcein AM, 1mM $CoCl_2$ and 1μM Hoechst in 1 mL No FBS culture medium. Image showed the changes of MPTP fluorescent in OVCAR3 cells before (left) and after SP9 treatment (right).

4.3.4 Beclin 1-targeting stapled peptides decreases Oxidative phosphorylation (OXPHOS) activity.

Oxidative phosphorylation (OXPHOS) is the final step of cellular respiration for ATP production, occurring in mitochondria. Defective OXPHOS activity result in mitochondria impairment with excessive ROS accumulation. The activity of OXPHOS was analyzed by measuring the oxygen consumption rate (OCR) of ovarian cancer cell line upon treatment by our Beclin 1-targeted peptides (Figure 4.10 A and C). FCCP is capable to uncouple oxygen consumption from ATP production then raises OCR to a maximal value, our result showed that after FCCP injection, cancer cells exhibit remarkably lower OCR value with higher concentration of peptides treatment in both cell lines OVCAR3 and SK-OV3 (Figure 4.10 B and D left plot), indicating the maximal respiration of cells decreasing to response peptide treatment by dosage dependent. Additionally, in SK-OV3 cell line, the OCR value already present difference after first injection of peptide compare with vehicle group, suggesting the basal respiration is detrimentally affected by peptide in certain cell line (Figure 4.10 D right plot). Overall, our data revealed that our Beclin 1-targeted peptides can impair the OXPHOS activity in ovarian cancer cell lines.

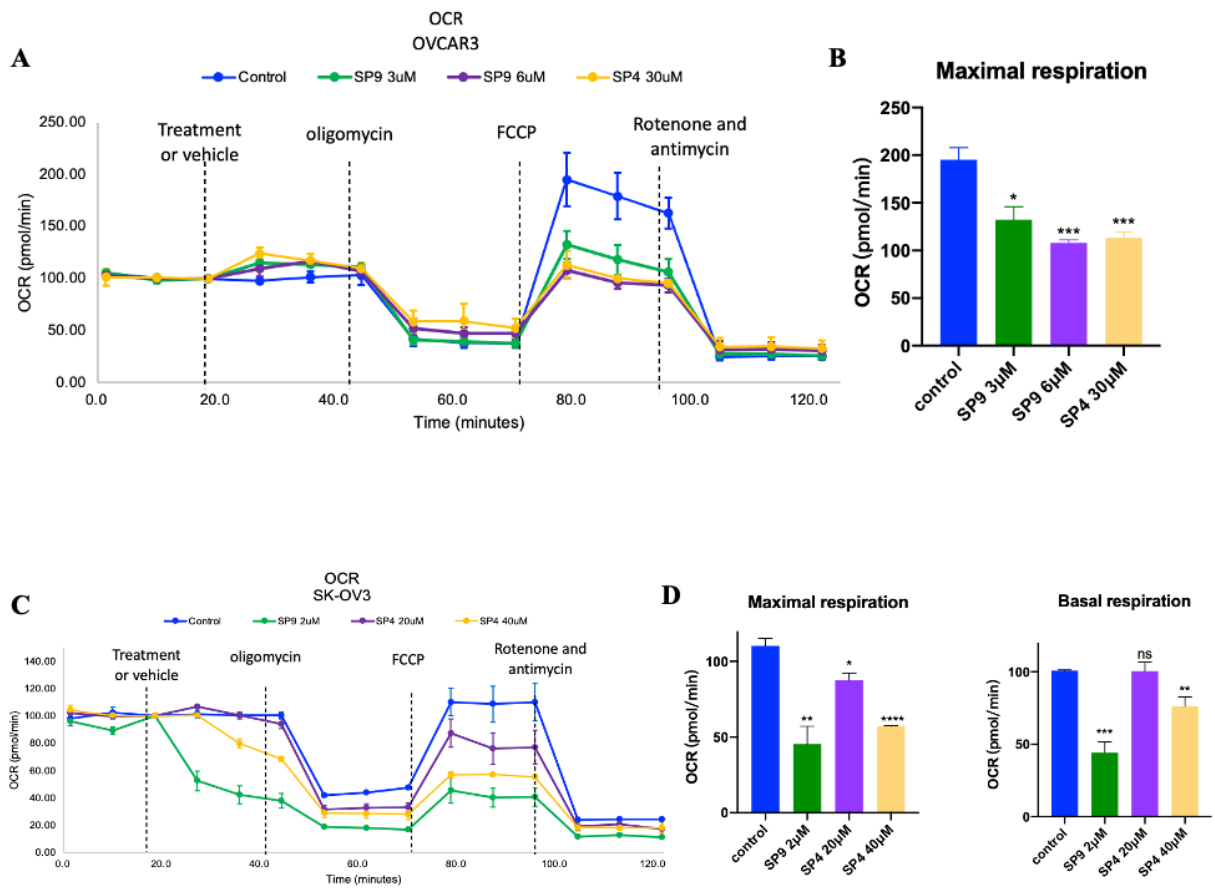

Figure 4. 10 SP9 decrease maximal oxygen consumption rate (OCR) in ovarian cancer cell lines. A. OCR was conducted using Mito Stress Test and measured by Agilent Seahorse Analyzer. OVCAR3 cells were treated with either SP9 or vehicle (control), 1μM oligomycin, 1μM FCCP, and 0.5μM rotenone and antimycin A sequentially. Each data point represented a real-time OCR measurement. B. maximal oxygen consumption, which refers to the OCR after FCCP treatment in OVCAR3. C. SK-OV3cells were treated with either 2μM SP9 or 20μM/40μM SP4 or vehicle (control), 1μM oligomycin, 1μM FCCP, and 0.5μM rotenone and antimycin A sequentially. Each data point represented the relative OCR compared to the base level. D. relative maximal oxygen consumption and basal oxygen consumption in SK-OV3 after treatment of FCCP. Results shown represent mean ± SEM (n=5). ns, not significant, *P <0.5, ** P<0.01, ***P <0.001, **** P<0.0001; t-test.

In conclusion, we have conducted a series of mitochondrial metabolism assay to delineate the impact of a Beclin 1-targeting stapled peptide on mitochondrial function in ovarian cancer cells. Mitochondria are recognized as the primary source of cellular ROS, which are by-products of respiration and closely linked to mitochondrial function. Using the CellROX™ Green reagent to quantify the intracellular ROS level, we observed that our Beclin-1 targeted peptide increased intracellular ROS levels in a dosage-dependent manner (Figure 4.7). Furthermore, we assessed mitochondrial membrane potential using TMRM fluorescent dye, and our results indicated that the peptide induced a dosage-dependent loss of mitochondrial membrane potential in ovarian cancer cells (Figure 4.8). Additionally, we utilized the MitoProbeTM Transition Pore Assay Kit to investigate the impact of our Beclin 1-targeting stapled peptides on MPTP dynamics, revealing the peptide's capability to induce MPTP opening (Figure 4.9). Given the essential role of mitochondria in ATP production through OXPHOS, we further explored OXPHOS activities by measuring the OCR (Figure 4.10). Our data demonstrated that our Beclin 1-targeting stapled peptides impaired OXPHOS activity in ovarian cancer cell lines. Collectively, our findings indicate that Beclin 1-targeting stapled peptides substantially influence mitochondrial function in ovarian cancer cells.

4.4 Involvement of the calcium signalling pathway in Beclin 1-targeting stapled peptides treatment.

4.4.1 Amelioration of Beclin 1-targeting stapled peptides-induced cell death by exogenous calcium.

As one of the most essential second messenger, intracellular calcium ion engage in diverse physiological activities. The dysregulation of calcium homeostasis usually is detrimental and involved with pathological occurrence, including tumorigenesis. Furthermore, the mitochondria-associated membranes indicate the contact site between mitochondria and endoplasmic reticulum (ER), which is described as hotspot for Ca^{2+} communication and being responsible for Ca^{2+} regulation. It is proved by our previous data that peptide can impact mitochondria function, so we wonder if peptide mediate cell death by interrupting calcium homeostasis. In this assay, 3.6mM $CaCl_2$ was added to test if extra Ca^{2+} can affect the potency of peptide. Our result showed after addition of 3.6mM $CaCl_2$, the IC50 value of SP9 raise from 6.68μM to 13.38μM in OVCAR3 cell lines (Figure 4.11 A), similar result is observed in SK-OV3 cell lines (Figure 4.11 B), IC50 value increased from 4.129μM to 9.157μM. This observation implies that Ca^{2+} rescue the cell death caused by peptides, we proposed that $CaCl_2$ supplement buffer calcium unbalance caused by peptide leading higher tolerance of cancer cell to peptide treatment.

We further employ BAPTA-AM, a cell-permeant chelator highly selective for Ca^{2+}, to confirm the rescue effect of Ca^{2+}. We adopted 2 hours 10μM BAPTA-AM pretreatment scheme since it showed no significant effect to the cell survival with or without 6 μM SP9 treatment. In control group, Ca^{2+} addition presented no influence on cell viability; but in 6 μM SP9 treated group, 3.6 mM $CaCl_2$ supplement increased the cell viability noticeably, Ca^{2+} did not improve the cell death induced by SP9 when cells are pretreated with 10μM BAPTA-AM 2 hours first (Figure 4.11C), indicating that the rescue effect of Ca^{2+} got offset with BAPTA-AM pretreatment and validating the critical role of calcium in Beclin 1-targeting stapled peptide induced cell death mechanism.

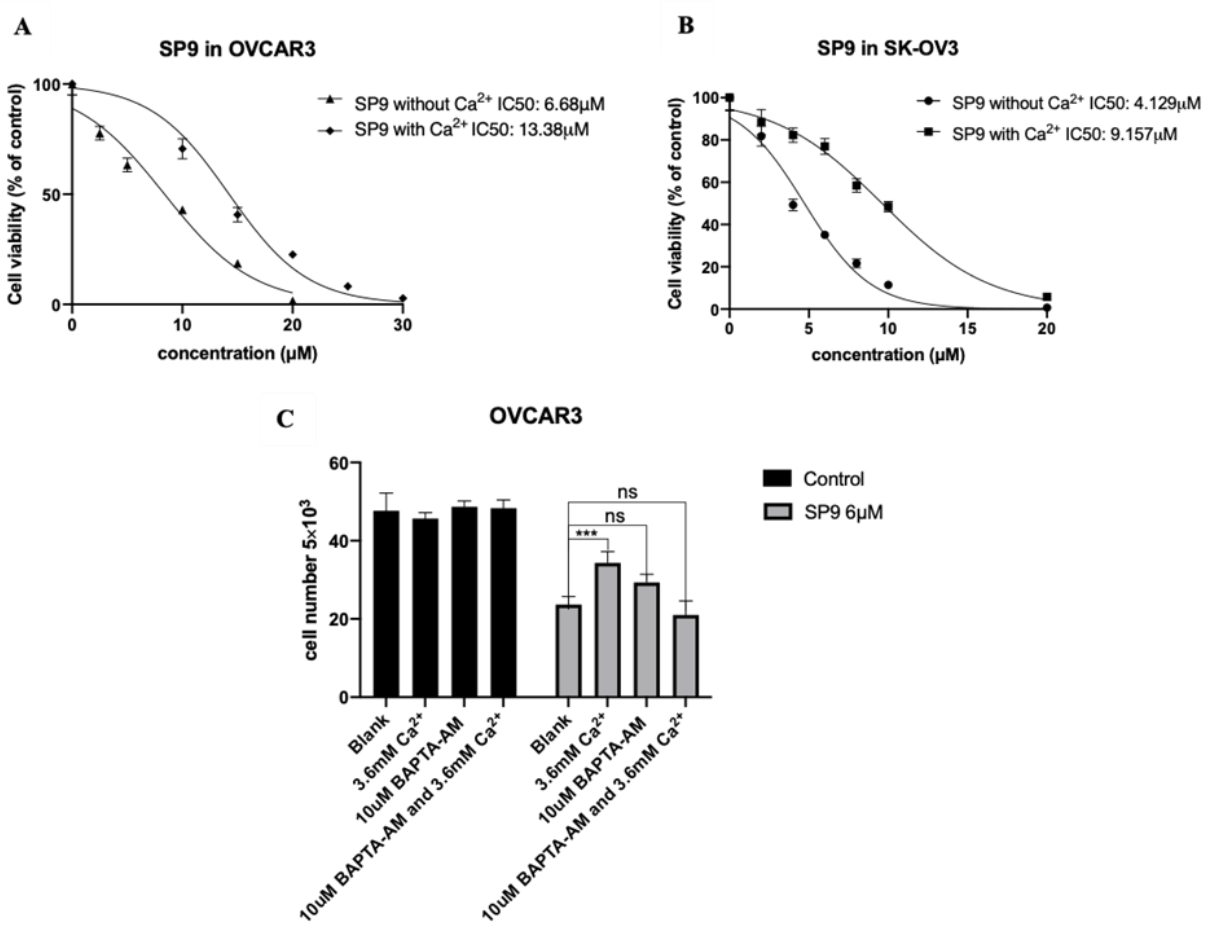

Figure 4. 11 SP9 induced cell death can be rescue by extra calcium in ovarian cancer cell lines A and B. Determination of IC50 value of SP9 with or without extra Ca^{2+} addition in OVCAR3 and SK-OV3. C. Survival plot of OVCAR3 cells with or without 6μM SP9 treatment in the exposure of only 3.6mM Ca, only 10μM BAPTA-AM and both 3.6mM Ca and 10μM BAPTA-AM included. Results shown represent mean ± SEM. ns, not significant, *** P<0.001, t-test.

4.4.2 Beclin 1-targeting stapled peptides treatment modulates intracellular calcium flux, alleviated by autosis inhibitor digoxin.

Intracellular calcium dynamic mainly concerns with the calcium ions cycling between the mitochondria and endoplasmic reticulum situated at the mitochondria-associated endoplasmic reticulum membrane named as MAM and cytosolic calcium fluctuation followed. To observe how peptide affect the intracellular calcium flux, OVCAR3 cells were transfected with cytosolic, mitochondrial and ER calcium sensor plasmids over 48 hours incubation, the fluorescence of the calcium sensors could be observed by inverted epifluorescence microscopy. the alteration of calcium concentration after peptide treatment was monitored and detected by CCD camera.

Our quantitative data presented how intracellular calcium signal changed with SP9 treatment in Ca^{2+} -absent or Ca^{2+} -present HBSS buffer, the real-time change of calcium signal represented by the relative fluorescence ratio. To the cell cultured in Ca^{2+} free HBSS buffer, when 2μM SP9 was added, cytosolic calcium signal and mitochondria calcium signal raised slightly first then fall back to base line over time. When the flux tended to be stable, 2 mM Ca^{2+} was further added, cytosolic and mitochondria calcium signal ascended again, cytosolic calcium then fall back to initial level steadily (Figure 4.12 A left plot), yet mitochondria calcium raised more dramatically even up to 1.5 folds (Figure 4.12 A middle plot). While ER calcium signal descended relatively obvious after 2μM SP9 added, around 25%, ER calcium signal then further fell away precipitously to 70%

followed by 2mM Ca^{2+} supplement but pick up to original level gradually along with time (Figure 4.12 A right plot). These phenomena indicated that SP9 can cause ER releasing Ca^{2+} and mitochondria Ca^{2+} intake. Additionally, extracellular calcium could further extend raised Ca^{2+}level. In 1.2 mM Ca^{2+} HBSS buffer cultured cells, similar trend is observed but with more noticeable range of variation, 2μM SP9 triggered cytosolic and mitochondria calcium level raising to around 2-3 folds compared with the change level in Ca^{2+} free HBSS buffer (Figure 4.12 B left and middle plot), descending of ER Ca^{2+} was about 60%, but the supplement of 2mM Ca^{2+} did not change the tendency of cytosol and mitochondria calcium level, yet still leading the ER Ca^{2+} grow back to original level, which is understandable considering the buffer effect of ER(Figure 4.12 B right plot). These results demonstrated that SP9 can impact the intracellular calcium homeostatic in OVCAR3 cells via inducing ER calcium release, mitochondrial and cytosolic calcium increase.

Our previous data proved that the cytostatic effect of SP9 can be inhibited by digoxin (Figure 4.6), subsequently Ca^{2+} rescue effect to SP9 induced cell death also be verified which support our conjecture that SP9 might cause cell death through calcium signal pathway, so we wonder if digoxin also restrain the calcium signal alteration motivated by SP9. Before adding 2μM SP9 to the transfected cells, we pretreated these transfected cells with 7.5μM digoxin 5 hours, then conducted the same procedure with no digoxin pretreated group as control group. In Ca^{2+} free HBSS buffer, it was observed that cytosolic and mitochondria

calcium signal show no detectable change when 2 μM SP9 is added compare with control group (black curves), but it showed similar tendency with control group after 2mM extracellular Ca^{2+} is added (Figure 4.12 A left and middle plot), whereas ER calcium signal maintained steady in whole course (Figure 4.12 A right plot). In 1.2 mM Ca^{2+} HBSS buffer, SP9 supplement still arouse mitochondria calcium signal increment but relatively light (from 3 folds to 1.5 folds compare with control group as shown in Figure 4.12 B middle plot), cytosolic calcium concentration showed no apparent change (Figure 4.12 A left plot) and ER calcium signal lowered steadily (Figure 4.12 A right plot), this result might issue from the fact that the extracellular Ca^{2+} is already existing, and the 2 mM Ca^{2+} did not alter the calcium signal trend of cells with or without digoxin pretreatment anymore.

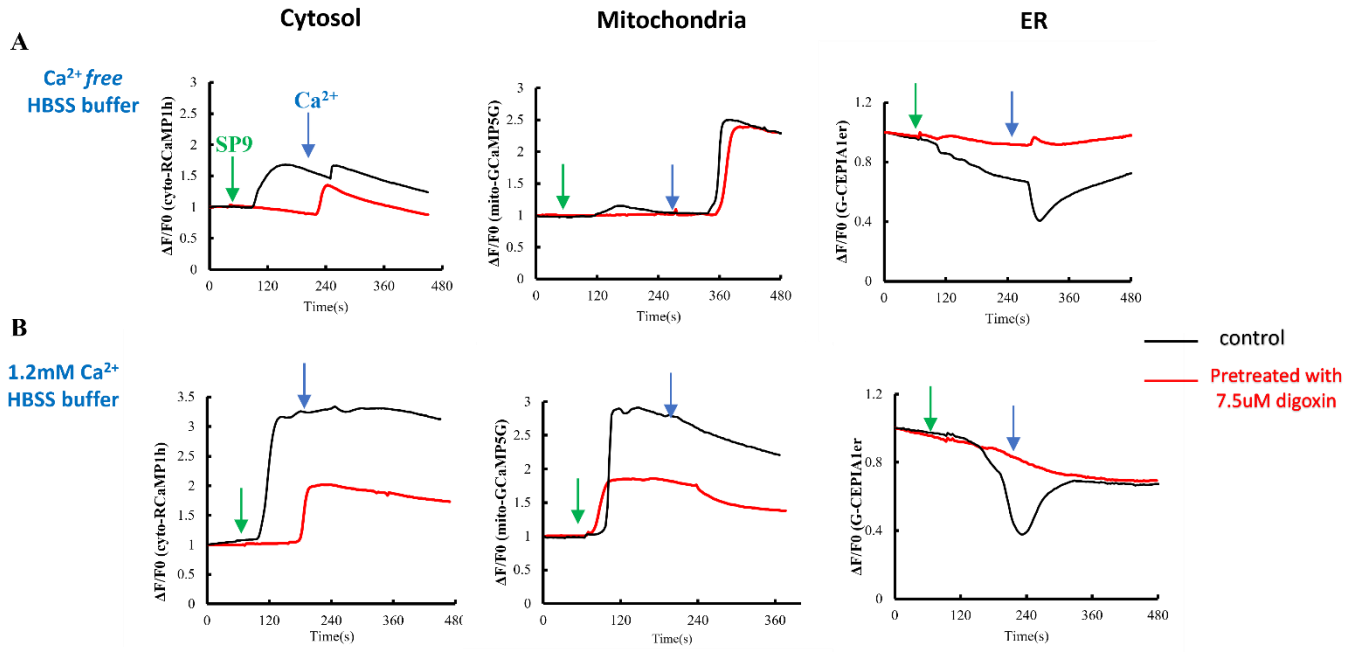

Figure 4. 12 SP9 disrupts intracellular calcium homeostasis in OVCAR3 cells and digoxin mitigates this effect A. From left to right, the relative fluorescence ratio of plasmid cyto-RCaMP1h indicated the changes of cytosolic calcium; the relative fluorescence ratio of plasmid mito-GCaMP5G indicated the changes in mitochondrial calcium; the relative fluorescence ratio of plasmid G-CEPIA1er indicated the changes in ER calcium. Transfected OVCAR3 cells were cultured in extracellular Ca^{2+} free HBSS buffer B. Transfected OVCAR3 cells were cultured in extracellular 1.2mM Ca^{2+} HBSS buffer. Green arrow indicates that cells are treated with 2μM SP9 at around 1min point, bule arrow indicates that additional 2mM $CaCl_2$ are added at the around 4 min point. Black curves indicate transfected OVCAR3 cells without any pretreatment. Red curves indicate the transfected OVCAR3 cells have been pretreated with 7.5μM digoxin 5 hours before the assay.

Overall, the addition of Ca^{2+} has been observed to modify the impact of SP9 on calcium signalling, attenuating the cytotoxic effects of SP9 through a rescue mechanism. This rescue effect was further substantiated by the counteractive response of the cell-permeant Ca^{2+} chelator BAPTA-AM (Figure 4.11). Our quantitative data additionally confirmed that SP9 influences calcium homeostasis by inducing the release of ER calcium, as well as increasing mitochondrial and cytosolic calcium levels (Figure 4.12 black curve). Consequently, we posit that SP9-induced cell death is associated with calcium signalling pathways. This supposition was further supported by our observation of calcium signal levels following pretreatment with digoxin in OVCAR3 cells. The results demonstrated that digoxin could restrain the fluctuation in calcium signalling induced by SP9 (Figure 4.12 red curve), affirming that digoxin can inhibit the cytostatic effects of SP9 by suppressing the alteration in calcium flux caused by SP9.

4.5 Evaluation of the anti-proliferative effectiveness of Beclin 1-targeting stapled peptides in an animal-based model of ovarian cancer

4.5.1 Optimized Beclin 1-targeting stapled peptides demonstrate potent anti-proliferative efficacy in ovarian cancer model

After confirming the cytostatic ability of our optimized Beclin 1-targeting stapled peptide in ovarian cancer cells, we further verify its anti-tumor potency in vivo

study. In our previous cellular experiments, OVCAR3 is one of the most sensitive ovarian cancer cell lines to SP9 and it has high tumor formation rate in vivo. Thus, the in vivo anti-proliferative efficacy of SP9 to ovarian cancer was studied on OVCAR3 xenograft model. We established the xenograft model by subcutaneously implanting 5×10^6 OVCAR3 cells on 4 to 6-week-old female nude mice. It takes about 20 days for tumor volume reached $100mm^3$ and the administration was started from that time point. The dosage of 10mg/kg SP9 were administrated via daily intraperitoneal (i.p.) injection and PBS was injected to mice in control group as placebo. The anti-tumor effect of SP9 in vivo was evaluated by measuring tumor volume.

The tumor volume was defined as $width^2 \times length/2$. The tumor volume was recorded every other day and drawn as growth curve shown in Figure 4.13 A, demonstrating that SP9 treated group can restrain the tumor growth by reducing the tumor volume significantly. After 25 days post-treatment, all tumors were harvested and weighed up. The results showed that SP9 treated group can prohibit the tumor growth with notably lower tumor weigh as compare with control group (Figure 4.13 B and C). The body weight of animal was also recorded every other day as shown in Figure 4.13 D, presenting no significant difference between SP9 treated group and control group. Furthermore, there were no discernible color or morphological abnormalities in the organs (Figure 4.13 E), suggesting the absence of toxic effects of SP9 on the organism at the effective dosage of 10mg/kg.

In short, the in vivo animal experiment revealed that our optimized Beclin 1-targeting stapled peptide displayed notable anti-proliferative efficacy (Figure 4.13), as evidenced by the deceleration of tumor growth and reduction in tumor weight in the OVCAR3 cell-driven xenograft model, without any observable toxic side effects.

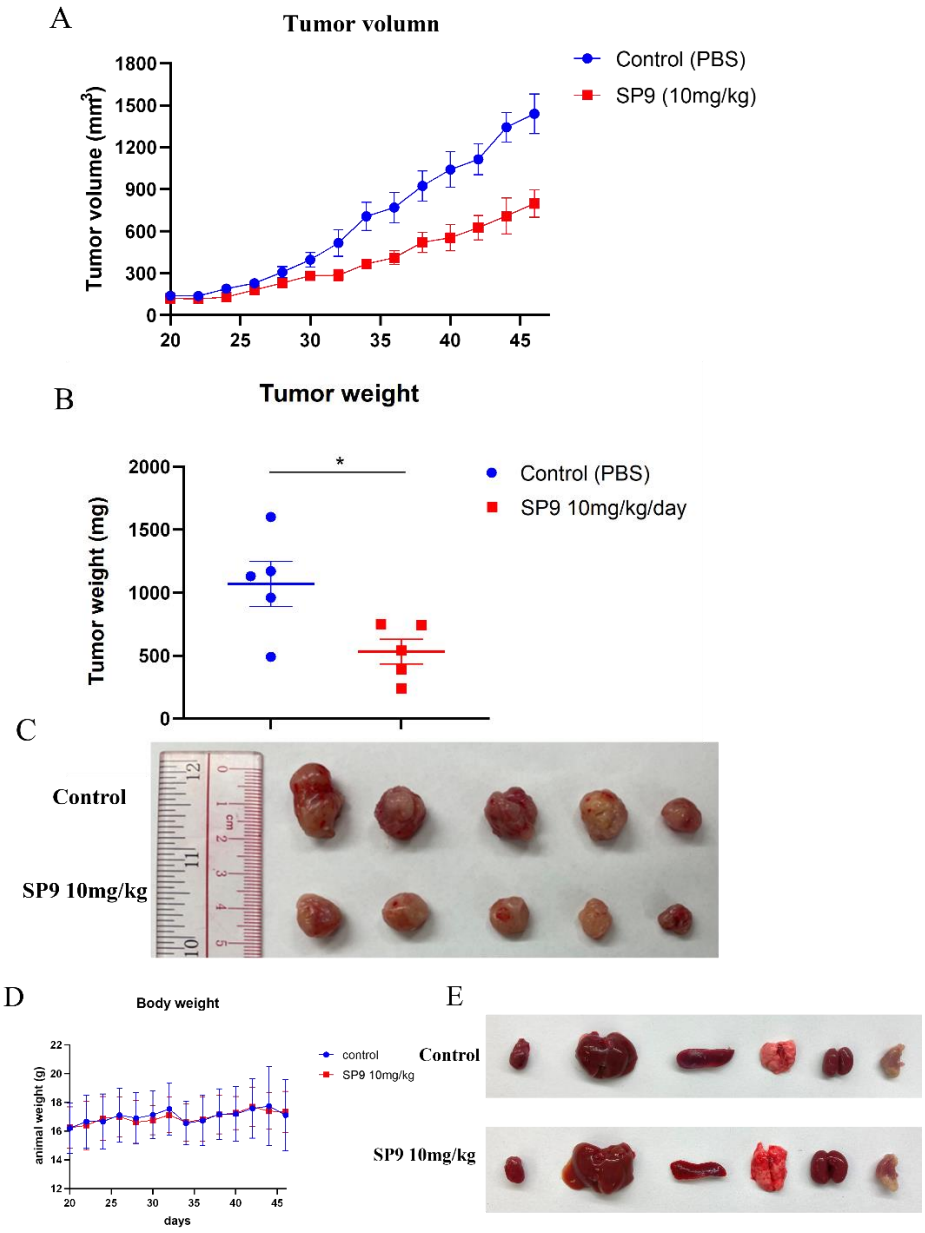

Figure 4. 13 The anti-tumor effect of SP9 and cisplatin in OVCAR3 xenografts animal model. A. The tumor growth curve of OVCAR3 xenograft animal model. 5×10^6 OVCAR3 cells were subcutaneously injected into nude mice. The administration of 10mg/kg SP9 when the tumor volume reached about 100 mm^3(assigned as day0). The tumor volume was recorded every other day. B. The plot of tumor weight on Day 25. Data represents mean ± SEM, n=5; *P< 0.05; unpaired t-test. C. Image of tumors at the end of time point (Day 25) from each treated group. D. The changes of mice body weight during treatment for each group. E. Image of vital organs from control group and SP9 treated group.

4.6 Enhanced cell death efficacy of Beclin 1-targeting stapled peptides and chemotherapeutic drugs combination treatment in ovarian cancer cells.

4.6.1 The combination treatment of Beclin 1-targeting stapled peptides and cisplatin shows stronger cell death efficacy than drug alone in ovarian cancer cells.

Cisplatin is one of the most frequently used chemotherapy to ovarian cancer treatment, its efficacy is impressive in the early stage of therapeutic scheme but inevitably develop with cisplatin resistance and tumor recurrence in later stage. Combination therapy with cisplatin is recommended to overcome these limitations in ovarian cancer treatment. We next investigate the cytostatic effect of SP9 and cisplatin combination treatment to ovarian cancer cells. Cell survival plot data showed the significant difference of the cell viability between 2.5μM cisplatin group with or without 2μM SP9 addition in ovarian cancer cell lines (Figure 4.14 A). In OVCAR3, cisplatin cell death rate of combination treatment group (SP9 + cis) is about 47.2%, the cell death rate of only cisplatin group and only SP9 group is 30.1% and 3.5% respectively (Figure 4.15 A. left), which proved that the inhibitory effect of combination group is not only stronger than single drug but also greater than the sum of individual effects of any of them. Akin result is observed in SK-OV3 cell lines that SP9 and cisplatin combination treatment show stronger cytotoxicity than individual treatment (Figure 4.14 A.

right), implying the SP9 and cisplatin might exert synergistic effect in ovarian cancer cells. However, when we performed the same combination scheme with non-cancer cell lines LO-2 and HEK-293 cells, data presented that the cell death rate of combination group exhibits no substantial difference from the single drug (Figure 4.14 B), indicating there may not have combination effect of SP9 and cisplatin in non-cancer cell line.

To study this combination effect in different effective dosage of SP9, we measured the 48 hours IC50 value of SP9 with or without the exposure of 2.5μM cisplatin. The results showed that 48 hours IC50 value of SP9 in OVCAR3 and SK-OV3 is about 7.109μM and 6.621μM respectively, while the IC50 value decline to 1.78μM and 2.81μM respectively with the cotreatment of 2.5μM cisplatin (Figure 4.14 C and D). Then, we further confirm the efficacy of combination treatment by performing the colony formation assay, which is considered as gold standard for determining the potency of cytotoxic agents on cancer cells in vitro, it facilitate to visualize cell growth ability after combination treatment. Ovarian cancer cells were seeded in 6-wells cell culture plate then treated with single agent of SP9, cisplatin, and combination treatment of these two agents at different concentration as shown in Figure 4.14 E and F. Results demonstrated that combination treatment of SP9 and cisplatin exert stronger growth inhibition effect to colony formation than individual agent treatment in ovarian cancer cells by dosage dependent, which are corresponding with the cell

viability assay in 96-wells cell culture plate (Figure 4.14 A, C and D), suggesting cisplatin and SP9 exert synergistic effect in ovarian cancer cells.

Taken together, our cellular studies demonstrated that the combination treatment of cisplatin and SP9 presented increased potency of inducing cell death in ovarian cancer cell lines compared to individual drug treatments, with no significant impact observed in non-cancerous cell lines.

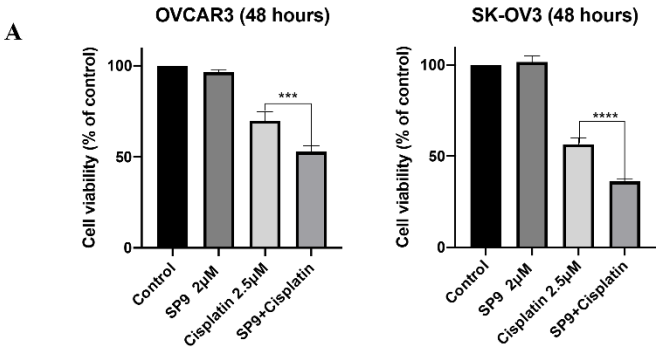

Cell death rate:

OVCAR3 (48 hours)		SK-OV3 (48 hours)	
Cis: 30.1%		Cis: 43.5%	
SP9: 3.5%	SP9+Cis:47.2%	SP9: 0%	SP9+Cis:63.8%

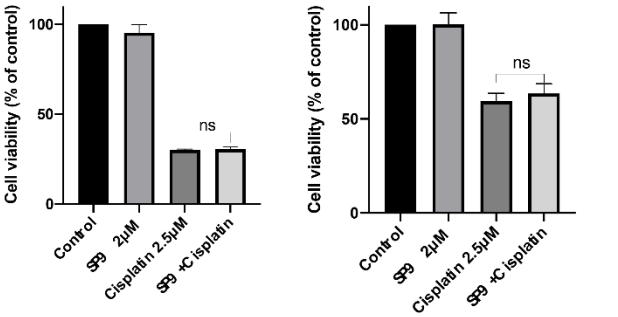

Cell death rate:

L-O2 (48 hours)		HEK293 (48 hours)	
Cis: 69.90%		Cis: 40.70%	
SP9: 4.83%	SP9+Cis: 69.54%	SP9: 0%	SP9+Cis: 36.58%

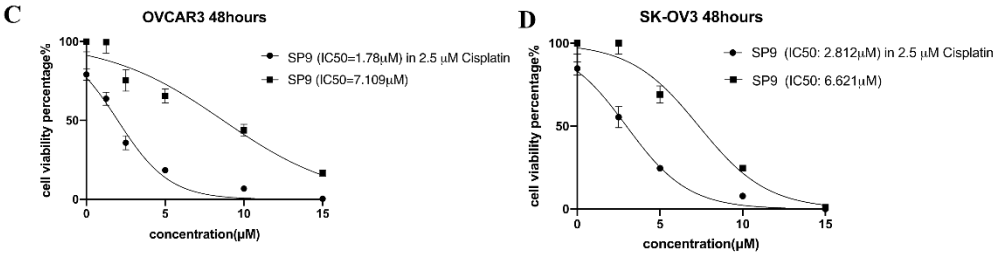

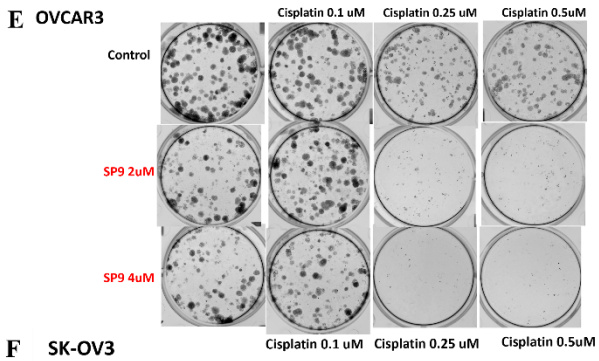

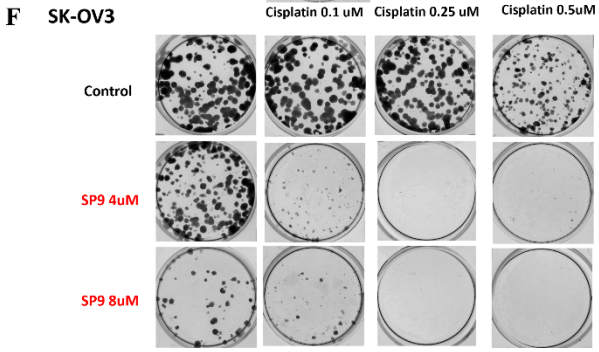

Figure 4. 14 The cytostatic effect of SP9 and cisplatin combination treatment. A. The survival plots of ovarian cancer cell lines OVCAR3 and SK-OV3 treated with indicated concentration of single drug (SP9 and cisplatin) and combination treatment. B. The survival plots of non-cancerous cell lines LO-2 and HEK293 treated with indicated concentration of single drug (SP9 and cisplatin) and combination treatment. C. The determination of 48 hours IC50 value of SP9 in OVCAR3 cells. D. The determination of 48 hours IC50 value of SP9 in SK-OV3 cells. E. Colony result of OVCAR3 treated with indicated concentration of SP9 and cisplatin. F. Colony result of SK-OV3 treated with indicated concentration of SP9 and cisplatin Results shown represent mean ± SEM (n=5). ns, not significant, ***P <0.001, **** P<0.0001; t-test.

4.6.2 Combination index indicates the synergistic effect of cisplatin and Beclin 1-targeting stapled peptides in vitro.

To further verify the synergistic effect of cisplatin and SP9 in ovarian cancer cell lines, we calculate the combination index based on the multiple drug-effect equation of Chou-Talalay with CalcuSyn software. The 1:1 constant ration was adopted to SP9 and cisplatin combination treatment, the Dose-effect curve and Fa (Fraction affected)-CI plot are obtained to reflect the relationship between effective dosage and combination index (Figure 4.15). Fa values was calculated by CalcuSyn software based on the standard Trypan Blue exclusion assay data. CI values change with Fa, the averaged CI of SP9 and cisplatin mixture at ED (Effective Dosage)50, ED75, and ED90 are used and summarized in table 4.2. It is shown in table that all CI value at specific ED is less than <1 in both ovarian cancer cell lines OVCAR3 and SK-OV3, affirming the synergistic effect of SP9 and cisplatin combination in vitro.

The dose-reduction index [30] quantifies the extent to which the individual doses of the drugs can be reduced when used in combination compared to when used alone, while still achieving the same level of effect, so the DRI is important in clinical situations, where dose-reduction leads to reduced toxicity toward the host while retaining the therapeutic efficacy. A DRI greater than 1 indicates that the combination is more effective than the individual drugs alone, allowing for a reduction in the doses of the drugs while achieving the desired therapeutic effect. This is particularly important in reducing potential side effects and toxicity

associated with higher drug doses. The higher the DRI value, the greater the degree of synergy. Table 4.2 displayed the DRI parameters for SP9 and cisplatin at different Fraction affected and DRI values are greater than 1 at all Fraction affected (except Fa<0.2 in OVCAR3 cell lines). With CalcuSyn software analyzation, we obtain the CI and DRI data to validate the synergism of SP9 and cisplatin in ovarian cancer cells in vitro.

Table 4. 1 Combination index values at ED50, ED75 and ED90, Dm, m and linear correlation coefficient r.

Drug	ED 50	ED75	ED90	Dm	m	r
Mixture (SP9+Cisplain) OVCAR3	**0.71875**	**0.61363**	**0.52555**	2.53254	2.67339	0.98308
Mixture (SP9+Cisplatin) SK-OV3	**0.50269**	**0.44647**	**0.39703**	1.90155	2.66893	0.97998

Dm is the median-effect dose signifying the potency. It is determined from the x-intercept of the median-effect plot; m is an exponent signifying the sigmoidal (shape) of the dose effect curve, which is determined by the slope of the median- effect plot.

Table 4. 2Dose-Reduction Index parameters for SP9 and cisplatin

OVCAR3	DRI		SK-OV3	DRI	
Fa	**SP9**	**Cisplatin**	**Fa**	**SP9**	**Cisplatin**
0.002890	**0.837**	**0.022**	0.0477612	**2.2130**	**2.959**
0.190751	**4.949**	**0.835**	0.0686567	**2.7107**	**1.766**
0.690751	**8.748**	**3.787**	0.549254	**11.8805**	**3.203**
0.864162	**7.873**	**5.284**	0.904478	**34.9867**	**4.107**
0.945087	**9.178**	**9.346**	0.955224	**53.6699**	**3.977**

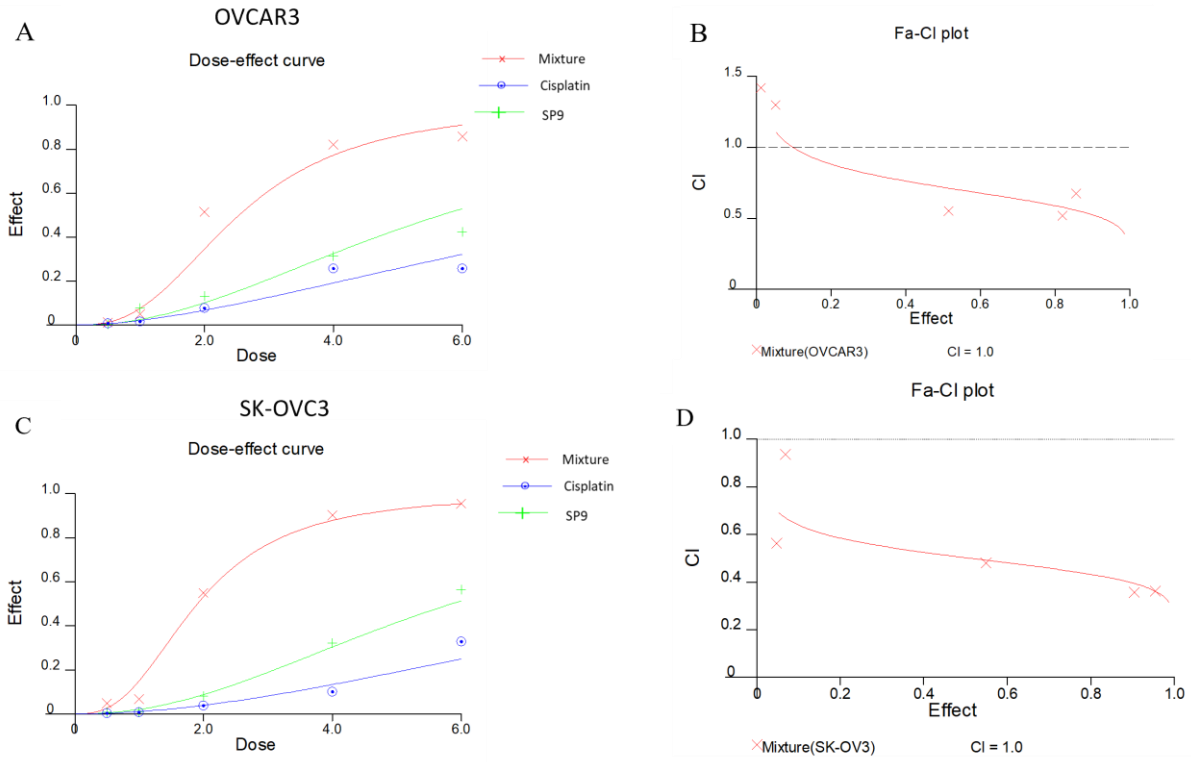

Figure 4. 15 The dose-effect curve and Fa-CI plot generated by CalcuSyn software base on the survival data of combination treatment in ovarian cancer cell lines. A. Dose-effect curve of OVCAR3 for SP9, cisplatin, and Mixture (SP9 mixed cisplatin in 1:1 constant ratio), respectively. Dose unit is μM. B.CI value-Fa (Fa: fraction affected level) curve for Mixture generated from CalcuSyn based on the dose-response curves shown in (A). It demonstrated that synergistic effect is starting from 10% effective level (Fa = 0.1) and this synergistic effect continues to increase (CI < 1) at higher effect levels in Mixture. C. Dose-effect curve of SK-OV3 for SP9, cisplatin, and Mixture (SP9 mixed cisplatin in 1:1 constant ratio), respectively. Dosage unit is μM. D.CI value-Fa (Fa: fraction affected level) curve for Mixture generated from CalcuSyn based on the dose-response curves shown in (C). It demonstrated that synergistic effect is starting from very low effective level (Fa > 0) and this synergistic effect continues to increase (CI < 1) at higher effect levels in Mixture.

4.6.3 Lack of synergistic effect of Beclin 1-targeting stapled peptides and cisplatin in ovarian cancer cell derived xenograft animal model.

Based on our previous in vivo study, the tumor inhibition effect of 10mg/kg SP9 is verified in OVCAR3 cells xenograft animal model (Figure 4.14). Therefore, we determined the dosage scheme as 10mg/kg SP9 every day and 0.75mg/kg cisplatin twice a week and their combination (10mg/kg SP9 and 0.75mg/kg cisplatin), PBS as placebo in control group, all treated group were administrated via i.p. injection The tumor volume was recorded every other day and drawn as growth curve shown in Figure 4.16 A, demonstrating that all treated group can restrain the tumor growth by decreasing the tumor volume compare with control group. After 25 days post-treatment, all tumors were harvested and weighed up. The results suggest that all treated group can reduce the tumor growth, and combination group with cisplatin and SP9 showed the most prominent efficacy with the lowest tumor weight (Figure 4.16 B and C). Though our results suggested the combination treatment can repress tumor growth more significantly than single drug in vivo compare with control group, the combination effect showed no significance between combination group and single agent treated group neither cisplatin nor SP9 (Figure 4.16.C).

The body weight of animal was also recorded every other day as shown in Figure 4.16 D, presenting cisplatin and combination group caused notable body weight loss. From the observation of major organ, the morphological abnormality of liver is observed in cisplatin and combination group but not in single SP9 treated group

(Figure 4.16 E Arrows). Accordingly, we consider the toxicity effect might attribute to the side effect of chemotherapy. Besides, spleen augmentation is observed in this OVCAR3 xenograft model (Figure 4.16 Blue arrow with dashed), yet all treated group presents notably abbreviated spleen, especially the combination group. It is known that increase in size of the spleen in response to the presence of transplanted cancer cells. The growth and proliferation of cancer cells in the host organism can lead to an increased workload for the immune system, including the spleen. This increased tumor burden can contribute to the enlargement of the spleen as it works to combat the presence of cancer cells. This phenomenon not only reflect the anti-proliferative efficacy of treatment to tumor growth but also provide valuable insights into the interactions between the immune system and cancer cells.

In summary, we conducted cell viability and colony formation assays to investigate the combined effect of our Beclin 1-targeting stapled peptide and a chemotherapeutic agent at the cellular level. The preliminary results demonstrated that combination treatment exerts more significant anti-proliferative effect than individual drug treatment, indicating synergistic effect of SP9 and cisplatin (Figure 4.14). Additionally, the combination index (CI) and dose reduction index (DRI) were utilized to assess the combined effect of SP9 and cisplatin. The synergism between SP9 and cisplatin was confirmed through analysis using CalcuSyn software (Figure 4.15, Table 4.1 & 4.2). Furthermore, in vivo studies were conducted to evaluate the anti-proliferative effect of the

combination treatment of SP9 and cisplatin in OVCAR3 xenograft animal models. While the combination treatment potentiated the inhibition of tumor growth, no apparent synergistic effect was observed in this animal model (Figure 4.16). It is suggested that other suitable ovarian cancer animal models be considered to further investigate the combined effect of our Beclin 1-targeting stapled peptides and chemotherapeutic agents in in vivo studies.

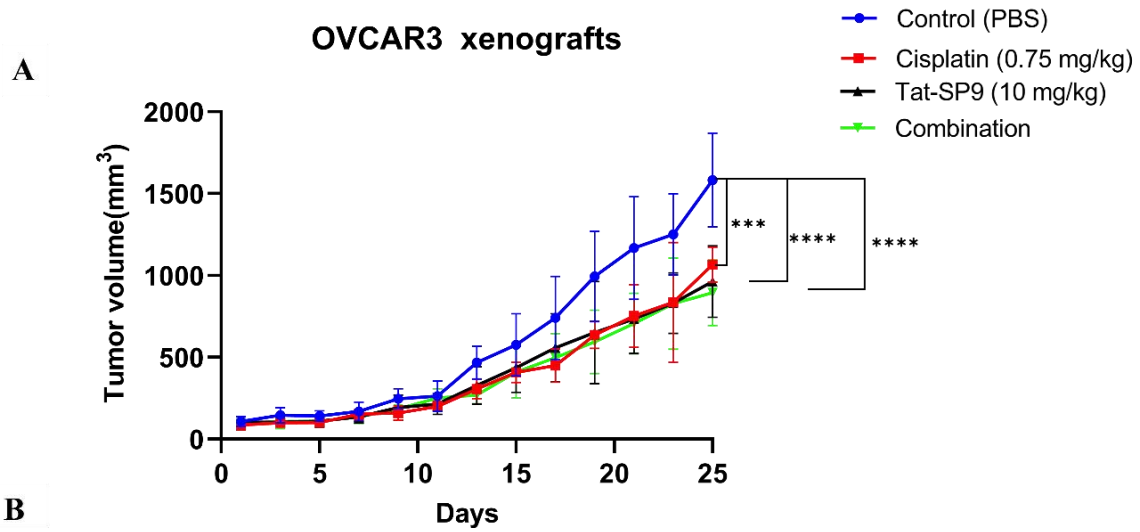
A
OVCAR3 xenografts
Control (PBS)
Cisplatin (0.75 mg/kg)
Tat-SP9 (10 mg/kg)
Combination
Tumor volume(mm3)
2000
1500
1000
500
0
0
5
10
15
20
25
Days
***
****
****


B
Control(PBS)
Cisplatin (0.75mg/kg)
SP9 (0.75mg/kg)
Combination

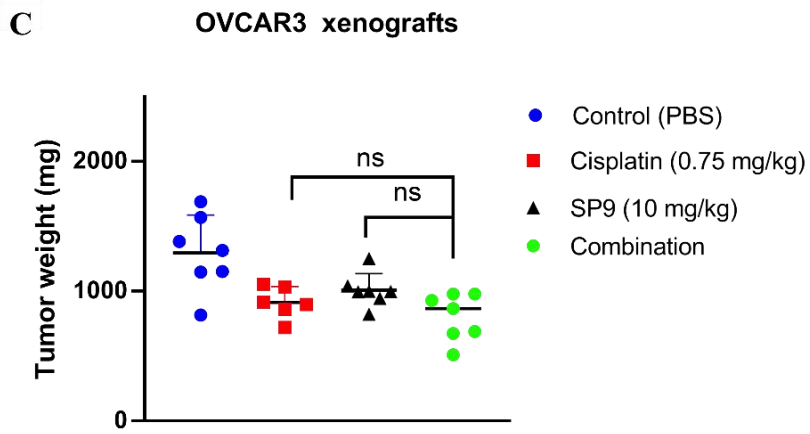
C
OVCAR3 xenografts
Tumor weight (mg)
2000
1000
0
ns
ns
Control (PBS)
Cisplatin (0.75 mg/kg)
SP9 (10 mg/kg)
Combination

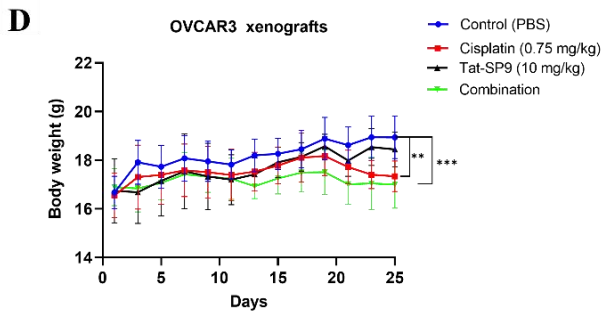
D
OVCAR3 xenografts
Control (PBS)
Cisplatin (0.75 mg/kg)
Tat-SP9 (10 mg/kg)
Combination
Body weight (g)
22
20
18
16
14
0
5
10
15
20
25
Days
**
***

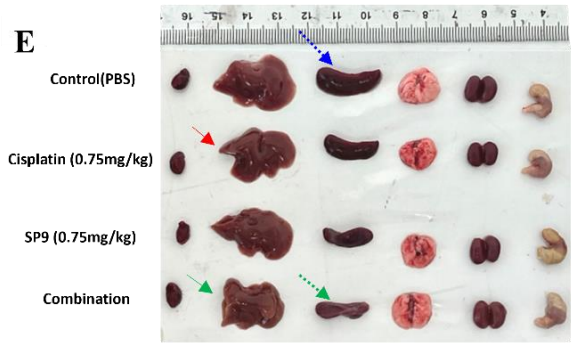
E
Control(PBS)
Cisplatin (0.75mg/kg)
SP9 (0.75mg/kg)
Combination

Figure 4. 16 The anti-tumor effect of SP9 and cisplatin in OVCAR2 xenografts animal model. A. The tumor growth curve of OVCAR3 xenograft animal model. 5×10^6 OVCAR3 cells were subcutaneously injected into nude mice. The administration of 10mg/kg SP9, 0.75mg/kg and combination (10mg/kg SP9 and 0.75mg/kg cisplatin) when the tumor volume reached about 100 mm^3(assigned as day0). The tumor volume was recorded every other day. Data represents mean ± SEM, n=7; ***P<0.001; ****P<0.0001; One-way ANOVA. B. Image of tumors at the end of time point from control and all treatment groups. C. The plot of tumor weight on Day 25. Data represents mean ± SEM, n=7; *ns*> 0.05; unpaired t-test. D.The changes of mice body weight during treatment for each group. E. Image of vital organs from each group. Regular arrows indicate liver morphology abnormality, blue arrow with dash shows the spleen augmentation, green arrow with dash shows spleen shrinkage.

5.Discussion and future work

Autophagy, a cellular self-degradation process, is perceived as a complex factor in oncological treatment, with its role contingent upon the specific cancer type and disease stage [157]. Proper manipulation of autophagy can augment anti-neoplastic efficacy and inhibit tumor relapse. Current oncological research is heavily focused on the modulation of autophagy within neoplastic cells. Beclin 1 is a pivotal protein in the regulation of autophagy, which collaborates with other factors such as Atg14L, UVRAG, Rubicon, and Ambra1 to modulate the lipid kinase Vps34 protein. This interaction promotes the formation of the Beclin 1-Vps34/Vps15 core complex, thereby regulating autophagic activity [158]. Despite the long-standing identification of Beclin 1 as a tumor suppressor [86], modulating Beclin 1 or Beclin 1-mediated autophagy activity for oncological therapy remains a challenging endeavor.

Our laboratory has previously demonstrated that the Beclin 1 coiled-coil domain can readily form a dissociable homodimer, facilitating ATG14 and UVRAG binding to the Beclin 1 coiled-coil domain [91]. Our research is pioneering in its design of a stapled peptide that disrupts the self-association of Beclin 1 and boosts the consitution of the Beclin 1-Atg14L or -UVRAG complex to regulate autophagy [91]. We have engineered a series of Beclin 1-derived stapled peptides that target the coiled-coil domain of Beclin 1. Our in vitro study revealed that these peptides not only exhibit strong binding affinity to Beclin 1 but also remarkably inhibit the self-association of the Beclin 1 coiled-coil domain and

promote the formation of the Beclin 1–Atg14L/UVRAG complex [97]. We further optimized the designed peptides Tat-SP4 by introducing new staples and residue mutations, resulting in a new generation peptide with a stronger binding affinity to Beclin 1 [159]. Our previous research identified two peptides, i7-01s-20 and i7-01s-31, which demonstrated binding affinities approximately 10-fold and 30-fold greater than Tat-SP4, respectively. Evaluation of these peptides' impact on cellular autophagic activity, via detection of LC3 and p62 protein levels, confirmed that the optimized Beclin 1-targeting stapled peptides effectively stimulate autophagy. Of these, peptide i7-01s-31, now referred to as SP9 in this project, was selected for further investigation.

Ovarian cancer, characterized by late-stage diagnosis and the highest mortality rate among all gynecological cancers, currently lacks specific early-stage biomarkers and effective curative treatments [8]. Consequently, the prognosis remains poor with existing therapies, underscoring the urgent need for more potent interventions. Our prior research demonstrated that the novel peptide SP9 exhibits a stronger binding affinity to the tumor suppressor Beclin 1 compared to its predecessor, Tat-SP4, following optimization. Furthermore, anti-proliferative effect of SP9 on cancer cells has been corroborated, and its capacity to induce autophagy has been confirmed. Given the increasing interest in the potential of autophagy activators as adjunctive therapies in ovarian cancer treatment, SP9 is anticipated to be a promising agent of ovarian cancer therapy.

Our optimized Beclin 1-targeting stapled peptides exhibited potent anti-proliferative efficacy in vitro with using a panel of ovarian cancer cell lines: SK-OV3, OVCAR3, HEY-T30 and CAOV3. These four cell lines all belongs to High-grade serous ovarian cancer (HGSC) which is the most common and aggressive type of epithelial ovarian cancer, and the epithelial tumor is the most common type in ovarian cancer [160]. Whereas it is found that relatively low cytotoxicity of SP9 in non-cancer cells compare with ovarian cancer cells, suggesting SP9 might provide a therapeutic window between efficacy and toxicity for ovarian cancer treatment. Chemotherapy remains the first line treatment of ovarian cancer, yet the toxicity side effect and chemo resistant issues are unneglectable [161]. Our findings demonstrated that SP9 presents significant anti-proliferative effects on ovarian cancer cells, while displaying lower cytotoxicity towards non-cancerous cells in comparison to conventional chemotherapeutic agents. These results suggested that our Beclin 1-targeting stapled peptides, through its distinct mechanism, may offer a therapeutic advantage by providing a favourable balance between efficacy and toxicity for the treatment of ovarian cancer.

Subsequently, we explored the combined application of SP9 and cisplatin, a platinum-based chemotherapeutic agent commonly utilized for advanced ovarian cancer. Despite its demonstrated efficacy in enhancing survival rates in patients with advanced disease, cisplatin's effectiveness can be curtailed by the emergence of drug resistance, a prevalent challenge in ovarian cancer treatment. To mitigate

toxicity and circumvent cisplatin chemoresistance, combination therapy is frequently implemented, integrating cisplatin with other pharmaceutical agents or treatment approaches to achieve superior therapeutic outcomes. Our cellular-level findings demonstrated a synergistic interaction between SP9 and cisplatin. This synergy was further substantiated by the combination index (CI) and dose-reduction index (DRI). However, this synergy effect failed to be validated with *in vivo* OVCAR3 xenograft model. For this result we consider the administration dosage scheme of combination treatment need to be further optimized to achieve enhanced outcome of tumor inhibition. Furthermore, we suspect the immunocompromised characteristic of xenograft model may also contribute to the lack of synergistic effect. Thought the cytotoxic effect of cisplatin is independent of immune system activation, the combination of cisplatin may lead to enhanced antitumor effects through various immune pathways such as the modulation of tumor microenvironment by reducing immunosuppressive factors [162] and immunomodulatory effects with releasing of tumor-associated antigens. These effects may complement the action of SP9 combined with cisplatin. Therefore, the immunocompetent animal model and the precise mechanism underlying this synergistic interaction with cisplatin warrants further investigation.

In this study, it is already proved SP9 induce cell death predominantly rely on autosis, which is a form of cell death that can stimulate an immune response [163]. Besides combination with cisplatin, our previous study has proved that the

prototype Tat-SP4 may confer potential synergy with anti-PD1 approach. We found Tat-SP4 induce autosis with the release of ATP and damage-associated molecular patterns (DAMPs) in hepatoma carcinoma cell, indicating our designed peptides can trigger immunogenic cell deaths. In 2022, Zheng et al. demonstrates that myxoma virus-infected T cells can induce autosis in cancer cells, enhancing the effectiveness of immunotherapy and overcomes resistance [164]. With anti-PD-1 therapy working to block the interaction between PD-1 on T cells and PD-L1 on tumor cells [165], we suspect SP9-elicited autosis function may active immune response to achieve synergy effect for tumor clearance. We believe our autophagy-targeting peptide SP9 exhibit potential as robust anti-tumor therapeutic candidates for use in combination with existing therapies to enhance treatment outcomes for cancer.

It is well-established that cisplatin primarily induces cell death in ovarian cancer through its interaction with DNA, thereby activating the p53-dependent apoptotic pathway [166]. For mechanistic studies of SP9-caused cell death, our findings showed that SP9-induced cell death could be rescued by autosis inhibitor, digoxin, but not other inhibitors of other programmed cell death. Cardiac glycoside-induced toxicity is associated with excessive inhibition of Na^+/K^+-ATPase, accumulation of Ca^{2+} ions [167]. Autosis is a Na^+/ K^+-ATPase–regulated form of programmed cell death that is characterized by the presence of autophagic features and is dependent on the presence of functional autophagy-related genes [163]. With using autophagy inhibitor 3-MA, our result proved that SP9-induced

cell death can be rescued by 3-MA exposure, suggesting autophagy activity is involved in SP9-triggered cell death event. Though we proved the effect of SP9 depend on autophagy, Beclin-1 targeting efficiency need to be further confirm given off-target effect might exist. Our lab has been adopted BECN 1 knockout HEK cells and BECN 2 knockout HEK cells to access the cytotoxic effect of prototype Tat-SP4, the results found there is no significance difference between wild type HEK and BECN 1 or BECN 2 knockout cells toward cytostatic effect of SP9. It is understandable given BECN 1 and BECN 2 may compensate for each other for executing Beclin-1 function in single knockout cells. Whereas double knockout of BECN 1 and BECN 2 is not recommended to perform in cells, since it might lead to significant effects on the cellular autophagy process and overall cell function [168], given the essential role of Beclin 1 in cells.

Additionally, calcium ions in autosis cell death has been a subject of research interest, as calcium signalling is known to play a crucial role in various cellular processes [145]. Research has posited that calcium signalling may play a role in the inhibition of autosis cell death [169], a notion supported by our findings. Our data revealed that the introduction of Ca^{2+} can modulate the effects of SP9 on calcium signalling, mitigating cytotoxic effects of SP9 via rescue mechanism. This rescue effect was further corroborated by the counteractive response elicited by the cell-permeant Ca^{2+} chelator. We believe the extra Ca^{2+} influx can counteract the imbalance of calcium homeostasis caused by SP9 in ovarian cancer cells, resulting in mitigation effect to SP9 cytotoxicity effect. Quantitative

analysis of calcium signalling confirmed that SP9 disrupts calcium homeostasis by inducing the release of endoplasmic reticulum (ER) calcium and elevating mitochondrial and cytosolic calcium levels. Changes in mitochondrial calcium levels influence the activity of proteins involved in autophagy, we believe Ca^{2+} influx caused by SP9 contribute to the cytostatic effects of SP9 by regulation of autophagy, yet the specific target need to be further investigated. As hypothesized, digoxin was able to curb the SP9-induced fluctuations in calcium signalling, thereby validating that digoxin can inhibit the cytostatic effects of SP9 by suppressing the alterations in calcium flux instigated by SP9.

In addition, calcium signalling has been implicated in the regulation of mitochondrial function [170], and dysregulation of mitochondrial calcium levels can lead to mitochondrial dysfunction and the initiation of cell death pathways, including autosis [171]. Autosis is also characterize as defective mitochondria with electron dense morphology changes [163]. Consistently, our optimized Beclin 1-targeting stapled peptides SP9 triggered cell death was accompanied by mitochondrial dysfunction including accumulation of Reactive oxygen species (ROS), depolarization of mitochondria membrane potential (MMP), and reduction in mitochondrial permeability transition pore (MPTP) opening and mitochondrial oxidative phosphorylation (OXPHOS) activity. ROS are byproducts of OXPHOS and can cause MMP depolarization. This depolarization can trigger the opening of the mPTP, leading to mitochondrial dysfunction and ultimately, cell death [115]. In cancer cells, elevated ROS levels can induce DNA

damage and genomic instability, contributing to cancer progression[172]. However, excessive ROS can also trigger cell death, suggesting a potential therapeutic strategy. Changes in MMP, often observed in cancer cells, the opening of MPTP can lead to cell death, providing another potential therapeutic target [173]. In line with our data that SP9 induces cell death along with depolarization of MMP, enhanced ROS level and mPTP opening in dosage dependent manner. Furthermore, researcher found that tumor cells desensitize the PTP to Ca^{2+} and ROS increasing their resistance to death. OXPHOS, though typically reduced in many cancer cells in favor of glycolysis (the Warburg effect), has been found to be upregulated in some ovarian cancers. This metabolic shift may contribute to chemoresistance, and targeting OXPHOS could potentially enhance the effectiveness of cancer treatments. Our findings revealed that SP9 can reduce OXPHOS activity, this might also explain the synergies between SP9 and cisplatin in ovarian cancer cells.

Next, we further validated the anti-neoplastic efficacy of SP9 through in vivo studies utilizing an OVCAR3 cell xenograft model. Our findings demonstrated that SP9, at a dosage of 10mg/kg, significantly impeded tumor growth and reduced tumor weight, with no discernible toxicity observed. Hence, the combined effect of SP9 and cisplatin was investigated in vivo using animal models. However, our findings indicate that the combination treatment only marginally enhances the inhibition of tumor growth in OVCAR3 xenograft animal models, without demonstrating a clear synergistic effect. Furthermore, the

combination treatment resulted in toxic side effects, which were not observed in the group treated with SP9 alone. Previous studies have shown that cisplatin enhances immune recognition and immune-mediated tumor elimination in ovarian cancer [174]. It is proved that cisplatin causes increased immune activity of monocytes and cytotoxic T-cells, intensifying anti-tumor activity in a murine model of epithelial ovarian cancer [175]. Therefore, we propose that the lack of a synergistic effect between cisplatin and SP9 in our in vivo study may be attributed to the immune-compromised nature of the xenograft animal models.

For future investigations, we plan to explore more specific molecular targets to elucidate the molecular mechanism underlying the disruption of intracellular calcium homeostasis and induction of mitochondrial dysfunction by our Beclin 1-targeting stapled peptides. Our previous work has established that these peptides promote autophagy by interacting with Beclin 1 with high binding affinity and enhancing the formation of the Beclin 1-Atg14L/UVRAG complex. Based on our calcium signal and mitochondria metabolism study, we hypothesize that our designed Beclin 1-targeting stapled peptides may impact plasma membrane potential, possibly leading to Ca^{2+} influx due to the cationic TAT sequence. Given the positive charge of the Beclin 1-targeting stapled peptides, potential targets may include Ca^{2+} channel regulatory proteins such as IP3R, TOM20, and Na+/K+ ATPase [176]. We anticipate that specific Ca^{2+} channel inhibitors may block the effects of our designed Beclin 1-targeting stapled

peptides, thereby identifying the channels as potential targets. However, further efforts are required to delineate the exact molecular processes involved.

Furthermore, to enhance the therapeutic potential of our leading candidate, SP9, in the treatment of ovarian cancer, we plan to conduct additional in vivo studies to investigate its combination effects. We intend to utilize a synergic ovarian cancer model with ID8 murine cells, which closely mimics key aspects of human ovarian cancer. The ID8 model not only provides a platform for studying the complex tumor microenvironment in ovarian cancer [177], but also allows researchers to study the interactions between the tumor and the immune system in the context of ovarian cancer [178], which is crucial given the essential role of the immune response in ovarian cancer development and progression. [179].

Finally, we will assess the safety profile of our optimized Beclin 1-targeting stapled peptides using both cell- and animal-based model. Cytotoxicity will be evaluated in multiple cell lines, including normal somatic cells and human primary ovarian epithelial cells, as well as in BALB/c mice to assess acute toxicity. Additionally, haematological tests and histological structural analysis of vital organs, particularly the liver and spleen.

In summary, our lead candidate of our designed Beclin 1-trageting stapled peptides, SP9, has demonstrated potent anti-proliferative effects in a panel of ovarian cancer cell lines and has shown potential for synergistic efficacy with chemotherapeutic agents in inhibiting tumor growth. Our mechanistic studies have revealed that SP9 induces autosis cell death by interfering with calcium

signalling and mitochondrial function. The findings from xenograft animal models have confirmed the tumor inhibition effect of SP9, underscoring the potential of our designed Beclin 1-targeting stapled peptides in ovarian cancer therapy.

6.Reference

1. *American Cancer Society, Cancer Facts and Statistics*. 2023; Available from: https://cancerstatisticscenter.cancer.org/.
2. *National Cancer Institute.The Surveillance, Epidemiology, and End Results (SEER)*. 2023; Available from: https://seer.cancer.gov/statfacts/html/ovary.html). .
3. *Hong Kong Cancer Registry*. 2023; Available from: http://www3.ha.org.hk/cancereg.
4. Chen, X., et al., *Trends and projections of ovarian cancer incidence in Hong Kong: A population-based study.* Acta Obstetricia et Gynecologica Scandinavica, 2023. **102**(7): p. 942-949.
5. Khanlarkhani, N., et al., *Metabolic risk factors of ovarian cancer: a review*. JBRA Assisted Reproduction, 2021.
6. Unzeitig, V., *Contraception for the premenopausal woman.* Contraception and Family Planning, 2006. **8**: p. 143.
7. Kobayashi, H., et al., *Hereditary breast and ovarian cancer susceptibility genes.* Oncology reports, 2013. **30**(3): p. 1019-1029.
8. Stewart, C., C. Ralyea, and S. Lockwood, *Ovarian Cancer: An Integrated Review.* Semin Oncol Nurs, 2019. **35**(2): p. 151-156.
9. McLachlan, J., M. Gore, and S. Banerjee, *Targeting the mitogen-activated protein kinase pathway in low-grade serous carcinoma of the ovary.* Pharmacogenomics, 2016. **17**(12): p. 1353-1363.
10. Rojas, V., et al., *Molecular Characterization of Epithelial Ovarian Cancer: Implications for Diagnosis and Treatment.* Int J Mol Sci, 2016. **17**(12).
11. O'Shea, A.S., *Clinical Staging of Ovarian Cancer*, in *Ovarian Cancer: Methods and Protocols*, P.K. Kreeger, Editor. 2022, Springer US: New York, NY. p. 3-10.
12. Amin, M.B., et al., *AJCC cancer staging manual*. Vol. 1024. 2017: Springer.
13. Prat, J., *Staging classification for cancer of the ovary, fallopian tube, and peritoneum.* International Journal of Gynecology & Obstetrics, 2014. **124**(1): p. 1-5.
14. Arora T, M.S., Lekkala MR, *Ovarian Cancer*. 2023, Treasure Island (FL): StatPearls [Internet].
15. Jayson, G.C., et al., *Ovarian cancer.* The Lancet, 2014. **384**(9951): p. 1376-1388.
16. Orr, B. and R.P. Edwards, *Diagnosis and Treatment of Ovarian Cancer.* Hematology/Oncology Clinics of North America, 2018. **32**(6): p. 943-964.
17. Zhang, M., et al., *Roles of CA125 in diagnosis, prediction, and oncogenesis of ovarian cancer.* Biochimica et Biophysica Acta (BBA) - Reviews on Cancer, 2021. **1875**(2): p. 188503.
18. Olson, S.H., et al., *Symptoms of ovarian cancer.* Obstetrics & Gynecology, 2001. **98**(2): p. 212-217.
19. Kashiwagi, S. and H.S. Choi, *Ovarian cancer-targeted near-infrared fluorophores for fluorescence-guided surgery.* Annals of Translational Medicine, 2023. **11**(6).
20. DiSilvestro, P., et al., *Overall Survival With Maintenance Olaparib at a 7-Year Follow-Up in Patients With Newly Diagnosed Advanced Ovarian Cancer and a BRCA Mutation: The SOLO1/GOG 3004 Trial.* Journal of Clinical Oncology, 2022. **41**(3): p. 609-617.
21. Dindere, M.E., et al., *Intraoperative Tumor Detection Using Pafolacianine.* International Journal of Molecular Sciences, 2022. **23**(21): p. 12842.
22. Bose, R.N., *Biomolecular targets for platinum antitumor drugs.* Mini reviews in medicinal chemistry, 2002. **2**(2): p. 103-111.

23. Lazarević, T., A. Rilak, and Ž.D. Bugarčić, *Platinum, palladium, gold and ruthenium complexes as anticancer agents: Current clinical uses, cytotoxicity studies and future perspectives.* European journal of medicinal chemistry, 2017. **142**: p. 8-31.
24. Armstrong, D.K., et al., *NCCN Guidelines(R) Insights: Ovarian Cancer, Version 3.2022.* J Natl Compr Canc Netw, 2022. **20**(9): p. 972-980.
25. Markman, M. and J.L. Walker, *Intraperitoneal chemotherapy of ovarian cancer: a review, with a focus on practical aspects of treatment.* Journal of clinical oncology, 2006. **24**(6): p. 988-994.
26. Zoń, A. and I. Bednarek, *Cisplatin in Ovarian Cancer Treatment—Known Limitations in Therapy Force New Solutions.* International Journal of Molecular Sciences, 2023. **24**(8): p. 7585.
27. Rocha, C.R.R., et al., *DNA repair pathways and cisplatin resistance: an intimate relationship.* Clinics, 2018. **73**: p. e478s.
28. Cisplatin Ghosh, S., *The first metal based anticancer drug.* Bioorg Chem, 2019. **88**: p. 102925.
29. Raudenska, M., et al., *Unexpected therapeutic effects of cisplatin.* Metallomics, 2019. **11**(7): p. 1182-1199.
30. Gentric, G., et al., *PML-Regulated Mitochondrial Metabolism Enhances Chemosensitivity in Human Ovarian Cancers.* Cell Metab, 2019. **29**(1): p. 156-173 e10.
31. Ledermann, J.A., et al., *Newly diagnosed and relapsed epithelial ovarian carcinoma: ESMO Clinical Practice Guidelines for diagnosis, treatment and follow-up.* Ann Oncol, 2013. **24 Suppl 6**: p. vi24-32.
32. Galluzzi, L., et al., *Systems biology of cisplatin resistance: past, present and future.* Cell death & disease, 2014. **5**(5): p. e1257-e1257.
33. Wang, H., et al., *The impact of the tumor microenvironment on macrophage polarization in cancer metastatic progression.* International journal of molecular sciences, 2021. **22**(12): p. 6560.
34. Yang, L., et al., *Molecular mechanisms of platinum-based chemotherapy resistance in ovarian cancer (Review).* Oncol Rep, 2022. **47**(4).
35. Monk, B.J., L. Minion, and R. Coleman, *Anti-angiogenic agents in ovarian cancer: past, present, and future.* Annals of oncology, 2016. **27**: p. i33-i39.
36. Montemorano, L., M.D. Lightfoot, and K. Bixel, *Role of olaparib as maintenance treatment for ovarian cancer: the evidence to date.* OncoTargets and therapy, 2019. **12**: p. 11497.
37. Tan, S., D. Li, and X. Zhu, *Cancer immunotherapy: Pros, cons and beyond.* Biomedicine & Pharmacotherapy, 2020. **124**: p. 109821.
38. Reinthaller, A., *Antiangiogenic therapies in ovarian cancer.* Memo, 2016. **9**(3): p. 139-143.
39. Liu, Y., et al., *Autosis is a Na+,K+-ATPase-regulated form of cell death triggered by autophagy-inducing peptides, starvation, and hypoxia-ischemia.* Proc Natl Acad Sci U S A, 2013. **110**(51): p. 20364-71.
40. Dizdar, O., C. Arslan, and K. Altundag, *Advances in PARP inhibitors for the treatment of breast cancer.* Expert Opinion on Pharmacotherapy, 2015. **16**(18): p. 2751-2758.
41. Jiang, X., et al., *PARP inhibitors in ovarian cancer: Sensitivity prediction and resistance mechanisms.* Journal of cellular and molecular medicine, 2019. **23**(4): p. 2303-2313.
42. Ramus, S.J. and S.A. Gayther, *The contribution of BRCA1 and BRCA2 to ovarian cancer.* Mol Oncol, 2009. **3**(2): p. 138-50.
43. Irtan, S., P.F. Ehrlich, and K. Pritchard-Jones. *Wilms tumor: "State-of-the-art" update, 2016*. in *Seminars in pediatric surgery*. 2016. Elsevier.

44. Constantinidou, A., C. Alifieris, and D.T. Trafalis, *Targeting programmed cell death-1 (PD-1) and ligand (PD-L1): a new era in cancer active immunotherapy.* Pharmacology & Therapeutics, 2019. **194**: p. 84-106.
45. Shimizu, M., et al., *Immunohistochemical detection of the Wilms' tumor gene (WT1) in epithelial ovarian tumors.* International journal of gynecological pathology, 2000. **19**(2): p. 158-163.
46. Maslak, P.G., et al., *Phase 2 trial of a multivalent WT1 peptide vaccine (galinpepimut-S) in acute myeloid leukemia.* Blood advances, 2018. **2**(3): p. 224-234.
47. Manning-Geist, B.L., et al., *Phase I Study of a Multivalent WT1 Peptide Vaccine (Galinpepimut-S) in Combination with Nivolumab in Patients with WT1-Expressing Ovarian Cancer in Second or Third Remission.* Cancers, 2023. **15**(5): p. 1458.
48. Mei, C., et al., *Anti-angiogenic therapy in ovarian cancer: Current understandings and prospects of precision medicine.* Front Pharmacol, 2023. **14**: p. 1147717.
49. Belpomme, D., et al., *Gemcitabine combined with cisplatin as first-line treatment in patients with epithelial ovarian cancer: a phase II study.* Gynecologic oncology, 2003. **91**(1): p. 32-38.
50. Moufarij, M.A., D.R. Phillips, and C. Cullinane, *Gemcitabine potentiates cisplatin cytotoxicity and inhibits repair of cisplatin-DNA damage in ovarian cancer cell lines.* Molecular pharmacology, 2003. **63**(4): p. 862-869.
51. Mini, E., et al., *Cellular pharmacology of gemcitabine.* Annals of oncology, 2006. **17**: p. v7-v12.
52. Medina, T.M. and K.D. Lewis, *The evolution of combined molecular targeted therapies to advance the therapeutic efficacy in melanoma: a highlight of vemurafenib and cobimetinib.* OncoTargets and therapy, 2016: p. 3739-3752.
53. Nami, B., H. Maadi, and Z. Wang, *Mechanisms underlying the action and synergism of trastuzumab and pertuzumab in targeting HER2-positive breast cancer.* Cancers, 2018. **10**(10): p. 342.
54. Arany, I., et al., *Cisplatin-induced cell death is EGFR/src/ERK signaling dependent in mouse proximal tubule cells.* American Journal of Physiology-Renal Physiology, 2004. **287**(3): p. F543-F549.
55. Carrato, A., J. Gallego-Plazas, and C. Guillen-Ponce, *Capecitabine plus oxaliplatin for the treatment of colorectal cancer.* Expert Review of Anticancer Therapy, 2008. **8**(2): p. 161-174.
56. Vodenkova, S., et al., *5-fluorouracil and other fluoropyrimidines in colorectal cancer: Past, present and future.* Pharmacology & therapeutics, 2020. **206**: p. 107447.
57. Vaishampayan, U., et al., *Taxanes: an overview of the pharmacokinetics and pharmacodynamics.* Urology, 1999. **54**(6): p. 22-29.
58. de Weger, V.A., et al., *A phase 1 dose-escalation study of low-dose metronomic treatment with novel oral paclitaxel formulations in combination with ritonavir in patients with advanced solid tumors.* Clinical Pharmacology in Drug Development, 2021. **10**(6): p. 607-621.
59. Lee, J.J., et al., *Interaction index and different methods for determining drug interaction in combination therapy.* Journal of biopharmaceutical statistics, 2007. **17**(3): p. 461-480.
60. Demidenko, E. and T.W. Miller, *Statistical determination of synergy based on Bliss definition of drugs independence.* PLoS One, 2019. **14**(11): p. e0224137.
61. Chou, T.-C., *Drug combination studies and their synergy quantification using the Chou-Talalay method.* Cancer research, 2010. **70**(2): p. 440-446.

62. Matthews, H., et al., *Investigating antimalarial drug interactions of emetine dihydrochloride hydrate using CalcuSyn-based interactivity calculations.* PLOS ONE, 2017. **12**(3): p. e0173303.
63. Chou, T.-C., *Preclinical versus clinical drug combination studies.* Leukemia & lymphoma, 2008. **49**(11): p. 2059-2080.
64. Loewe, S., *The problem of synergism and antagonism of combined drugs.* Arzneimittel-forschung, 1953. **3**(6): p. 285-290.
65. Ianevski, A., A.K. Giri, and T. Aittokallio, *SynergyFinder 2.0: visual analytics of multi-drug combination synergies.* Nucleic acids research, 2020. **48**(W1): p. W488-W493.
66. Pellegrini, P., et al., *Acidic extracellular pH neutralizes the autophagy-inhibiting activity of chloroquine: implications for cancer therapies.* Autophagy, 2014. **10**(4): p. 562-571.
67. Tang, J., K. Wennerberg, and T. Aittokallio, *What is synergy? The Saariselkä agreement revisited.* Frontiers in pharmacology, 2015. **6**: p. 181.
68. Bliss, C.I., *The toxicity of poisons applied jointly 1.* Annals of applied biology, 1939. **26**(3): p. 585-615.
69. Yadav, B., et al., *Searching for Drug Synergy in Complex Dose–Response Landscapes Using an Interaction Potency Model.* Computational and Structural Biotechnology Journal, 2015. **13**: p. 504-513.
70. Ryter, S.W., D. Bhatia, and M.E. Choi, *Autophagy: a lysosome-dependent process with implications in cellular redox homeostasis and human disease.* Antioxidants & redox signaling, 2019. **30**(1): p. 138-159.
71. Dice, J.F., *Lysosomal pathways of protein degradation*. 2000: CRC Press.
72. Wong, P.-M., et al., *The ULK1 complex: sensing nutrient signals for autophagy activation.* Autophagy, 2013. **9**(2): p. 124-137.
73. Galluzzi, L., et al., *Metabolic control of autophagy.* Cell, 2014. **159**(6): p. 1263-1276.
74. Saha, S., et al., *Autophagy in health and disease: A comprehensive review.* Biomedicine & Pharmacotherapy, 2018. **104**: p. 485-495.
75. LEE, J.W., et al., *Somatic mutations of BECN1, an autophagy-related gene, in human cancers.* APMIS, 2007. **115**(6): p. 750-756.
76. Levy, J.M.M., C.G. Towers, and A. Thorburn, *Targeting autophagy in cancer.* Nature Reviews Cancer, 2017. **17**(9): p. 528-542.
77. Yao, T.-P., *The role of ubiquitin in autophagy-dependent protein aggregate processing.* Genes & cancer, 2010. **1**(7): p. 779-786.
78. Zorova, L.D., et al., *Mitochondrial membrane potential.* Analytical biochemistry, 2018. **552**: p. 50-59.
79. Wu, Q., et al., *Overexpression of p62 induces autophagy and promotes proliferation, migration and invasion of nasopharyngeal carcinoma cells through promoting ERK signaling pathway.* Current Cancer Drug Targets, 2020. **20**(8): p. 624-637.
80. Lamark, T., S. Svenning, and T. Johansen, *Regulation of selective autophagy: the p62/SQSTM1 paradigm.* Essays in biochemistry, 2017. **61**(6): p. 609-624.
81. Yang, Z.J., et al., *The role of autophagy in cancer: therapeutic implications.* Molecular cancer therapeutics, 2011. **10**(9): p. 1533-1541.
82. Shao, M., et al., *Encapsulation of chloroquine and doxorubicin by MPEG-PLA to enhance anticancer effects by lysosomes inhibition in ovarian cancer.* International Journal of Nanomedicine, 2018: p. 8231-8245.
83. Moosavi, M.A., et al., *Phytochemicals as potent modulators of autophagy for cancer therapy.* Cancer Letters, 2018. **424**: p. 46-69.

84. Ma, L., et al., *Autophagic flux promotes cisplatin resistance in human ovarian carcinoma cells through ATP-mediated lysosomal function.* International Journal of Oncology, 2015. **47**(5): p. 1890-1900.
85. Peracchio, C., et al., *Involvement of autophagy in ovarian cancer: a working hypothesis.* Journal of ovarian research, 2012. **5**: p. 1-10.
86. Yue, Z., et al., *Beclin 1, an autophagy gene essential for early embryonic development, is a haploinsufficient tumor suppressor.* Proceedings of the National Academy of Sciences, 2003. **100**(25): p. 15077-15082.
87. Valente, G., et al., *Expression and clinical significance of the autophagy proteins BECLIN 1 and LC3 in ovarian cancer.* BioMed research international, 2014. **2014**.
88. Hu, Y.-J., et al., *Autophagy-related beclin 1 and head and neck cancers.* OncoTargets and therapy, 2020: p. 6213-6227.
89. Lee, E.F., et al., *The BECN1 N-terminal domain is intrinsically disordered.* Autophagy, 2016. **12**(3): p. 460-471.
90. Oberstein, A., P.D. Jeffrey, and Y. Shi, *Crystal structure of the Bcl-XL-Beclin 1 peptide complex: Beclin 1 is a novel BH3-only protein.* Journal of Biological Chemistry, 2007. **282**(17): p. 13123-13132.
91. Li, X., et al., *Imperfect interface of Beclin1 coiled-coil domain regulates homodimer and heterodimer formation with Atg14L and UVRAG.* Nature communications, 2012. **3**(1): p. 662.
92. Marat, A.L. and V. Haucke, *Phosphatidylinositol 3-phosphates—at the interface between cell signalling and membrane traffic.* The EMBO journal, 2016. **35**(6): p. 561-579.
93. Tanida, I., *Autophagosome formation and molecular mechanism of autophagy.* Antioxidants & redox signaling, 2011. **14**(11): p. 2201-2214.
94. Wu, S., et al., *Targeting the potent Beclin 1-UVRAG coiled-coil interaction with designed peptides enhances autophagy and endolysosomal trafficking.* Proc Natl Acad Sci U S A, 2018. **115**(25): p. E5669-E5678.
95. Hu, Y.J., et al., *Autophagy-Related Beclin 1 and Head and Neck Cancers.* Onco Targets Ther, 2020. **13**: p. 6213-6227.
96. Li, X., et al., *Imperfect interface of Beclin1 coiled-coil domain regulates homodimer and heterodimer formation with Atg14L and UVRAG.* Nat Commun, 2012. **3**: p. 662.
97. Wu, S., et al., *Targeting the potent Beclin 1–UVRAG coiled-coil interaction with designed peptides enhances autophagy and endolysosomal trafficking.* Proceedings of the National Academy of Sciences, 2018. **115**(25): p. E5669-E5678.
98. Romani, B., S. Engelbrecht, and R.H. Glashoff, *Functions of Tat: the versatile protein of human immunodeficiency virus type 1.* Journal of general virology, 2010. **91**(1): p. 1-12.
99. Shoji-Kawata, S., et al., *Identification of a candidate therapeutic autophagy-inducing peptide.* Nature, 2013. **494**(7436): p. 201-206.
100. Ramsey, J.D. and N.H. Flynn, *Cell-penetrating peptides transport therapeutics into cells.* Pharmacology & therapeutics, 2015. **154**: p. 78-86.
101. Yang, Q., et al., *Optimization of beclin 1-targeting stapled peptides by staple scanning leads to enhanced antiproliferative potency in cancer cells.* Journal of Medicinal Chemistry, 2021. **64**(18): p. 13475-13486.
102. Halliwell, B. and J.M. Gutteridge, *Free radicals in biology and medicine*. 2015: Oxford university press, USA.
103. Lee, H.-C. and Y.-H. Wei, *Mitochondrial role in life and death of the cell.* Journal of biomedical science, 2000. **7**(1): p. 2-15.

104. Pieczenik, S.R. and J. Neustadt, *Mitochondrial dysfunction and molecular pathways of disease.* Experimental and molecular pathology, 2007. **83**(1): p. 84-92.
105. Pathania, D., M. Millard, and N. Neamati, *Opportunities in discovery and delivery of anticancer drugs targeting mitochondria and cancer cell metabolism.* Advanced drug delivery reviews, 2009. **61**(14): p. 1250-1275.
106. Kuznetsov, A.V., et al., *Changes in mitochondrial redox state, membrane potential and calcium precede mitochondrial dysfunction in doxorubicin-induced cell death.* Biochimica et Biophysica Acta (BBA)-Molecular Cell Research, 2011. **1813**(6): p. 1144-1152.
107. Dashty, M., *A quick look at biochemistry: carbohydrate metabolism.* Clinical biochemistry, 2013. **46**(15): p. 1339-1352.
108. Rigoulet, M., A. Mourier, and A. Devin, *Organization and regulation of mitochondrial oxidative phosphorylation*. 2007: Wiley-VCH Verlag GmbH&Co. KGaA: Weinheim, Darmstadt, Germany.
109. Mitchell, P. and J. Moyle, *Chemiosmotic hypothesis of oxidative phosphorylation.* Nature, 1967. **213**(5072): p. 137-139.
110. Lenaz, G., et al., *The role of Coenzyme Q in mitochondrial electron transport.* Mitochondrion, 2007. **7**: p. S8-S33.
111. Nicholls, D.G., *Bioenergetics*. 2013: Academic press.
112. Koppenol, W.H., P.L. Bounds, and C.V. Dang, *Otto Warburg's contributions to current concepts of cancer metabolism.* Nature Reviews Cancer, 2011. **11**(5): p. 325-337.
113. Moreno-Sánchez, R., et al., *The bioenergetics of cancer: is glycolysis the main ATP supplier in all tumor cells?* Biofactors, 2009. **35**(2): p. 209-225.
114. Ho, J., et al., *Importance of glycolysis and oxidative phosphorylation in advanced melanoma.* Molecular cancer, 2012. **11**(1): p. 1-13.
115. Zorov, D.B., M. Juhaszova, and S.J. Sollott, *Mitochondrial reactive oxygen species (ROS) and ROS-induced ROS release.* Physiological reviews, 2014. **94**(3): p. 909-950.
116. Maciag, A.E., et al., *Nitric oxide-releasing prodrug triggers cancer cell death through deregulation of cellular redox balance.* Redox biology, 2013. **1**(1): p. 115-124.
117. Arfin, S., et al., *Oxidative stress in cancer cell metabolism.* Antioxidants, 2021. **10**(5): p. 642.
118. Arnér, E.S. and A. Holmgren, *Physiological functions of thioredoxin and thioredoxin reductase.* European journal of biochemistry, 2000. **267**(20): p. 6102-6109.
119. Sobhakumari, A., et al., *Susceptibility of human head and neck cancer cells to combined inhibition of glutathione and thioredoxin metabolism.* PLoS One, 2012. **7**(10): p. e48175.
120. Endo, T., H. Yamamoto, and M. Esaki, *Functional cooperation and separation of translocators in protein import into mitochondria, the double-membrane bounded organelles.* Journal of cell science, 2003. **116**(16): p. 3259-3267.
121. Giacomello, M., et al., *The cell biology of mitochondrial membrane dynamics.* Nature reviews Molecular cell biology, 2020. **21**(4): p. 204-224.
122. Zoratti, M. and I. Szabó, *Electrophysiology of the inner mitochondrial membrane.* Journal of bioenergetics and biomembranes, 1994. **26**: p. 543-553.
123. Lenaz, G. and M.L. Genova, *Structure and organization of mitochondrial respiratory complexes: a new understanding of an old subject.* Antioxidants & redox signaling, 2010. **12**(8): p. 961-1008.
124. Begum, H.M. and K. Shen, *Intracellular and microenvironmental regulation of mitochondrial membrane potential in cancer cells.* WIREs Mechanisms of Disease, 2023. **15**(3): p. e1595.

125. Perry, S.W., et al., *Mitochondrial membrane potential probes and the proton gradient: a practical usage guide.* Biotechniques, 2011. **50**(2): p. 98-115.
126. Morciano, G., et al., *The mitochondrial permeability transition pore: an evolving concept critical for cell life and death.* Biological Reviews, 2021. **96**(6): p. 2489-2521.
127. Hunter, D.R., R. Haworth, and J. Southard, *Relationship between configuration, function, and permeability in calcium-treated mitochondria.* Journal of Biological Chemistry, 1976. **251**(16): p. 5069-5077.
128. Hurst, S., J. Hoek, and S.-S. Sheu, *Mitochondrial Ca 2+ and regulation of the permeability transition pore.* Journal of bioenergetics and biomembranes, 2017. **49**: p. 27-47.
129. Ikeda, G., et al., *Nanoparticle-mediated targeting of cyclosporine A enhances cardioprotection against ischemia-reperfusion injury through inhibition of mitochondrial permeability transition pore opening.* Scientific reports, 2016. **6**(1): p. 20467.
130. Bonora, M. and P. Pinton, *The mitochondrial permeability transition pore and cancer: molecular mechanisms involved in cell death.* Frontiers in oncology, 2014. **4**: p. 302.
131. McAinsh, M.R., C. Brownlee, and A.M. Hetherington, *Calcium ions as second messengers in guard cell signal transduction.* Physiologia Plantarum, 1997. **100**(1): p. 16-29.
132. Endo, M., *Calcium ion as a second messenger with special reference to excitation-contraction coupling.* Journal of pharmacological sciences, 2006. **100**(5): p. 519-524.
133. Krebs, J., L.B. Agellon, and M. Michalak, *Ca2+ homeostasis and endoplasmic reticulum (ER) stress: An integrated view of calcium signaling.* Biochemical and biophysical research communications, 2015. **460**(1): p. 114-121.
134. Rizzuto, R., et al., *Ca2+ transfer from the ER to mitochondria: when, how and why.* Biochimica et Biophysica Acta (BBA)-Bioenergetics, 2009. **1787**(11): p. 1342-1351.
135. Bustos, G., et al., *Endoplasmic reticulum–mitochondria calcium communication and the regulation of mitochondrial metabolism in cancer: a novel potential target.* Frontiers in oncology, 2017. **7**: p. 199.
136. Karaki, H., et al., *Calcium movements, distribution, and functions in smooth muscle.* Pharmacological reviews, 1997. **49**(2): p. 157-230.
137. Bourinet, E., et al., *Calcium-permeable ion channels in pain signaling.* Physiological reviews, 2014. **94**(1): p. 81-140.
138. DeLuca, H.F. and G.W. Engstrom, *Calcium uptake by rat kidney mitochondria.* Proceedings of the National Academy of Sciences, 1961. **47**(11): p. 1744-1750.
139. Shoshan-Barmatz, V. and S. De, *Mitochondrial VDAC, the Na+/Ca 2+ Exchanger, and the Ca 2+ Uniporter in Ca 2+ dynamics and signaling.* Membrane Dynamics and Calcium Signaling, 2017: p. 323-347.
140. Machaca, K., *Ca2+ signaling, genes and the cell cycle.* Cell calcium, 2010. **48**(5): p. 243-250.
141. LaFerla, F.M., *Calcium dyshomeostasis and intracellular signalling in Alzheimer's disease.* Nature Reviews Neuroscience, 2002. **3**(11): p. 862-872.
142. Kawamoto, E.M., C. Vivar, and S. Camandola, *Physiology and pathology of calcium signaling in the brain.* Frontiers in pharmacology, 2012: p. 61.
143. Brini, M., *Ca2+ signalling in mitochondria: mechanism and role in physiology and pathology.* Cell Calcium, 2003. **34**(4-5): p. 399-405.
144. Caravia, L., et al., *Altered organelle calcium transport in ovarian physiology and cancer.* Cancers, 2020. **12**(8): p. 2232.

145. Patergnani, S., et al., *Various aspects of calcium signaling in the regulation of apoptosis, autophagy, cell proliferation, and cancer.* International journal of molecular sciences, 2020. **21**(21): p. 8323.
146. Lencesova, L., et al., *Hypoxic conditions increases H 2 S-induced ER stress in A2870 cells.* Molecular and cellular biochemistry, 2016. **414**: p. 67-76.
147. Chakraborty, P.K., et al., *MICU1 drives glycolysis and chemoresistance in ovarian cancer.* Nature communications, 2017. **8**(1): p. 14634.
148. Wang, S.-F., L.-M. Tseng, and H.-C. Lee, *Role of mitochondrial alterations in human cancer progression and cancer immunity.* Journal of Biomedical Science, 2023. **30**(1): p. 61.
149. Ivanova, H., et al., *Endoplasmic reticulum–mitochondrial Ca2+ fluxes underlying cancer cell survival.* Frontiers in oncology, 2017. **7**: p. 70.
150. Mesquita, K.d.A., *Role of mitochondria and DNA damage responses in cancer stem cells resistance to chemotherapy*. 2016.
151. Rasola, A. and P. Bernardi, *Mitochondrial permeability transition in Ca2+-dependent apoptosis and necrosis.* Cell calcium, 2011. **50**(3): p. 222-233.
152. Görlach, A., et al., *Calcium and ROS: A mutual interplay.* Redox biology, 2015. **6**: p. 260-271.
153. Landriscina, M., et al., *Adaptation to oxidative stress, chemoresistance, and cell survival.* Antioxidants & redox signaling, 2009. **11**(11): p. 2701-2716.
154. Humeau, J., et al., *Calcium signaling and cell cycle: Progression or death.* Cell calcium, 2018. **70**: p. 3-15.
155. Panda, S., et al., *Targeting Ca2+ signaling: A new arsenal against cancer.* Drug Discovery Today, 2022. **27**(3): p. 923-934.
156. Ravikumar, B., et al., *Regulation of mammalian autophagy in physiology and pathophysiology.* Physiological reviews, 2010. **90**(4): p. 1383-1435.
157. He, C. and D.J. Klionsky, *Regulation mechanisms and signaling pathways of autophagy.* Annual review of genetics, 2009. **43**: p. 67-93.
158. Kang, R., et al., *The Beclin 1 network regulates autophagy and apoptosis.* Cell Death & Differentiation, 2011. **18**(4): p. 571-580.
159. Yang, Q., et al., *Optimization of Beclin 1-Targeting Stapled Peptides by Staple Scanning Leads to Enhanced Antiproliferative Potency in Cancer Cells.* J Med Chem, 2021. **64**(18): p. 13475-13486.
160. Domcke, S., et al., *Evaluating cell lines as tumour models by comparison of genomic profiles.* Nature communications, 2013. **4**(1): p. 2126.
161. Pokhriyal, R., et al., *Chemotherapy resistance in advanced ovarian cancer patients.* Biomarkers in cancer, 2019. **11**: p. 1179299X19860815.
162. Chen, S.-H. and J.-Y. Chang, *New insights into mechanisms of cisplatin resistance: from tumor cell to microenvironment.* International journal of molecular sciences, 2019. **20**(17): p. 4136.
163. Liu, Y. and B. Levine, *Autosis and autophagic cell death: the dark side of autophagy.* Cell Death & Differentiation, 2015. **22**(3): p. 367-376.
164. Zheng, N., et al., *Induction of tumor cell autosis by myxoma virus-infected CAR-T and TCR-T cells to overcome primary and acquired resistance.* Cancer Cell, 2022. **40**(9): p. 973-985. e7.
165. Chen, L. and X. Han, *Anti–PD-1/PD-L1 therapy of human cancer: past, present, and future.* The Journal of clinical investigation, 2015. **125**(9): p. 3384-3391.
166. Basu, A. and S. Krishnamurthy, *Cellular responses to Cisplatin-induced DNA damage.* Journal of nucleic acids, 2010. **2010**.

167. Bers, D.M., *Calcium cycling and signaling in cardiac myocytes.* Annu. Rev. Physiol., 2008. **70**: p. 23-49.
168. An, Z., et al., *Beth Levine's Legacy: From the Discovery of BECN1 to Therapies. A Mentees' Perspective.* Frontiers in Cell and Developmental Biology, 2022. **10**.
169. Nah, J., D. Zablocki, and J. Sadoshima, *Autosis: a new target to prevent cell death.* Basic to Translational Science, 2020. **5**(8): p. 857-869.
170. Duchen, M.R., *Mitochondria and calcium: from cell signalling to cell death.* The Journal of physiology, 2000. **529**(1): p. 57-68.
171. Li, N., et al., *Perturbation of Autophagy by a Beclin 1-Targeting Stapled Peptide Induces Mitochondria Stress and Inhibits Proliferation of Pancreatic Cancer Cells.* Cancers, 2023. **15**(3): p. 953.
172. Renaudin, X., *Reactive oxygen species and DNA damage response in cancer.* International Review of Cell and Molecular Biology, 2021. **364**: p. 139-161.
173. Zamzami, N., N. Larochette, and G. Kroemer, *Mitochondrial permeability transition in apoptosis and necrosis.* Cell death and differentiation, 2005. **12**(S2): p. 1478.
174. Grabosch, S., et al., *Cisplatin-induced immune modulation in ovarian cancer mouse models with distinct inflammation profiles.* Oncogene, 2019. **38**(13): p. 2380-2393.
175. Hopkins, D., et al., *Cisplatin increases immune activity of monocytes and cytotoxic T-cells in a murine model of epithelial ovarian cancer.* Translational Oncology, 2021. **14**(12): p. 101217.
176. Catterall, W.A. and A.P. Few, *Calcium channel regulation and presynaptic plasticity.* Neuron, 2008. **59**(6): p. 882-901.
177. Ceci, C., et al., *Role of VEGFs/VEGFR-1 signaling and its inhibition in modulating tumor invasion: Experimental evidence in different metastatic cancer models.* International journal of molecular sciences, 2020. **21**(4): p. 1388.
178. Wang, W., et al., *CD8+ T cells regulate tumour ferroptosis during cancer immunotherapy.* Nature, 2019. **569**(7755): p. 270-274.
179. Odunsi, K., *Immunotherapy in ovarian cancer.* Annals of oncology, 2017. **28**: p. viii1-viii7.